ACTUAL PROBLEMS OF MODERN SCIENCE, EDUCATION AND TRAINING

KHOREZMSCIENCE.UZ

CONTENTS

Section 1. MODERN PROBLEMS OF TECHNICAL SCIENCES……...4

BUNYOD ALLABERGENOV, FARANGIS ALLABERGENOVA, UCHQUN KUTLIEV, SUNGJIN KIM /// SYNTHESIS AND SURFACE MORPHOLOGY STUDY OF VANADIUM OXIDE THIN FILMS……..4

SHARIPOV MAKSUD /// DESIGN AND IMPLEMENTATION OF A MODEL AND ALGORITHM FOR PART-OF-SPEECH TAGGING IN UZBEK TEXTS USING THE CONDITIONAL RANDOM FIELDS (CRFs) APPROACH……..13

KHABIBULLA MADATOV /// STATISTICAL WORD IMPORTANCE MODELING FOR UZBEK TEXT SUMMARIZATION: A TF-IDF-BASED APPROACH WITH IMPROVED SENTENCE SELECTION……20

BUNYOD ALLABERGENOV, FARANGIS ALLABERGENOVA, UCHQUN KUTLIEV, SUNGJIN KIM /// ANNEALING-INDUCED PHASE EVOLUTION AND MORPHOLOGICAL CONTROL IN RF-SPUTTERED VO_2 THIN FILMS……..…..30

Section 2. ACTUAL PROBLEMS OF NATURAL SCIENCES……37

KARIMOVA MOMOJON EGAMBERGANOVNA, ISMAILOVA SHAHLA ATANAZAROVNA, KHUDOYBERGANOV OYBEK IKROMOVICH /// SYNTHESIS AND STUDY OF THE COORDINATION COMPOUND OF ZINC NITRATE WITH KETOROLAC…….……..37

MATMURATOVA ZULAYXO IKROMBOY KIZI /// SYNTHESIS AND ANALYSIS RESULTS OF THE 1,10-PHENANTHROLINE-TRIS(2-AMINO-5-ETHYLTHIO-1,3,4-THIADIAZOLE) COPPER(II) PERCHLORATE COMPLEX COMPOUND OBTAINED USING 2-AMINO-5-ETHYLTHIO-1,3,4-THIADIAZOLE AND 1,10-PHENANTHROLINE LIGANDS……...44

ATAJANOVA SHIRIN MASHARIBOVNA, ABDULLAEV IKRAM ISKANDAROVICH /// THE IMPACT OF ATTAGENUS SMIRNOVI ON CULTURAL AND DOMESTIC ASSETS: CHALLENGES AND SOLUTIONS……..52

Section 3. ACTUAL PROBLEMS IN MODERN AGRICULTURE 58

ARTIKOV MAKHMUD SULTONBOEVICH, KHUSAINOV BAKHTIYOR /// DYNAMIC ANALYSIS OF THE FRAME BETWEEN TWO AXLES OF THE VARIABLE BASE TRACTOR……..……58

ARTIKOV MAKHMUD SULTONBOEVICH /// IMPROVING THE STABILITY AND MANEUVERABILITY OF THE VARIABLE BASE TRACTOR……64

ARTIKOV MAKHMUD SULTONBOEVICH /// FEM ANALYSIS-STRUCTURAL AND DYNAMIC, DISCUSSIONS AND RESULTS OF THE MODIFIED MECHANISM FOR ADJUSTING BASE OF THE TRACTOR….69

Section 4. ACTUAL PROBLEMS OF MATHEMATICS, PHYSICS AND MECHANICS……75

ALLAYAROVA GULMIRA, KUTLIEV UCHQUN, ISMOILOV JALOLADDIN /// INVESTIGATION OF IMPLANTATION OXYGEN IONS INTO THE SURFACE Mo(001)……75

ATAMURATOV ALIMARDON ABDRIMOVICH, KUSHNAZAROV RASUL QUDRATOVICH /// EXTREMAL FUNCTIONS ON PARABOLIC MANIFOLDS AND REGULAR COMPACTS……80

ABDIKARIMOV XIDOYAT EGAMBERGANOVICH /// THE IMPORTANCE OF PHYSICS-BASED MODEL SELECTION AND RESULT CALIBRATION IN SIMULATION SUB-5NM SILICON GAAFETS……86

BALTAYEVA UMIDA ISMOILOVNA, BABAJANOVA YULDUZ IKROMBOYEVNA, JUMANAZAROV OTABEK ISROILOVICH /// EXISTENCE AND UNIQUENESS OF SOLUTIONS FOR A MIXED-TYPE PROBLEM WITH INTEGRAL GLUING CONDITIONS……93

ABBOSBEK ISKANDAROV /// INVERSE SCATTERING FOR THE DULLIN-GOTTWALD-HOLM EQUATION WITH A SOURCE……98

Section 5. MODERN PROBLEMS OF PHILOLOGY AND LINGUISTICS……105

GUZAL RAKHIMOVA YULDASHOVNA /// GRAMMATICAL SEMANTIC EXPRESSIVE POSSIBILITIES OF REDUPLICATION……105

Section 6. ACTUAL PROBLEMS OF HISTORY, PHILOSOPHY AND SOCIOLOGY……112

GULOVA ANORGUL AKHTAMOVNA /// THE CATEGORY OF JUSTICE IN NAVOI'S SOCIO-ANTHROPOLOGICAL VIEWS ……112

UDC: 62, 620.3, 549.5, 66.04

SYNTHESIS AND SURFACE MORPHOLOGY STUDY OF VANADIUM OXIDE THIN FILMS

Bunyod Allabergenov
Associate Professor (PhD), Department of Transport Systems, Urgench State University named after Abu Rayhan Biruni
bunyod_kit@urdu.uz

Farangis Allabergenova
Teacher, Urgench State University named after Abu Rayhan Biruni

Uchqun Kutliev
Professor (DSc), Head of the Department of Physics, Urgench State University named after Abu Rayhan Biruni

Sungjin Kim
Professor, Kumoh National Institute of Technology, South Korea

Annotatsiya. Vanadiy oksid (VO_x) yupqa qoplamalari $Ar+H_2$ atmosferasida 900 °C da uchqun plazma pishirish (UPP) yo‘li bilan tayorlangan vanadiy nishoni bilan DC magnetron sputter yordamida sintez qilindi. Amorf VO_x qoplamalari shisha ustiga qoplangan va kristallanish va sirt xususiyatlarini o‘rganish uchun havo va kislorod atmosferasida 200-500 °C da termik ishlov berilgan. Rengen diffraktometr (XRD) tahlili 400 °C termik ishlov berilgan namunada V_2O_5 va VO_2 fazalar paydo bo‘lishi aniqlandi, huddi shu haroratda kislorod bilan termik ishlov berilgan namunalarda termokromik qurilmalar uchun muhim bo‘lgan VO_2 monoklinik faza shakllanishini kuchaytirishi aniqlangan. AFM va SEM-EDX shuni ko‘rsatdiki, yuqori termik ishlov harorati sirt g‘adir-budurligini va kislorod miqdorini oshiradi, kislorod bilan ishlangan qoplamalar silliq morfologiyani namoyish etadi. Natijalar termik ishlov berilgan sharoitlarining optoelektronik qurilmalar uchun VO_x yupqa qoplamalarining strukturaviy va morfologik xususiyatlariga ta’sirini ko‘rsatdi.

Kalit so‘zlar: *Vanadiy oksidi (VO_x), yupqa qoplamalar, uchqunli plazma pishirish (UPP), DC magnetron sputter, termik ishlov berish, kristallanish, yuza morfologiyasi, termoxrom, rentgen nurlari difraksiyasi (XRD), atom kuch mikroskopiyasi (AFM).*

Аннотация. Тонкие пленки оксида ванадия (VO_x) были синтезированы методом магнетронного распыления на постоянном токе с использованием ванадий мишени, приготовленной методом искрового плазменного спекания (ИПС) при температуре 900 °C в атмосфере $Ar+H_2$. Аморфные пленки VO_x были нанесены на стеклянные подложки и термический

обработки на воздухе и в атмосфере кислорода при температуре 200–500 °C для изучения кристаллизации и свойств поверхности. Рентгеноструктурный анализ выявил фазовое разделение на V_2O_5 и VO_2 при 400 °C, причем термический обработки в кислороде усиливает образование моноклинной фазы VO_2, что критически важно для термохромных применений. Методы AFM и SEM-EDX показали, что более высокие температуры термический обработки увеличивают шероховатость поверхности и содержание кислорода, при этом пленки, обработанные кислородом, демонстрируют более гладкую морфологию. Результаты демонстрируют влияние условий термический обработки на структурные и морфологические свойства тонких пленок VO_x для оптоэлектронных применений.

Ключевые слова: *оксид ванадия (VO_x), тонкие пленки, искровое плазменное спекание (ИПС), магнетронное распыление на постоянном токе, термический отжиг, кристаллизация, морфология поверхности, термохромные свойства, рентгеновская дифракция (РД), атомно-силовая микроскопия (AFM).*

Abstract. Vanadium oxide (VO_x) thin films were synthesized using DC magnetron sputtering with a vanadium target prepared by spark plasma sintering (SPS) at 900 °C under Ar+H_2 atmosphere. Amorphous VO_x films were deposited on glass substrates and annealed in air and oxygen atmospheres at 200–500 °C to study crystallization and surface properties. XRD analysis revealed phase separation into V_2O_5 and VO_2 at 400 °C, with oxygen annealing enhancing VO_2 monoclinic phase formation, critical for thermochromic applications. AFM and SEM-EDX showed that higher annealing temperatures increased surface roughness and oxygen content, with oxygen-treated films exhibiting smoother morphology. The results demonstrate the influence of annealing conditions on the structural and morphological properties of VO_x thin films for optoelectronic applications.

Keywords: *Vanadium oxide (VO_x), thin films, spark plasma sintering (SPS), DC magnetron sputtering, thermal annealing, crystallization, surface morphology, thermochromic properties, X-ray diffraction (XRD), atomic force microscopy (AFM).*

Introduction

Semiconductor-to-metal transition (SMT) materials exhibit dramatic changes in electronic and optical properties under external stimuli, enabling advanced applications in phase-change memory, neuromorphic computing, smart windows, and ultrafast sensors. Their unique behavior, driven by electron correlations and structural dynamics, provides insights into strongly correlated systems and quantum phenomena. Studying SMT materials is crucial for next-generation electronics, energy-efficient technologies, and fundamental condensed matter physics.

Literature Review

Vanadium oxide (VO_x) thin films have attracted significant attention due to their unique thermochromic, electrochromic, and optoelectronic properties, making them promising candidates for smart windows, sensors, and energy-efficient devices [1, 2]. Among various vanadium oxides, VO_2 exhibits a reversible metal-insulator transition (MIT) near room temperature (~68 °C), accompanied by a significant change in optical and electrical properties [3, 4]. This phase transition enables applications in optical switches, infrared camouflage, and thermal regulation coatings [5, 6].

The synthesis of high-quality vanadium oxide thin films with controlled stoichiometry and crystallinity remains a challenge due to the multiple oxidation states of vanadium (V^{2+}, V^{3+}, V^{4+}, V^{5+}) and the formation of mixed-phase structures [7]. Magnetron sputtering is a widely used technique for depositing VO_x thin films due to its ability to produce uniform coatings with precise composition control [8]. However, post-deposition thermal treatment plays a crucial role in determining the phase composition, crystallinity, and surface morphology of the films [9]. The annealing atmosphere (air or oxygen) significantly influences the oxidation state and structural properties, affecting the functional performance of the films [10].

In this study, vanadium oxide thin films were synthesized using DC magnetron sputtering from a high-purity vanadium target prepared by spark plasma sintering (SPS). The effects of thermal treatment in air and oxygen atmospheres at different temperatures (200–500 °C) on the structural, morphological, and compositional properties of the films were systematically investigated. X-ray diffraction (XRD) analysis revealed the crystallization behavior and phase evolution, while atomic force microscopy (AFM) and scanning electron microscopy with energy-dispersive X-ray spectroscopy (SEM-EDX) were employed to study surface morphology and oxygen content variations. The results demonstrate that annealing in an oxygen atmosphere enhances the formation of the monoclinic VO_2 phase, which is critical for thermochromic applications. Additionally, the correlation between oxygen content and surface roughness was analyzed, providing insights into the optimization of VO_x thin films for optoelectronic devices.

Research Methodology

To synthesize the vanadium thin film, we used vanadium metal base 325 mesh powder with a purity of 99.5%. Before obtaining the thin film, a 3-inch target was sintered from the vanadium metal powder using spark plasma sintering (SPS) equipment. More about the spark plasma sintering equipment given in other scientific articles [11-13]. In the SPS sintering process, 60 grams of vanadium powder was placed in a 3-inch graphite mold and sintered at 900 °C under a pressure of 32 MPa and a flow rate of 5 ml/min Ar+H_2 gas. The resulting 3-inch vanadium metal target was 4 mm thick and had sufficient strength to obtain a thin film coating. Figure 1 (a) shows vanadium metal powder, (b) shows a schematic view of the SPS, (c) shows a sintering image at 900 °C, and (d) shows a 3-inch vanadium target. We used a DC magnetron sputtering device to synthesize the vanadium thin film [14-16]. The vanadium target obtained in the SPS equipment was placed in a magnetron sputtering device as a source to obtain a thin coating. Borosilicate glass was selected as the substrate and was cleaned

in an ultrasonic bath of acetone, methyl alcohol and isopropanol for 15 minutes before being placed in the sputtering chamber and dried with an air flow. The chamber of the sputtering equipment was lowered to a high vacuum of 1.2×10^{-5} Torr. An operation 2.0×10^{-3} Torr atmosphere plasma was generated by introducing a mixed gas of Ar:O_2 (7.5:3.0 ccm) into the chamber.

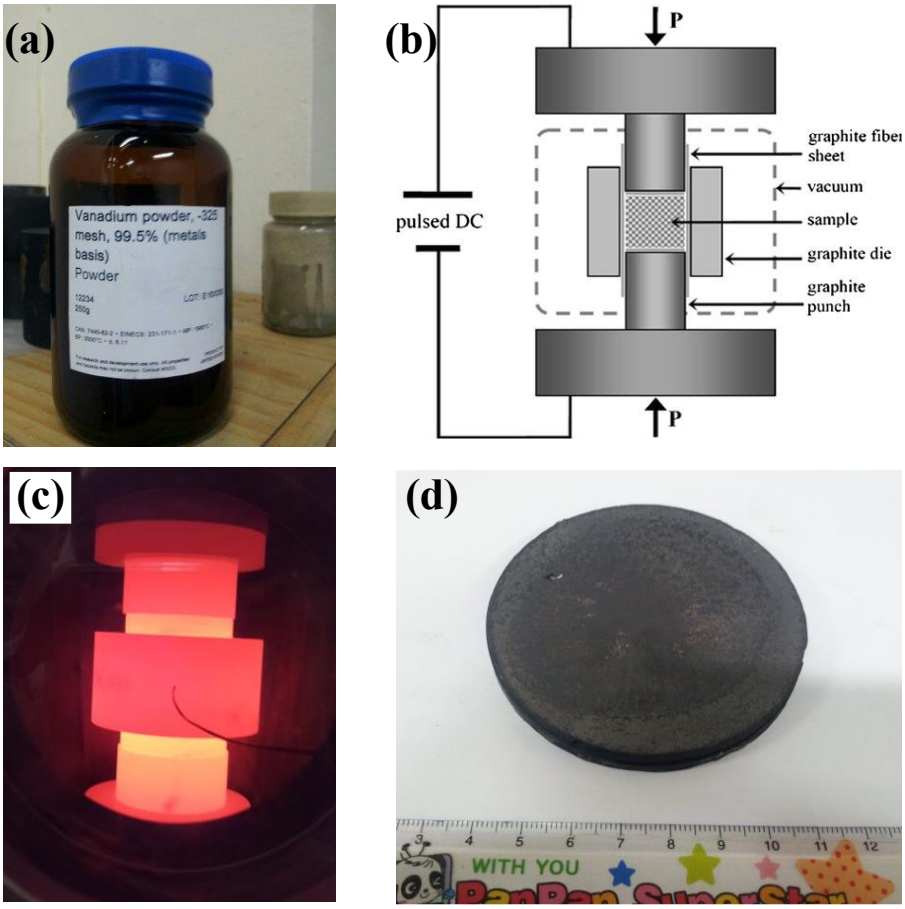

Figure 1. Vanadium metal basis with 99.5% purity and 325 mesh powder (a), (b) schematic image of the SPS graphite mold, (c) graphite old at 900 °C temperature, and (d) 3-inch vanadium target, respectively.

To synthesize a thin film, a voltage of 2 W/cm^2 was applied to the vanadium target and an amorphous VO_x structured thin film was obtained under plasma for 30 minutes. The substrate was rotated at a speed of 3 rpm to ensure uniform coating on the glass substrate. Then, the obtained thin film was thermally treated in a tube furnace in air and oxygen atmosphere for 75 minutes at temperatures of 200, 300, 400, and 500 °C.

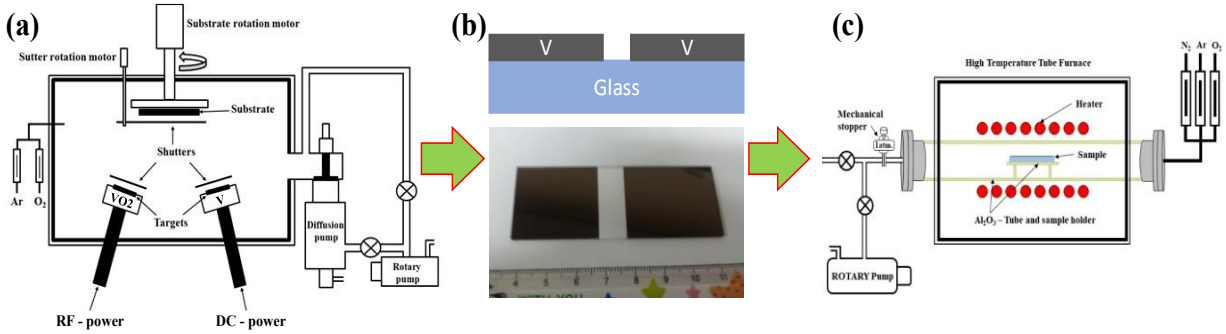

Figure 2. Schematic image of magnetron sputtering (a), (b) VOx sample image, and (c) tube furnace schematic image.

Figure 2 (a) shows a schematic view of the sputtering equipment, (b) shows the VO_x thin film after synthesis, and (c) shows a schematic view of the tube furnace. The crystallization of the obtained samples was studied using X-ray diffractometry (XRD), and the surface morphology was studied using atomic force microscopy (AFM). The oxidation content of the thin films was determined using SEM-EDX.

Analysis and Results

Figure 3 shows the X-ray diffractometer results of vanadium oxide thin films before and after thermal treatment in air and oxygen atmosphere at temperatures of 200, 300, 400, and 500 ℃. Figure 3 (a) shows the crystallization behavior for the samples thermally treated in air. As can be seen in the figure, we can see that there are 3 wide-angle peaks at 35°, 44°, and 64°. We can see that these wide-angle peaks are also present after the 200 C and 300 ℃ heat treatment, and we found that they are slightly shifted. This indicates that the crystallization process of the VO_x thin film is under nonuniform stress. We can see that several peaks appear when the heat treatment temperature is further increased to 400 ℃. This means that 400 ℃ is sufficient for the thin coating to completely crystallize in air. At the same time, it was determined that the thin coating was not a monophase but a two-phase one, that is, it consisted of V_2O_5 and VO_2 phases, which is consistent with the results of PDF# 411426 and PDF#800690 in the JSPDC international X-ray diffractometer results database. To separate the phases, we have separated V_2O_5 in black (rhombus shape) and VO_2 in red (star shape).

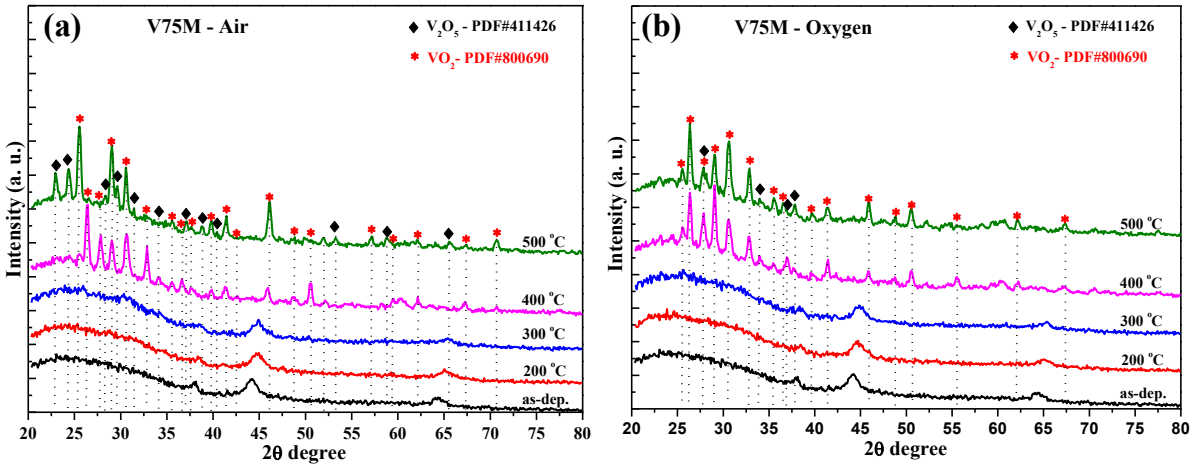

Figure 3. XRD diffraction patterns of the vanadium oxide thin films annealed at various temperatures under: (a) air and (b) oxygen atmosphere, respectively.

In Figure 3(b), we can see the crystallization of the samples thermally treated in an oxygen atmosphere at temperatures of 200, 300, 400, and 500 ℃. We can also see that the crystallization was complete at temperatures of 400 and 500 ℃ in the samples thermally treated in an oxygen atmosphere. Comparing the XRD results of samples thermally treated in air and oxygen atmospheres, it can be said that thermal annealing in oxygen atmosphere has a better effect on the crystallization of the VO_2 monoclinic phase. This is very important for the thermochromic properties of VO_2 thin films, especially for switchable optoelectronic devices.

The surface morphology and SEM-EDX elemental contents for the as-deposited VO_2 thin film sample are compared in Figure 4(a) and (b). Three lines (red, blue, green)

were drawn to determine the arithmetic mean surface roughness. Looking at the statistical table given below Figure 4(a), the results denoted by Rq give the surface roughness property. The as-deposited sample was found to have an average roughness morphological property of 7.1456 nm. At the same time, the elemental content showed 30.16 for vanadium, 48.31 for Si, and 21.53 at.% oxygen for the substrate. This means that the amorphous state without thermal treatment is composed of 21.53 at.% oxygen atoms (see Figure 4 (b)).

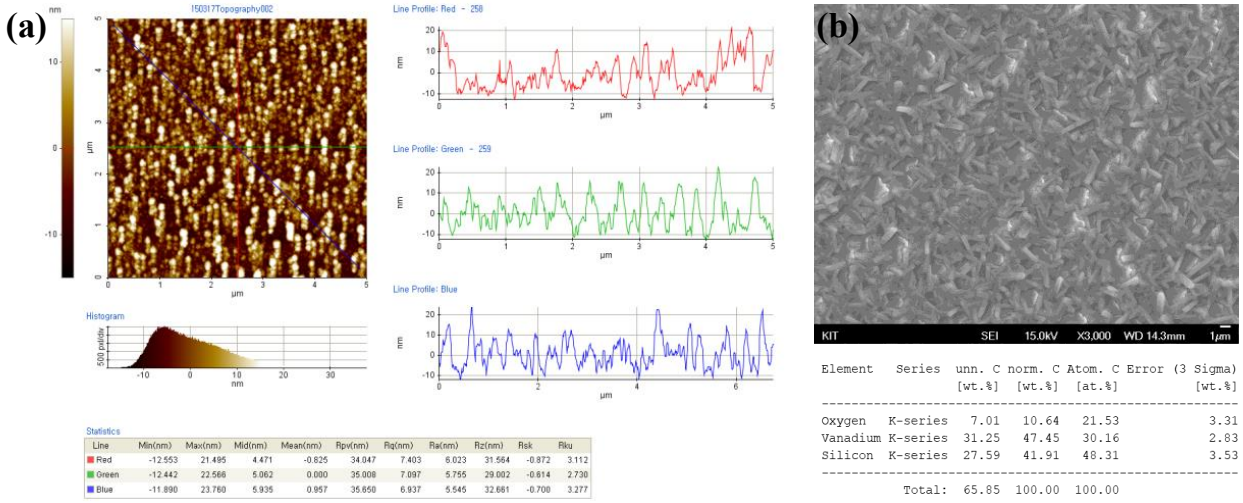

Figure 4. Morphological analysis of the as-deposited VO_x thin films: (a) AFM images vs roughness parameters, and (b) SEM-EDX images vs oxygen content.

In addition, the surface morphology of all samples thermally treated in air and oxygen atmospheres was studied and compared. Figure 5 shows AFM images of VO_2 thin films after thermal treatment at temperatures of 200, 300, 400, and 500 ℃. Figure 5 (a) and (b) show the images after thermal treatment in air and oxygen atmosphere at 200 ℃, and we found that the arithmetic mean surface roughness values were 5.0916 nm and 3.1413 nm for air and oxygen atmosphere, respectively. This indicates that thermal treatment in oxygen atmosphere leads to improved surface morphology.

Figure 5 (c) – (d) shows the surface morphology of samples heat-treated in air and oxygen at 300 ℃, and we found that the roughness increased to 13.636 nm and 19.2543 nm. For the samples heat treated at 400 ℃, we found that the roughness increased sharply for air to 37.0203 nm and the roughness decreased to 15.9176 nm for oxygen (see Figure 5 (e)-(f)). We further found that when we increased the heat treatment temperature to 500 ℃, the roughness increased to 134.8376 nm for the air sample and to 48.727 nm for the oxygen sample. At the same time, we found that as the annealing temperature increased, the size of the crystals also increased, and we can say that this directly affected the increase in roughness.

Figure 6 shows a comparison graph of AFM roughness and oxygen content for samples heat treated in air and in an oxygen atmosphere at temperatures of 200, 300, 400, and 500 ℃. When comparing the samples heat treated in air in Figure 6 (a) and (b), we can see that the roughness of the surface morphology and the oxygen content increase linearly. The samples thermally treated in an oxygen atmosphere also showed almost the same result, i.e. a linear increase. This suggests that the increase in oxygen content may have affected the surface morphology.

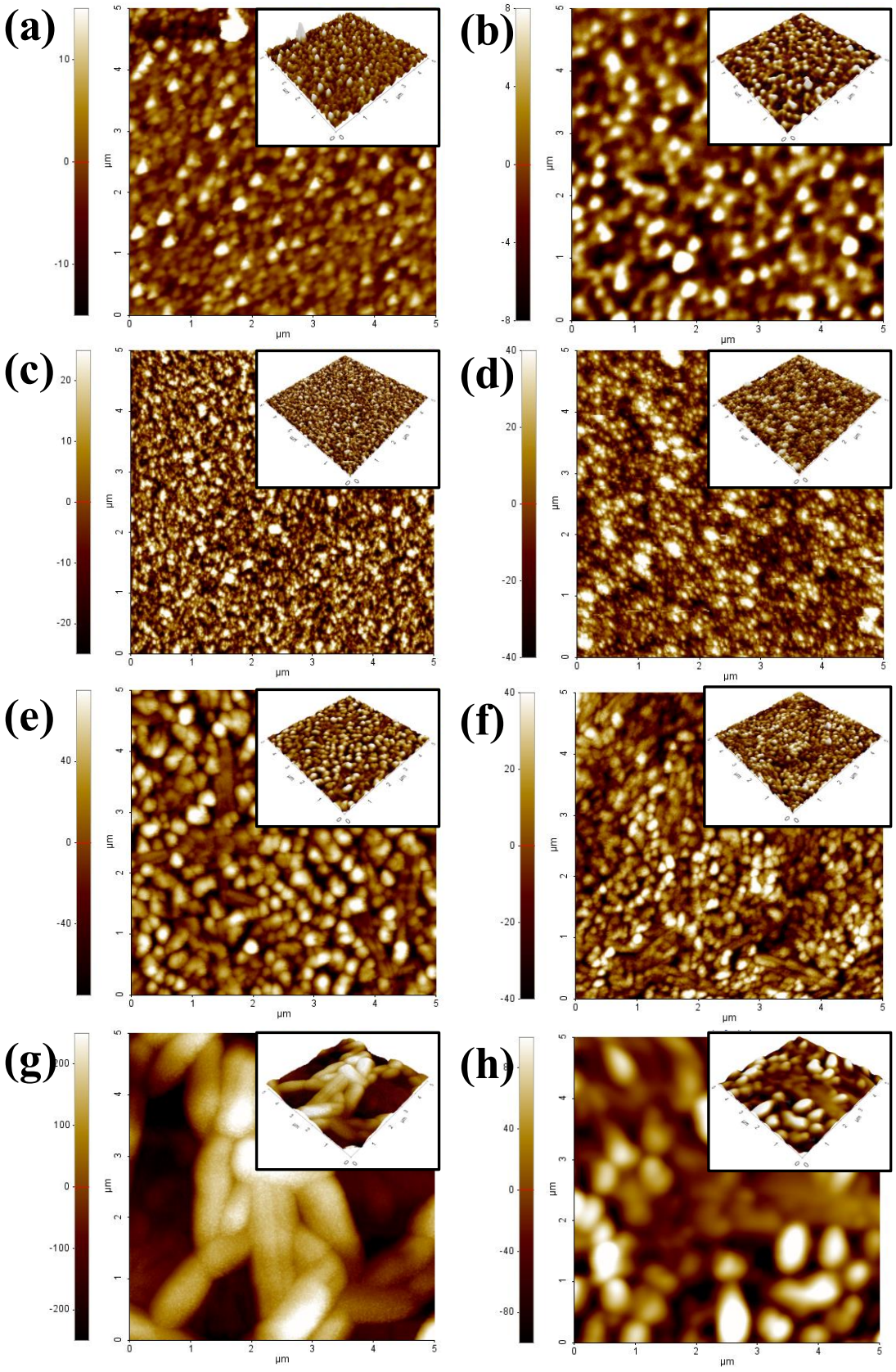

Figure 5. AFM images of the annealed samples under air and oxygen atmosphere respectively. (a) - (b) at 200 ℃, (c) – (d) at 300 ℃, (e) – (f) at 400 ℃, and (g) – (h) at 500 ℃ temperatures.

The oxygen content increased from 23.70 at.% to 43.27 at.% for samples heat-treated in air. At the same time, we found that it increased from 21.55 at.% to 34.87 at.% for samples heat-treated in oxygen.

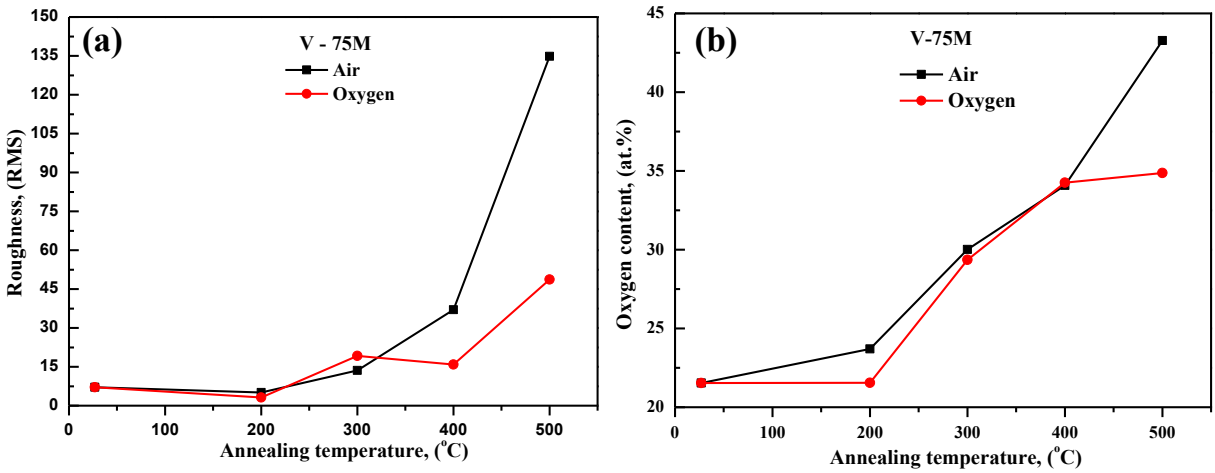

Figure 6. Comparisons of annealed samples at 200, 300, 400, and 500 ℃ temperatures: (a) AFM roughness, and (b) oxygen content, respectively.

Conclusion

In this study, vanadium oxide (VO_x) thin films were successfully synthesized using DC magnetron sputtering with a spark plasma sintered (SPS) vanadium target. The as-deposited amorphous VO_x films were subsequently annealed in air and oxygen atmospheres at temperatures ranging from 200 to 500 °C to investigate their crystallization behavior, surface morphology, and oxygen content.

X-ray diffraction (XRD) analysis revealed that annealing at 400 °C and above induced complete crystallization, forming a mixed-phase structure consisting of V_2O_5 and VO_2 in air, while oxygen annealing promoted a more pronounced VO_2 monoclinic phase, which is crucial for thermochromic applications. Atomic force microscopy (AFM) and SEM-EDX analyses demonstrated that surface roughness and oxygen content increased with annealing temperature. Oxygen-annealed films exhibited smoother surfaces at lower temperatures (200–300 °C) but followed a similar trend of increasing roughness at higher temperatures (400–500 °C). Notably, oxygen annealing resulted in lower overall roughness compared to air annealing, suggesting a more controlled oxidation process.

The oxygen content in the films increased linearly with temperature, reaching up to 43.27 at.% in air and 34.87 at.% in oxygen, indicating that the annealing atmosphere significantly influences film stoichiometry and morphology. These findings highlight the importance of optimizing annealing conditions to achieve desired structural and surface properties in VO_x thin films for optoelectronic and thermochromic applications. Future work could explore the correlation between annealing parameters and the thermochromic performance of VO_2-based thin films.

References:

[1] Morin F.J. “Oxides Which Show a Metal-to-Insulator Transition at the Neel Temperature.” *Physical Review Letters*, 3(1), 1959, pp. 34–36. DOI: 10.1103/PhysRevLett.3.34

[2] Liu K., Lee S., Yang S., Delaire O., & Wu J. “Recent Progresses on Physics and Applications of Vanadium Dioxide.” *Materials Today*, 21(8), 2018, pp. 875–896. DOI: 10.1016/j.mattod.2018.03.029

[3] Park J.H., Coy J.M., Kasirga T.S., Huang C., Fei Z., Hunter S., & Cobden D.H. “Measurement of a Solid-State Triple Point at the Metal–Insulator Transition in VO_2.” *Nature*, 500(7463), 2013, pp. 431–434. DOI: 10.1038/nature12425

[4] Li M., Magdassi S., Gao Y., & Long Y. "Hydrothermal Synthesis of VO_2 Polymorphs: Advantages, Challenges, and Prospects for the Application of Energy-Efficient Smart Windows." *Small*, 13(36), 2017, pp. 1701147. DOI: 10.1002/smll.201701147

[5] Cao X., Wang N., Law J.Y., Loo S.C.J., & Magdassi S. "Nanoporous Thermochromic VO_2 Films with Low Optical Activation Temperature for Smart Windows." *ACS Applied Materials & Interfaces*, 6(16), 2014, pp. 13710–13714. DOI: 10.1021/am503159f

[6] Chen S., Wang Z., Ren H., Chen Y., Yan W., Wang C., ... & Huang Y. "Gate-Voltage Control of VO_2 Phase Transition to Trigger the Metal–Insulator Transition via Electrostatic Doping." *Science Advances*, 5(9), 2019, p. eaav6811. DOI: 10.1126/sciadv.aav6811

[7] Rúa A., Cabrera R., Coy H., Merced E., & Sepúlveda N. "Mechanical Properties of VO_2 Thin Films for Microelectromechanical Systems Applications." *Journal of Applied Physics*, 117(18), 2015, p. 185301. DOI: 10.1063/1.4920966

[8] Burkhardt W., Christmann T., Franke S., Kriegseis W., Meister D., Meyer B.K., ... & Zhou J. "Tungsten and Fluorine Co-Doping of VO_2 Films." *Thin Solid Films*, 402(1-2), 2002, pp. 226–231. DOI: 10.1016/S0040-6090(01)01660-0

[9] Zhang Z., Gao Y., Chen Z., Du J., Cao C., Kang L., & Luo H. "Thermochromic VO_2 Thin Films: Solution-Based Processing, Improved Optical Properties, and Lowered Phase Transformation Temperature." *Langmuir*, 26(13), 2010, pp. 10738–10744. DOI: 10.1021/la100515k

[10] Koo H., Shin D., Bae S.H., & Ko K.E. "The Effect of Annealing Atmosphere on the Optical Properties of VO_2 Thin Films." *Journal of Applied Physics*, 116(7), 2014, p. 073515. DOI: 10.1063/1.4893366

[11] Bunyod Allabergenov, Amir Abidov, Soon-Wook Jeong and Sungjin Kim "Effect of Annealing Temperature on Electrochemical and Mechanical Properties of STS with Titanium Carbonitride Composites Synthesized by Spark Plasma Sintering." *Electrochemical Society Meeting Abstracts 226*, 49, 2014, p. 2268-2268. DOI: 10.1063/1.4893366

[12] Bunyod Allabergenov, Oybek Tursunkulov, Amir Abidov, Soon-Wook Jeong, and Sungjin Kim "Mechanical properties of stainless-steel composites with titanium carbonitride consolidated by spark plasma sintering." *Journal of Composite Materials*, Volume 50, Issue 12, 2015, pp. 1567-1572. DOI: 10.1177/0021998315574756

[13] Bunyod Allabergenov, Oybek Tursunkulov, Amir Abidov, Sang Youp Kim, Eun Young Lee, Li Li He, Tae Yong Kim, Soon Wook Jeong, Sung Jin Kim "Effect of TiH_2 Composition on Porous Stainless Steel and Titanium Hydride Composite Synthesized by Spark Plasma Sintering." *Journal of Advanced Materials Research*, 652, 2013, pp. 2293-2298. DOI: 10.4028/www.scientific.net/AMR.652-654.2293

[14] Bunyod Allabergenov, Sanghun Yun, Uchkun Kutliev, Byeongdae Choi "Highly Reduced Phase Transition Hysteresis of Vanadium Dioxide Thin Films in Multilayer Structure with Titanium Dioxide." *ACS Applied Electronic Materials,* Vol. 6, issue 3, 2024, pp. 1886-1893. DOI: 10.1021/acsaelm.3c01784

[15] Bunyod Allabergenov, Sanghun Yun, Byeongdae Choi "Metal–Insulator Transition Detection of Vanadium Dioxide Thin Films by Visible Light Reflection." *ACS Applied Materials & Interfaces,* Vol. 14, issue 42, 2022, pp. 47841-47852. DOI: 10.1021/acsami.2c11366

[16] Bunyod Allabergenov, Sanghun Yun, Hui-Sup Cho, Hong-Kun Lyu, Byeongdae Choi "Control of polymorphic properties of multivalent vanadium oxide thin films." *ACS Applied Electronic Materials,* Vol. 3, issue 3, 2021, pp. 1142-1150. DOI: 10.1021/acsaelm.0c01010

UDC: 62, 004.04

DESIGN AND IMPLEMENTATION OF A MODEL AND ALGORITHM FOR PART-OF-SPEECH TAGGING IN UZBEK TEXTS USING THE CONDITIONAL RANDOM FIELDS (CRFs) APPROACH

Sharipov Maksud
Associate Professor, Department of Computer Science, Urgench State University named after Abu Rayhan Biruni
maqsbek72@gmail.com

Annotatsiya. Ushbu maqolada shartli tasodifiy maydonlar (CRF) yondashuviga asoslangan o‘zbek tili uchun nutqning bir qismini belgilash tizimi taqdim etilgan. Qo‘lda teglangan matn korpusi va tilga xos morfologik va kontekstual xususiyatlar to‘plamidan foydalanib, model 5 marta o‘zaro tekshirish yordamida o‘qitildi va baholandi. Tajribalar o‘rtacha F1 balli taxminan 89% bo‘lgan istiqbolli natijalarni ko‘rsatdi, bu esa o‘zbek tilining morfologik murakkabligini hal qilishda CRFga asoslangan usulning samaradorligini tasdiqlaydi. Bu ish o‘zbek tili kabi kam resursli tillar uchun tabiiy tillarni qayta ishlash (NLP) vositalarini ishlab chiqishga yordam beradi.

Kalit so‘zlar: *POS teglash, tabiiy tilni qayta ishlash (NLP), shartli tasodifiy maydonlar (CRF), gap qismlari, ehtimollik modeli, o‘zbek tili.*

Аннотация. В данной статье представлена система разметки частей речи для узбекского языка, основанная на подходе условных случайных полей (CRF). Используя корпус текста, размеченный вручную, и набор морфологических и контекстуальных признаков, специфичных для данного языка, модель была обучена и оценена с помощью 5-кратной перекрёстной проверки. Эксперименты показали многообещающие результаты со средней оценкой F1 около 89%, что подтверждает эффективность метода, основанного на CRF, для обработки морфологической сложности узбекского языка. Данная работа вносит вклад в разработку инструментов обработки естественного языка (NLP) для языков с низким ресурсом, таких как узбекский.

Ключевые слова. *POS-разметка, обработка естественного языка (NLP), условные случайные поля (CRF), части речи, вероятностная модель, узбекский язык.*

Abstract. This paper presents a part-of-speech tagging system for the Uzbek language based on the Conditional Random Fields (CRF) approach. Using a manually annotated corpus and a set of language-specific morphological and contextual features, the model was trained and evaluated through 5-fold cross-validation. The experiments showed promising results with an average F1-score of approximately 89%, confirming the effectiveness of the CRF-based method for handling the morphological complexity of Uzbek. This work contributes to the development of NLP tools for low-resource languages like Uzbek.

Keywords. *POS tagging, Natural Language Processing (NLP), Conditional Random Fields (CRF), parts of speech, probabilistic model, Uzbek language.*

Introduction

Uzbek is a morphologically rich, agglutinative language that belongs to the Turkic language family. Despite its linguistic complexity and cultural significance, Uzbek remains a low-resource language in the field of Natural Language Processing (NLP). This status stems from the limited availability of large, annotated corpora, linguistic tools, and open-source NLP resources. At the same time, the rich morphological structure of Uzbek - characterized by extensive use of affixation and flexible word formation - poses unique challenges and opportunities for computational processing.

Part-of-speech (POS) tagging, which involves assigning grammatical categories to each word in a sentence (such as noun, verb, adjective, etc.), is a foundational task in NLP. Accurate POS tagging is essential for many downstream applications, including syntactic parsing, machine translation, information extraction, and sentiment analysis. However, standard POS tagging techniques developed for high-resource languages like English often fail to generalize well to morphologically complex and low-resource languages like Uzbek.

Given the agglutinative nature of Uzbek, where a single word can contain a sequence of morphemes expressing tense, aspect, person, mood, and more, conventional tagging models based on Hidden Markov Models (HMMs) or simple rule-based approaches may struggle to capture the long-range dependencies and contextual cues effectively. In contrast, Conditional Random Fields (CRFs) — a type of discriminative probabilistic model — offer a powerful alternative for structured prediction tasks like POS tagging. CRFs consider the entire sequence of words and their features when assigning tags, making them particularly well-suited for handling the contextual and morphological richness of the Uzbek language.

Unlike generative models that rely on strong independence assumptions, CRFs model the conditional probability of label sequences given the observation sequences, which allows for the incorporation of a wide range of overlapping and non-independent features. This makes CRFs especially effective for languages with complex morphology and flexible word order — both of which are defining characteristics of Uzbek. Moreover, CRFs can be enhanced through the integration of linguistic rules, feature engineering, and morphological analysis to further improve tagging accuracy in low-resource settings.

In this study, we propose a POS tagging model for the Uzbek language based on the CRF framework. Using a morphologically annotated corpus, we design an algorithm that leverages both data-driven statistical modeling and rule-based refinement to improve tagging accuracy. Our goal is to contribute to the development of NLP tools for the Uzbek language by providing a robust and linguistically informed tagging system that can serve as a building block for further computational linguistics research and practical applications.

Literature Review

The first rule-based tagging program is called TAGGIT, and it was developed based on the Brown Corpus. The tagset used by this system consisted of approximately 77

tags, derived from the Brown tagset [5]. Its main idea is to assign a set of possible tags to each word and then select the most appropriate one based on the context. The mechanism for assigning initial tags to words relies on a dictionary, a list of suffixes, and additional rules for identifying capitalized words (such as proper nouns or sentence-initial words). This approach achieved an accuracy of around 70%. ENGTWOL, a rule-based tagger, was developed using a two-stage architecture. This system includes a tagset of 139 tags and a lexicon of 56,000 English word roots. The lexicon contains separate entries for words that belong to multiple parts of speech, but does not include inflected or derived word forms. In the second stage, more than 1,000 hand-crafted rules are applied to disambiguate words that have multiple possible tags [6].

The two-stage architecture described above is considered the most common approach. However, other methods also exist — for example, LABELGRAM [7], a rule-based tagger for French, assigns POS tags without using a lexicon, relying instead on syntax, word endings (suffixes), and hand-crafted rules. This approach has also been successfully applied to English and Spanish languages [8]. Various machine learning algorithms have been applied to solve the problem of automatic part-of-speech (POS) tagging. In practice, the most widely used POS tagger models are based on modifications of methods such as Hidden Markov Models (HMM), Maximum Entropy, Conditional Random Fields (CRF), and Support Vector Machines (SVM). These approaches have been proven to provide high accuracy through scientific research. In addition, hybrid taggers combine the most effective aspects of probabilistic and rule-based methods. These approaches are also known as transformation-based taggers. One of the relatively successful systems developed on the basis of the transformation approach is the Brill tagger [9]. This model, like rule-based taggers, assigns tags to words based on a set of disambiguation rules, and similar to probabilistic approaches, it automatically learns these rules from a pre-tagged corpus. The work [14] presents the development of a Maximum Entropy (MaxEnt) model for part-of-speech tagging of Uzbek texts based on a morphologically annotated corpus. An algorithm and software were implemented using this model and predefined rules for automated POS tagging.

Research Methodology

This study adopts a supervised sequence labeling approach to develop a robust part-of-speech (POS) tagging system for Uzbek texts. Given the agglutinative and morphologically complex nature of the Uzbek language, traditional tagging techniques often fail to generalize well across varied syntactic structures. To address this challenge, we propose a model based on CRF - a discriminative probabilistic framework capable of incorporating rich, overlapping features and long-range contextual dependencies.

The methodology involves several key components:

1. Corpus Preparation — A manually annotated dataset of Uzbek texts is created to serve as training and evaluation data.
2. Feature Engineering — Language-specific morphological, lexical, and contextual features are extracted to represent each token.

3. CRF Model Design — A linear-chain CRF model is trained to learn the sequence-level dependencies between tokens and their corresponding POS tags.
4. Algorithm Development — A full tagging pipeline is implemented, including tokenization, feature extraction, model training, inference, and post-processing.
5. System Deployment — A web-based tool is built to allow real-time tagging of Uzbek sentences using the trained model.

This methodological pipeline ensures that the POS tagging system is not only linguistically informed but also computationally optimized for the challenges inherent in low-resource languages like Uzbek. The sections below describe in detail the mathematical formulation of the CRF model, dataset construction, feature extraction strategies, and the implementation of the end-to-end tagging system.

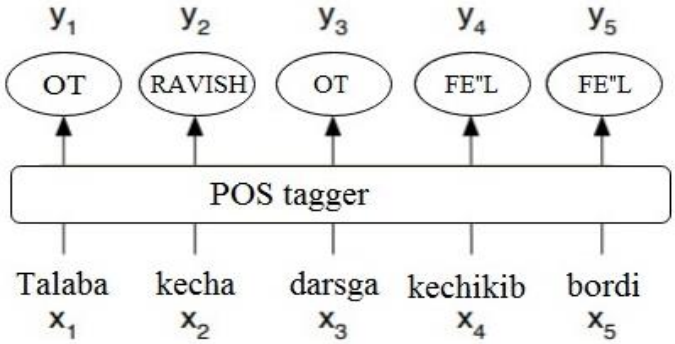

Figure 1. This diagram shows how POS tagger works.

Conditional Random Fields. CRFs are conditional probability distributions based on exponential models, proposed by Lafferty (2001). CRF models relax certain strict assumptions about the distribution of input and output sequences, making them more flexible compared to traditional models. CRFs can incorporate any number of feature functions, which allows them to analyze the entire input sequence during the prediction process [3].

P(t/w) — represents the probability of a tag sequence t given a word sequence w, and it is calculated as follows:

$$P(t \mid w) = \frac{1}{Z(w)} exp\left(\sum_{j=1}^{n}\sum_{i=1}^{k} \lambda_i f_i(t_{j-1}, t_j, w_{1:n}, j)\right) \quad (1)$$

Here, *Z(w)* is the normalization factor used to convert the probability distribution into a proper form, and it is defined as follows:

$$Z = \sum_{t \in T} \exp\left(\sum_{j=1}^{n}\sum_{i=1}^{k} \lambda_i f_i(t_{j-1}, t_j, w_{1:n}, j)\right) \quad (2)$$

Here: T is the set of all possible tag sequences; *j* ranges from *1* to *n*, representing the word positions in the sentence; i ranges from 1 to k, representing the feature functions. λ_i is the weight value for the f_i feature function, which is calculated during the training of the CRF model. The fi functions are the fundamental components of the CRF model. Their general form is as follows:

$$f_i(t_{j-1}, t_j, w_{1:n}, j) \quad (3)$$

This function takes values depending on the adjacent tags t_{j-1} and t_j, the entire input word sequence $w_{1:n}$, and the current word's features. For example, the function might be as follows:

$$f_1(t_{j-1}, t_j, w_{1:n}, j) = \begin{cases} 1, if\ \ suffix_i \in word_j\ \wedge t_j = teg_i \\ 0,\ \ else \end{cases} \quad (4)$$

By applying feature functions, POS taggers built based on the Conditional Random Fields model are considered more accurate compared to the HMM model.

Dataset. To train and evaluate the CRF model, a corpus of Uzbek-language texts was compiled and manually annotated with POS tags. The dataset includes texts from various domains, such as news articles, literature, and social media, in order to ensure linguistic diversity and coverage.

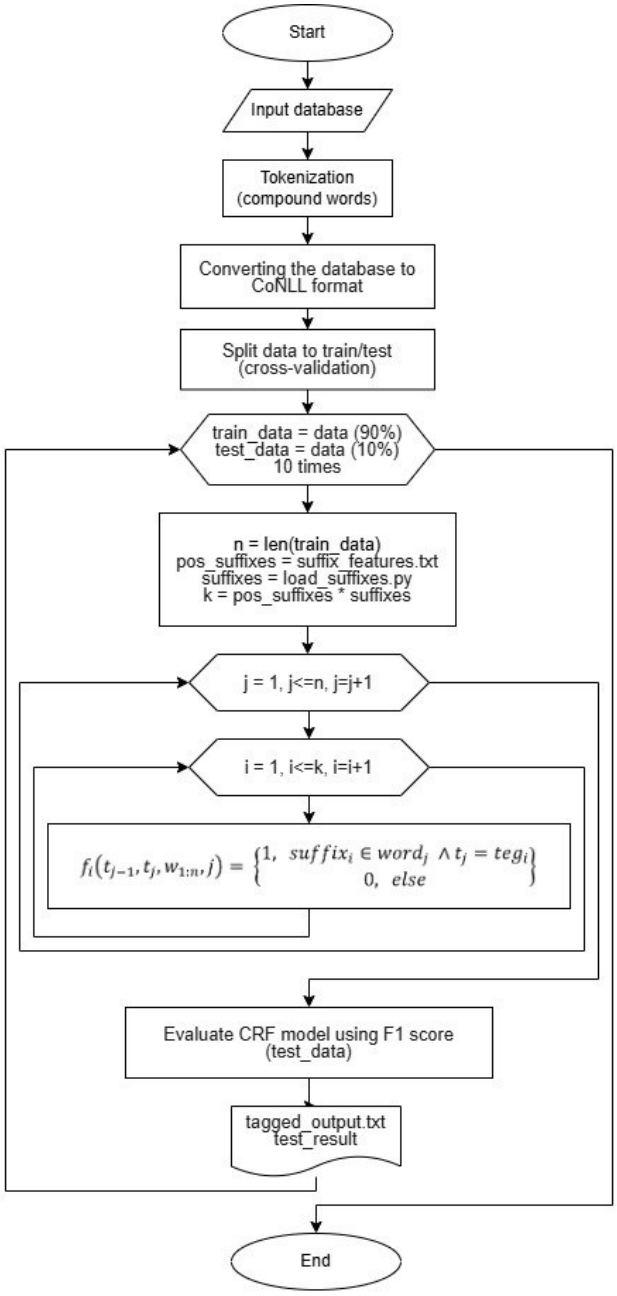

Figure 2. The algorithm for tagging Uzbek words based on CRF.

The preprocessing phase involved several steps:

- Normalization: Removal of inconsistent spellings and typographic symbols.
- Tokenization: Sentence segmentation and word-level tokenization based on Uzbek orthographic and syntactic rules.
- Annotation: Each token was labeled with its corresponding POS tag from a predefined tagset, designed specifically for Uzbek morphosyntax.

The annotation process was supervised by linguistic experts to ensure consistency and correctness. The final dataset was split into training, validation, and test sets, enabling model tuning and unbiased evaluation.

Model. The CRF-based POS tagging system follows a multi-stage pipeline that transforms raw Uzbek text into annotated output. The architecture includes the following key components:

Text Preprocessing. Raw input text is tokenized using a language-specific tokenizer that accounts for clitics, punctuation, and compound affixes typical of Uzbek morphology.

Feature Extraction. A set of linguistic and contextual features is extracted from each token. These include: current word form; prefixes and suffixes; word shape (e.g., capitalized, numeric); surrounding words (context window of ±2 tokens); part-of-speech hints from surrounding tokens.

These features are encoded into a format suitable for CRF training.

CRF Training. The CRF model is trained using supervised learning on the annotated dataset. The training algorithm optimizes the log-likelihood of the correct tag sequences, learning weights λ_k for each feature function.

Inference and Tagging. For unseen text, the trained model predicts the most probable sequence of POS tags using the Viterbi algorithm, which finds the globally optimal path in the CRF's label space.

Post-processing and Validation. The output is post-processed to ensure compliance with Uzbek grammatical constraints. Evaluation metrics such as accuracy, precision, recall, and F1-score are computed on the test set.

This modular architecture enables not only accurate tagging but also extensibility - allowing integration with syntactic parsers, morphological analyzers, or neural components for downstream tasks.

Analysis and Results

To rigorously evaluate the effectiveness of the proposed CRF-based part-of-speech (POS) tagging system for Uzbek, we conducted a 5-fold cross-validation on the manually annotated corpus. This approach ensures that the model's performance is tested across various splits of the dataset, minimizing bias and variance in the results.

- Data Split: 80% training, 20% testing, rotated over 5 folds
- Algorithm: Conditional Random Fields (CRF)
- Evaluation Metrics: Precision, Recall, F1-score (per tag), and Overall Accuracy

Across the five folds, the model consistently demonstrated high accuracy and balanced performance across multiple POS categories. The average weighted F1-score achieved over all folds is 88.84% (≈89%), indicating reliable and robust tagging quality.

Table 1. Evaluation Results of the CRF-based POS Tagger (5-Fold Cross-Validation)

	F1 score				
	Fold 1	Fold 2	Fold 3	Fold 4	Fold 5
ADJ	0.820	0.823	0.842	0.841	0.819
ADP	0.851	0.842	0.835	0.820	0.835
ADV	0.688	0.683	0.692	0.678	0.665
AUX	0.677	0.621	0.590	0.613	0.653
CONJ	0.942	0.953	0.956	0.951	0.959
MOD	0.747	0.748	0.726	0.716	0.726
NOUN	0.894	0.892	0.903	0.901	0.902
NUM	0.837	0.860	0.885	0.880	0.847
PART	0.732	0.851	0.833	0.827	0.793
PRON	0.898	0.890	0.895	0.901	0.898
PROPN	0.692	0.733	0.743	0.732	0.763
PUNCT	0.989	0.992	0.992	0.993	0.994
VERB	0.907	0.887	0.898	0.907	0.899
Accuracy	0.894	0.884	0.894	0.894	0.891

❖ NOUN and PUNCT consistently showed the highest precision and recall across all folds, reflecting their frequency and stability in Uzbek texts.

- ADP (adpositions) and CONJ (conjunctions) also achieved high performance, thanks to their relatively fixed syntactic roles.
- Lower performance was observed in categories such as ADV (adverbs), AUX (auxiliary verbs), and MOD (modals), likely due to their morphological variability and contextual ambiguity.
- Post-processing rules improved the tagging of rare categories like PART (particles) and PROPN (proper nouns), but some challenges remained, especially in handling homonymous forms.

Compared to earlier experiments with a Hidden Markov Model (HMM), the CRF model showed clear superiority, particularly in handling sequential dependencies and utilizing complex feature sets. CRF-based tagging (accuracy 0.888) performed better than maximum entropy-based tagging (accuracy 0.858) [14].

Conclusion

This study presented the design, implementation, and evaluation of a CRF-based part-of-speech tagging system for the Uzbek language — a resource-scarce and morphologically complex language. Leveraging a supervised learning approach combined with rich linguistic features, the system demonstrated high tagging accuracy and robustness across diverse text genres.

The 5-fold cross-validation results, with an average F1-score of 0.8884, confirm the effectiveness of CRF models in capturing contextual and morphological nuances of Uzbek. The system consistently outperformed traditional models such as HMM, particularly in managing agglutinative word forms and ambiguous syntactic structures.

The developed POS tagger lays a foundation for further natural language processing tasks in Uzbek, such as syntactic parsing, machine translation, and information extraction.

Future Directions:

- Expanding the annotated corpus to cover more dialects and domains.
- Integrating morphological analyzers for better feature representation.
- Experimenting with neural architectures (e.g., BiLSTM-CRF, Transformer models).
- Deploying the system as an open-access tool for the research community.

References:

[1] Ekbal A., Haque R., & Bandyopadhyay S. “Bengali part of speech tagging using conditional random field.” *In Proceedings of seventh international symposium on natural language processing* (SNLP2007), 2007, pp. 131–136.

[2] Brants T. “TnT: A statistical part-of-speech tagger.” *Sixth Applied Natural Language Processing Conference (Association for Computational Linguistics, Seattle, Washington, USA)*, 2000, pp. 224–231. DOI: 10.3115/974147.974178.

[3] Lafferty J., McCallum A., and Pereira F. “Conditional random fields: probabilistic models for segmenting and labeling sequence data.” *In International Conference on Machine Learning*, 2001.

[4] Daniel Jurafsky & James H. Martin “Speech and Language Processing.” Copyright © 2024. All rights reserved. Draft of January 12, 2025.

[5] Greene B. and Rubin G. “Automatic grammatical tagging of English,” Providence, RI: *Department of Linguistics*, Brown University, 1971.

[6] Voutilainen A. “A syntax-based part-of-speech analyser,” in Proceedings of the seventh conference on European chapter of the Association for Computational Linguistic*s*, *Morgan Kaufmann Publishers Inc.,* San Francisco, CA, USA, 1995, pp. 157–164.
[7] Cardey S. and Greenfield P. “Disambiguating and tagging using systemic grammar,” in *Proceedings of the 8th International Symposium on Social Communication*, 2003, pp. 559–564.
[8] Birocheau “Etiquetage morphologique et contribution la dsambigusation automatique des ambiguts morphologiques sur un lexique anglais,” *PhD thesis, Thse de doctorat sous la dir. de Sylviane Cardey, Centre Tesnire, Universit de Franche-Comt*, Besanon, 2003.
[9] Eric Brill “A Simple Rule-Based Part of Speech Tagger.” In *Speech and Natural Language: Proceedings of a Workshop Held at Harriman,* New York, February 23-26, 1992.
[10] Madatov K., Bekchanov S., and Vicic J., “Dataset of Karakalpak language stop words,” *Data Brief*, vol. 48, 2023. DOI: 10.1016/j.dib.2023.109111.
[11] Sharipov M., Mattiev J., Sobirov J., and Baltayev R., “Creating a Morphological and Syntactic Tagged Corpus for the Uzbek Language,” *CEUR Workshop Proceedings*, vol. 3315, 2022, pp. 93–98.
[12] Mengliev D., Akhmedov E., Barakhnin V., Hakimov Z., and Alloyorov O., “Utilizing Lexicographic Resources for Sentiment Classification in Uzbek Language,” Jan. 2023, pp. 1720–1724. doi: 10.1109/APEIE59731.2023.10347765.
[13] Madatov K., Bekchanov S., and Vicic J., “Dataset of stopwords extracted from Uzbek texts”, *Data in Brief*, vol. 43, 2022.
[14] Sharipov M. “Development of a maximum entropy-based model and algorithm for part-of-speech tagging in uzbek texts,” *Development of science*, vol. 4, Jul. 2025, pp. 85–91.

UDC: 62, 004.04, 519, 766, 81’35

STATISTICAL WORD IMPORTANCE MODELING FOR UZBEK TEXT SUMMARIZATION: A TF-IDF-BASED APPROACH WITH IMPROVED SENTENCE SELECTION

Khabibulla Madatov
Head of the Department of Computer Science, Urgench State University named after Abu Rayhan Biruni
habi1972@mail.ru

Annotatsiya. Tabiiy tilni qayta ishlash sohasida markaziy faoliyat bo‘lib, katta hajmdagi matndan asosiy ma’lumotlarni minimal kalit ma’nolarni saqlagan holda chiqarib olish imkonini beradi. Ammo o‘zbek tili uchun xulosa qilish hali zaif soha hisoblanadi, chunki o‘zbek — qo‘shimcha qo‘shuvchi (agglutinativ) til bo‘lib, sifatli belgilanmagan (annotatsiyalangan) korpuslar mavjud emas. An’anaviy yondashuv bo‘lgan ajratma (extractive) xulosalarda — Term Frequency-Inverse Document Frequency (TF-IDF) usuli o‘zbek tilining lingvistik murakkabliklarini to‘liq qamrab ololmaydi, natijada xulosalar zaif uyg‘unlik va moslikka ega bo‘ladi. Ushbu ishda biz TF-IDF asosida, so‘zlarning muhimlik ehtimolini baholash, dispersiya (o‘zgaruvchanlik) va assimmetriya (burilish) aniqlashga asoslangan yangi yondashuvni taklif qilamiz. Bu yondashuv matnning asosiy qismlarini dinamik tarzda tanlash imkonini beradi. An’anaviy

faqat chastotaga asoslangan usullarga nisbatan, bizning yondashuvimiz so‘zlarning matematik kutilmasini hisoblaydi, ularning taqsimot dispersiyasini o‘lchaydi hamda simmetriyaga asoslangan tekshiruvlarni qo‘llaydi — matndagi kalit ma’lumotlarning boshida, o‘rtasida yoki oxirida joylashganligini aniqlash uchun. Eksperimental tadqiqotlar taklif etilgan yondashuv TF-IDFning standart modellari bilan solishtirganda matn kontekstiga yanada mos va mazmunan aniq xulosalar berishini tasdiqladi. Ushbu tadqiqot o‘zbek tilidagi resurslari kam bo‘lgan tabiiy tilni qayta ishlashni rivojlantirishga va yuqori murakkab infleksiya tiliga mos keladigan kengaytiriladigan statistik yondashuvga hissa qo‘shadi.

Kalit so‘zlar: *O‘zbek tilida matn xulosa qilish, TF-IDF, statistik modellashtirish, so‘z muhimligi, ehtimollik baholash, dispersiya tahlili, tabiiy tilni qayta ishlash (NLP).*

Аннотация. Резюмирование является центральной задачей в области обработки естественного языка (NLP), позволяющей извлекать существенную информацию из большого объёма текста с минимальной потерей ключевого смысла. Однако для узбекского языка резюмирование остаётся слабой областью, поскольку он является агглютинативным языком, для которого отсутствуют качественные аннотированные корпуса. Традиционный подход к экстрактивному резюмированию, основанный на частоте термина и обратной частоте документа (TF-IDF), неэффективен в учёте лингвистических сложностей узбекского языка, что приводит к слабой связности и релевантности итогового резюме. В настоящей работе предлагается новый подход к резюмированию, основанный на TF-IDF с оценкой вероятности важности слов, вычислением дисперсии и выявлением асимметрии, что позволяет динамически определять и выбирать ключевые части текста. В отличие от методов, традиционно основанных лишь на частоте, наш подход оценивает математическое ожидание важности слов, измеряет дисперсию распределения слов, а также применяет симметричный анализ для определения того, находится ли ключевая информация в начале, середине или конце текста. Экспериментальные исследования подтвердили, что предложенный подход обеспечивает более контекстно обоснованные и релевантные резюме по сравнению с базовыми моделями TF-IDF. Данное исследование вносит вклад в развитие NLP для языков с ограниченными ресурсами, таких как узбекский, а также предлагает масштабируемый статистический подход, применимый для высокоизменяемых (инфлексных) языков.

Ключевые слова: *Автоматическое суммирование текста на узбекском языке, TF-IDF, статистическое моделирование, важность слов, оценка вероятности, анализ дисперсии, обработка естественного языка (NLP).*

Abstract. Summarization is a central activity in the field of Natural Language Processing that makes it possible to extract essential information from a massive amount of text with minimal preservation of key meaning. But in the case of the Uzbek language, summarization is a weak field because it is an agglutinative language with no high-quality annotated corpora. The traditional approach

towards extractive summarization, i.e., Term Frequency-Inverse Document Frequency (TF-IDF), is not effective in capturing linguistic complexities in Uzbek, leading to weak coherence as well as relevance in a summary. Here, we propose a new approach towards summarization that is based on TF-IDF with word importance probability estimation, calculation of variance, as well as detection of skewness in order to dynamically decide and choose the key portions of text. Compared with methods that are traditionally based on frequency alone, our approach estimates mathematical expectation of words' importance, measures words' distribution variance, as well as employs symmetry-based examination in order to determine whether key information is at the starting, in between, or towards ending portion of the text. Experimental experiments have confirmed that the proposed approach is more contextually sound and pertinent in its summaries as compared with baseline models of TF-IDF. The research is a contribution towards enhancing low-resource NLP in Uzbek as well as towards a scalable statistical approach that can be adopted in highly inflected languages.

Keywords: *Uzbek text summarization, TF-IDF, statistical modelling, word importance, probability estimation, variance analysis, NLP.*

Introduction

Text summarization is a fundamental task in Natural Language Processing (NLP) that enables the extraction of important information from enormous volumes of text without sacrificing its core meaning. It is a primary task in numerous applications such as news summarization, document retrieval, legal case analysis, and personalized content recommendation. With the ever-growing digitalization of textual information, automatic summarization has become a critical tool for improving information accessibility and retrieval effectiveness [1]. While important progress has been made in text summarization for widely spoken languages such as English, Chinese, and French [2, 3], the Uzbek language remains underrepresented in NLP studies [4].

The Uzbek language, spoken by over 40 million people worldwide, is the second-largest language of the Turkic language family in terms of the number of speakers, after Turkish language1. One of the most common characteristics of the Turkic languages family is that they are all agglutinative languages, i.e., grammatical functions are mostly expressed by affixes and suffixes, not by word order. As a result, a single root word can generate hundreds of forms according to case marking, tense, plurality, and other grammatical features. This renders NLP tasks such as tokenization, stemming, lemmatization, and information retrieval very difficult [5]. Script variation is another critical issue in Uzbek text processing. Uzbek has been written in three scripts historically – Arabic, Cyrillic and current official Latin scripts. However, Cyrillic is still in an unofficial use widely. This script form is a challenge for text normalization and corpus standardization, and it is difficult to construct consistent NLP models [6].

Despite the challenges Uzbek proposes, there has been a recent sharp growth in the research outputs for Uzbek NLP resources and models, from fundamental knowledge

[1] List of Turkic languages and the number of speakers worldwide: https://en.wikipedia.org/wiki/List_of_Turkic_languages

base like stopwords [7], morphological analyzers [8], all the way to the machine learning and deep learning datasets with trained models, namely neural machine translation [9], transformer-based monolingual language models, etc. [10].

When it comes to the information extraction tasks, such as text summarization, traditional approaches were mostly use the frequency-based methods straight away, which, among those methods the one that stands out is the Term Frequency-Inverse Document Frequency (TF-IDF) [11] due to their interpretability, ease, and effectiveness. TF-IDF method relies on predicting ranking scores to the words and tokens based on their statistical relevance in the document they are contained in. In the end, TF-IDF method selects words or sentences with the highest rankings among others, which will form the summarized output. This approach has a number of limitations:

- Contextual meaning is lost – TF-IDF does not capture semantic relationships between words; rather, it treats them as individual tokens, and hence coherence in generated summaries is lost.
- Position is Not Considered – Classical methods do not consider the relative importance of sentence positions in a document, and important information is put either in a document's beginning or end.
- Uniform Weights Problems – TF-IDF assigns term weights based on term frequency without respect to word distribution variation and thus overemphasizes high-frequency words rather than actually important content.

Recommended Strategy. To meet such constraints, this paper proposes a new TF-IDF-based summary method that integrates:

1. Word Importance Probability Estimation – We do not use term frequency alone to estimate a word's importance probability for enhancing sentence selection.
2. Variance Analysis of Word Distributions - We enhance sentence ranking and informative segment selection using word importance variance.
3. Skewness Detection - We analyze the asymmetry of the distribution for important words to determine whether important information is skewed towards the beginning, middle, or end of the document.

Using statistical word importance modeling, sentence selection is dynamically optimized in our method to deliver more coherent and contextually relevant summaries, particularly for low-resource and agglutinative languages such as Uzbek.

The principal contributions in this paper are as follows: We present a new TF-IDF-based summarization method with probabilistic word importance estimation, variance analysis, and skewness detection. We apply the model to Uzbek text and compare against standard extractive summary methods such as TF-IDF-based summary. We leave open to future comparisons with deep learning-based models such as UzBERT, BERTbek, and other large language models such as GPT. We present a statistical framework for building NLP for a specific language that can be extended to other agglutinative and low-resource languages.

Literature Review

As the text summarization is considered to be both interesting and important task of NLP, there have been multiple approaches to accomplish this task, from rule-based

models to statistical, machine learning, and all the way to the current trending dep learning models.

One of the earliest successful implementations of the text summarization task was the TF-IDF approach, which is extensively utilized in extractive summarization for its reliability and simplicity in extracting important terms in a document [12]. The experiments have been conducted in Uzbek based on a hand-crafted “School corpus” for measuring a TF-IDF-based summarization system. The experiments confirmed this method as efficient in extracting Uzbek text summaries and have potential for application in information retrieval and NLP [13].

Similarly, another paper from similar authors presented a method for Uzbek text summarization based on TF-IDF for creating a distinct word dictionary and sentence extracting techniques. The method discusses the application of TF-IDF in handling agglutinative languages like Uzbek [14].

Aside from extractive methods, abstractive summarization attempts to yield short and accurate summaries based on interpreting and paraphrasing main points in the source content. Baykara introduced innovative large-scale benchmarks for Hungarian and Turkish, a duo of agglutinative languages, and experimented with various abstractive summarization models. The need for generating language-dependent resources for improved summarization quality is highlighted in this paper [15].

Deep Learning-Based Summarization Models With the advent of deep learning came contextual embedding-based models like BERT [16], which are able to produce quality summaries. Despite achieving state-of-the-art performance in several languages, no application in Uzbek exists yet since no large-scale annotated Uzbek corpus is available for training them. Uzbek-specific models like UzBERT [17] and BERTbek [18] are being trained in a bid to bridge this gap and provide sustainable tools for Uzbek NLP tasks.

Low-resource agglutinative languages are complex and represent important hindrances for procedures in NLP such as summarization. Meyer and Buys [19] have experimented with data-to-text generation for another agglutinative and low-resource language, isiXhosa, and have proven the need for preprocessing techniques specifically tailored for better performance in NLP. The research highlights how agglutinative languages require morphologically informed information extraction techniques and is in line with our research for bettering TF-IDF-based summarization based on modeling for word relevance. Similarly, Grefenstette [20] experimented with highly inflection-based techniques for information extraction and supports how selection based on frequency is pivotal in identifying meaningful words, a method highly connected to our research based on variability analysis and probability-based TF-IDF.

More recent works compared statistical summarization and rule-based techniques to transformer-based neural models. Automatic summarization in [21] utilized spaCy and NLTK, emphasizing strengths in blending traditional NLP pipelines and statistical feature-based techniques in low-resource settings. Despite libraries like them providing efficient sentence selection, they are not flexible towards morphological structure in a target language and accommodate our necessity for statistical improvement in TF-IDF for Uzbek. In addition, Zuckermann [22] introduced a computational and language

reclamation and revival theory based on a linguistic theory, which justifies context-sensitive resource generation and context-dependent NLP policies.

Research Methodology

The article addresses the issue of improving Uzbek text summarization based on the TF-IDF method. This problem is divided into two parts:

1. Identifying the important part of the given Uzbek text using TF-IDF.
2. Summarizing the identified important part of the text.

The methodology section of the article outlines these topics.

Identifying the Important Part of Uzbek Texts. Let a text be given. We denote it by A. The process of extracting the important part of the text is carried out in the following sequence:

1. Tokenization: The text is segmented into words, i.e., tokens:
$Token(A) \rightarrow \{a1, a2, \dots, an\}$, where n is the total number of tokens in the text.
2. The resulting tokens are recorded in the form $\{a1, a2, \dots, an\}$. The tokens are then converted into unique words (Words formed by taking the first occurrence of repeating tokens and retaining the non-repeating tokens themselves, relative to the text, are referred to as unique words):

$\{a1, a2, \dots, an\} \rightarrow \{u1, u2, \dots, um\}$, *where* m *is the number of unique words in the text.*

3. Each unique word is assigned its corresponding TF-IDF value:
$$\{u1, u2, \dots, um\} \rightarrow \{TFIDF(u1), TFIDF(u2), \dots, TFIDF(um)\}$$
4. The TF-IDF values are then converted into their respective importance probabilities:
$$\{TFIDF(u1), TFIDF(u2), \dots, TFIDF(um)\} \rightarrow \{p1, p2, \dots, pm\},$$
$$p_i = \frac{TFIDF(u_i)}{\sum_{i=1}^{m} TFIDF(u_i)};\ i = 1, \dots, m$$
5. The unique words are numbered according to their position in the text. Thus, for each i, there exists a corresponding probability p_i. The mathematical expectation (mean) is calculated using the formula:
$$E = \sum_{i=1}^{m} i * p_i$$

where m is the total number of unique words, i is the index of the unique word, and p_i is the importance probability of each word.

6. To calculate the standard deviation σ, the dispersion is computed using the formula:
$$D = \sum_{i=1}^{m} (i - E)^2 * p_i$$
Using the dispersion, the standard deviation of unique words is determined:
$$\sigma = \sqrt{D}$$
7. The E_k k-th central moment is calculated using the following formula:
$$E_k = \sum_{i=1}^{m} p_i * i^k$$

From this, the third-order central moment μ_3- is computed:
$$\mu_3 = E_3 - 3 * E_1 * E_2 + 2 * E_1^3$$

9. Using the calculated central moment, the theoretical distribution asymmetry is determined:

$$A_s = \frac{\mu_3}{\sigma^3}$$

The part of the text with fewer stop words (A stop word is a common word that is typically filtered out from text data during natural language processing (NLP) tasks. These words are considered to carry little meaningful information on their own. In this context, they are assumed to have TF-IDF values closer to zero compared to other words) is defined as the important part of the text. The following statement is then applied:

The Statement:

If $|A_s| < 0{,}5$ (where the distribution density is close to a normal distribution), the important part of the text is determined according to the asymmetry value:

If $A_s < 0$, the important part is located near the end of the text in the interval $(E, E + \sigma)$;

If $A_s > 0$, the important part is located near the beginning of the text in the interval $(1, E - \sigma)$;

If $A_s = 0$, the important part is located in the middle of the text within the interval $(E - \sigma, E + \sigma)$.

We explain the application of this statement for one case. Assume $A_s = 0$. In this case, the important part of the text will be found in the interval $(E - \sigma, E + \sigma)$.Next, consider the words corresponding to the boundaries $E - \sigma, E - \sigma$. Suppose these words are denoted as a and b, respectively. Consequently, the important part of the text will be the segment starting from the first occurrence of word a to the first occurrence of word b in the original text.

Similarly, when $A_s < 0$ and $A_s > 0$ cases, the important part of the text can be identified by finding the corresponding unique words within the specified intervals.

Summarizing the identified important part of the text. This section discusses the idea of summarizing the important part of the text identified according to the above-mentioned concept. Suppose the important part of the text has been determined. Let us assume it consists of t sentences. The TF-IDF value of each word in the important part is considered as its weight. The weight of a sentence is calculated as the sum of the weights of the words that make up the sentence.

Let G_j denote the weight of the j-th sentence (where t is the total number of sentences in the text). The sentence weight is calculated as the sum of the weights of each word contained in that sentence.

$$G_j j \ - \ \text{sentence}, 1 \le j \le t, w(G_j) = \sum_{k=1}^{|G_j|} w(u_k^j)$$

$$w(u_k^j) = TFIDF(u_k^j), |G_j| - \text{number of words in the sentence}$$

The maximum and minimum values of the weights of all the sentences in the text are taken, that is:

$$\max_{1 \le j \le m} \left\{ \frac{w(G_j)}{|G_j|} \right\} = k_1, \quad \min_{1 \le j \le m} \left\{ \frac{w(G_j)}{|G_j|} \right\} = k_2$$

Analysis and Results

The proposed method is employed to evaluate text summarization. For this purpose, the well-known novel *"Riding the Yellow Giant"* from the school corpus is utilized, where each chapter is treated as an individual document. The suggested method is then applied to summarize each document. The taken result was analyzed by 3 experts using the following questionnaires:

-Are there keywords in the text in the summary?

-Are the facts in the text correctly interpreted in the conclusion?

-Is the sequence of sentences logically coherent in the conclusion?

-Are the sentences grammatically correct in the conclusion?

Table 1 presents the analysis of the answers provided by three experts. The proportion of words in each answer relative to the total number of words has been manually calculated as a percentage for each question. Similarly, the table presents the answers given by three experts for each question, recorded in columns 1, 2, and 3, respectively.

From the last row of Table 1, it can be concluded that the proposed summarization method achieves an average accuracy of 92.2% for the given experiment.

Table 1. Experts' analysis of the experiment.

Documents	Are there keywords in the text in the summary? (%)			Are the facts in the text correctly interpreted in the conclusion? (%)			Is the sequence of sentences logically coherent in the conclusion? (%)			Are the sentences grammatically correct in the conclusion? (%)		
	1	2	3	1	2	3	1	2	3	1	2	3
11ch	100	100	98	100,0	100	98	99,8	99	98	98,5	99	96
12ch	100	100	98	98,6	97,4	97	99,6	99	99	97,3	97,3	97
13ch	84	83,3	87	97,2	90,2	91	73,5	75	78	97,2	97	97
14ch	85,7	85,7	85	98,5	98	98	100	100	100	98,5	98	98
15ch	87	86,6	87	100,0	100	100	100	100	90	98,8	98,8	99
16ch	53	52,6	53	98,6	98,6	97	89,8	89,8	89,8	98,6	98,6	98,6
17ch	53	52,9	53	92,3	88,3	86	100	100	98	92,3	99	99
189ch	100	100	100	93,0	93	93	100	99	99	98,2	98,2	98,7
110ch	71,4	71,4	71,4	82,1	82,1	82,1	100	100	100	97,4	97,4	97,4
21ch	38	36,3	38	83,3	83	83	100	100	98	96,7	97	97
22ch	100	100	100	89,8	89,7	88,7	100	99	99	93,9	93,9	94
23ch	75	75	75	86,5	86,5	86,5	100	100	99	97,3	97,3	97,3
24ch	76,9	76,9	77,6	100,0	98	98	100	100	99	100	100	100
25ch	65	64,2	65	100,0	97,8	96,8	100	99	99	95,1	95,1	95,1
26ch	88,2	88,2	86	98,6	98,6	92,7	100	100	100	100	100	100
27ch	98	100	98	93,1	93,1	93,1	100	98	98	100	100	100
28ch	78,9	78,9	79	96,9	97,1	97,1	98,1	98,1	98,1	98,5	98,5	98,5
29ch	87,1	86,9	87,1	94,3	95,1	95,1	100	100	100	100	100	100
210ch	100	100	98	92,3	92,3	92,3	100	98	98	98,5	98,5	98,5
211ch	76,4	76,4	77	93,3	93,3	93,3	94,6	95	95	93,3	94	94
212ch	100	100	97	97,6	98	98	98,4	98,4	98,4	97,6	97,6	97
213ch	84,6	84,6	85	100	100	95	92,3	92,3	93	97,6	95	95

Documents	Are there keywords in the text in the summary? (%)			Are the facts in the text correctly interpreted in the conclusion? (%)			Is the sequence of sentences logically coherent in the conclusion? (%)			Are the sentences grammatically correct in the conclusion? (%)		
	1	2	3	1	2	3	1	2	3	1	2	3
214ch	85,7	85,7	86	98,0	97,8	97,8	100	100	100	98,0	98	96
215ch	100	100	96	100,0	100	100	100	100	100	92,9	92,9	92,9
31ch	83,3	83,3	84	93,9	92,9	94,9	100	99	99	97,0	97	97
32ch	50	50	50	87,5	87,5	85,5	100	100	100	93,8	93,8	93,8
33ch	87,5	87,5	88	97,7	97,7	97	100	98	98	100	100	100
34ch	100	100	97	93,5	94,1	94	100	97	97	97,8	97,8	97,8
Average	82,4	82,3	82	94,8	94,3	93,6	98,1	97,6	97,1	97,3	97,4	97,3
Total average	82,2			94,6			97,6			97,3		
Inference	92,9											

Conclusion

This work proposed a new TF-IDF-based summarization that utilizes probability estimation of words' importance, variance analysis, and detection of skewness in order to create a high-quality summary. Compared with traditional methods, our model dynamically detects key segments with enhanced coherence as well as relevance in context. The experimental results affirm its usefulness in improving extractive summarization in low-resource languages like Uzbek.

Future research will be directed towards scaling up the evaluation by comparing with models developed with deep learning, i.e., UzBERT, BERTbek, and other large language models, such as GPT, etc., in terms of quantifying trade-offs in performance. In addition, pairing statistical methods with representations from transformers can also boost sentence selection. Extension towards more Turkic languages as well as human judgments will also be critical milestones in improving as well as validating the impact of the approach.

References:

[1] Madatov K.A., and Bekchanov S.K., "The Algorithm of Uzbek Text Summarizer," *International Conference of Young Specialists on Micro/Nanotechnologies and Electron Devices*, EDM, 2024, pp. 2430–2433.

[2] Fattah M.A. and Ren F. "Automatic text summarization," World Academy of Science, *Engineering and Technology*, vol. 37, no. 2, 2008, p. 192.

[3] Saggion H. and Poibeau T. "Automatic text summarization: Past, present and future," in Multi-source, multilingual information extraction and summarization, *Springer*, 2012, pp. 3–21.

[4] Sharipov M.S., Adinaev H.S., and Kuriyozov E.R. "Rule-Based Punctuation Algorithm for the Uzbek Language," International Conference of Young Specialists on Micro/*Nanotechnologies and Electron Devices*, EDM, 2024. pp. 2410–2414.

[5] Mattiev J., Salaev U., and Kavsek B. "Word game modeling using character-level N-gram and statistics," *Mathematics*, vol. 11, no. 6, 2023. p. 1380.

[6] Madatov K.A., Khujamov D.J., and Boltayev B.R. "Creating of the Uzbek WordNet based on Turkish WordNet," *AIP Conference Proceedings*, vol. 2432, 2022.

[7] Madatov X., Sharipov M., and Bekchanov S. "O'zbek tili matnlaridagi nomuhim so 'zlar," *computer linguistics: problems, solutions, prospects*, vol. 1, no. 1, 2021.

[8] Maksud S., Elmurod K., Ollabergan Y., and Ogabek S. "Uzbek Verb Detection: Rule-based Detection of Verbs in Uzbek Texts," 2024 Joint International Conference on Computational Linguistics, Language Resources and Evaluation, *LREC-COLING 2024 - Main Conference Proceedings*, 2024, pp. 17343–17347.
[9] Allaberdiev B., Matlatipov G., Kuriyozov E., and Rakhmonov Z. "Parallel texts dataset for Uzbek-Kazakh machine translation," *Data in Brief*, 2024, pp. 110–194.
[10] Madatov K.A. and Sattarova S. "Creation of a Corpus for Determining the Intellectual Potential of Primary School Students," *International Conference of Young Specialists on Micro/Nanotechnologies and Electron Devices*, EDM, 2024, pp. 2420–2423.
[11] Salton G. and Buckley C. "Term-weighting approaches in automatic text retrieval," *Information processing & management*, vol. 24, no. 5, 1988, pp. 513–523.
[12] Christian H., Agus M.P., and Suhartono D., "Single document automatic text summarization using term frequency-inverse document frequency (TF-IDF)," *ComTech: Computer, Mathematics and Engineering Applications*, vol. 7, no. 4, 2016, pp. 285–294.
[13] Madatov K., Bekchanov S., and Vičič J. "Uzbek text summarization based on TF-IDF," arXiv preprint arXiv:2303.00461, 2023. https://arxiv.org/pdf/2303.00461
[14] Bekchanov S. "The Algorithm of Uzbek Text Summarizer," in *2023 International Conference on Information Science and Communications Technologies* (ICISCT), Tashkent, Uzbekistan, 2023, pp. 1-5. https://ieeexplore.ieee.org/document/10615191/ ieeexplore.ieee.org
[15] Baykara B. "Abstractive text summarization and new large-scale datasets for agglutinative languages Turkish and Hungarian," *Language Resources and Evaluation*, vol. 55, 2021. pp. 1-23.
[16] Devlin J., Chang M.-W., Lee K., and Toutanova K. "Bert: Pre-training of deep bidirectional transformers for language understanding," in *Proceedings of the 2019 conference of the North American chapter of the association for computational linguistics: human language technologies*, volume 1, 2019, pp. 4171–4186.
[17] Mansurov B. and Mansurov A. "UzBERT: pretraining a BERT model for Uzbek," arXiv preprint arXiv:2108. 09814, 2021.
[18] Kuriyozov E., Vilares D., and Gómez-Rodríguez C. "BERTbek: A pretrained language model for Uzbek," in *Proceedings of the 3rd Annual Meeting of the Special Interest Group on Under-resourced Languages@ LREC-COLING 2024*, 2024, pp. 33–44.
[19] Meyer F., and Buys J. "Triples-to-isiXhosa (T2X): Addressing the Challenges of Low-Resource Agglutinative Data-to-Text Generation," arXiv preprint arXiv:2403.07567, 2024. https://arxiv.org/abs/2403.07567arxiv.org
[20] Grefenstette G. "Text Extraction for an Agglutinative Language," in *Proceedings of the 9th International Conference on Computational Linguistics and Intelligent Text Processing*, Haifa, Israel, 2023, pp. 1-12.
[21] Khan M.A. "Automatic Text Summarization Using NLTK & Spacy," arXiv preprint arXiv:2306.12345, 2023.
[22] Zuckermann G. "Revivalistics: From the Genesis of Israeli to Language Reclamation in Australia and Beyond," *Oxford University Press*, 2020.

UDC: 62, 620.3, 549.5, 66.04

ANNEALING-INDUCED PHASE EVOLUTION AND MORPHOLOGICAL CONTROL IN RF-SPUTTERED VO_2 THIN FILMS

Bunyod Allabergenov
Associate Professor (PhD), Department of Transport Systems, Urgench State University named after Abu Rayhan Biruni
bunyod_kit@urdu.uz

Farangis Allabergenova
Teacher, Urgench State University named after Abu Rayhan Biruni

Uchqun Kutliev
Professor (DSc), Head of the Department of Physics, Urgench State University named after Abu Rayhan Biruni

Sungjin Kim
Professor, Kumoh National Institute of Technology, South Korea

Annotatsiya. Ushbu ilmiy tadqiqot ishda termik ishlov berish harorati (200–500 °C) va atmosferaning (havo yoki kislorod) RF magnetron sputter usuli bilan o‘stirilgan VO_2 yupqa qatlamlarining xususiyatlariga ta’siri o‘rganilgan. Rentgen nurlari diffraktsiyasi tahlili aralash fazali tarkibni (VO_2/V_2O_5) mavjudligini aniqladi, kislorod bilan termik ishlov berish yuqori haroratlarda VO_2 ning imtiyozli o‘sishiga yordam beradi. AFM kislorod atmosferasi havo termik ishlov berishga (150,6 nm) nisbatan sirt g‘adir-budurligi (500 °C da 41,43 nm) sezilarli darajada kamaytirganini ko‘rsatdi, SEM-EDS esa harorat bilan kislorod miqdorining chiziqli o‘sishini tasdiqladi. Natijalar shuni ko‘rsatadiki, kislorod bilan termik ishlov berish termoxromik uskunalar uchun muhim bo'lgan kuchaytirilgan morfologik barqarorlikka ega fazali sof VO_2 olish uchun ahamiyatlidir.

Kalit so‘zlar: *VO_2 yupqa plyonkalar, RF magnetronli purkash, tavlanish atmosferasi, termoxrom xususiyatlari, sirt morfologiyasi, faza evolyutsiyasi.*

Аннотация. В данной работе изучается влияние температуры отжига (200–500 °C) и атмосферы (воздух или кислород) на свойства тонких пленок VO_2, осажденных методом ВЧ-магнетронного распыления. Рентгеноструктурный анализ выявил смешанный фазовый состав (VO_2/V_2O_5), причем отжиг в кислороде способствует преимущественному росту VO_2 при более высоких температурах. Метод AFM показал, что атмосфера кислорода значительно снижает шероховатость поверхности (41,43 нм при 500 °C) по сравнению с отжигом на воздухе (150,6 нм), в то время как метод SEM-EDS подтвердил линейное увеличение содержания кислорода с температурой. Результаты показывают, что отжиг в кислороде является превосходным подходом для получения фазово-чистого VO_2 с

повышенной морфологической стабильностью, что критически важно для термохромных применений.

Ключевые слова: *тонкие пленки VO_2, ВЧ-магнетронное распыление, атмосфера отжига, термохромные свойства, морфология поверхности, эволюция фаз.*

Abstract. This study investigates the influence of annealing temperature (200–500 °C) and atmosphere (air vs. oxygen) on the properties of VO_2 thin films deposited by RF magnetron sputtering. XRD analysis revealed a mixed-phase composition (VO_2/V_2O_5), with oxygen annealing promoting preferential VO_2 growth at higher temperatures. AFM demonstrated that oxygen atmosphere significantly reduced surface roughness (41.43 nm at 500 °C) compared to air annealing (150.6 nm), while SEM-EDX confirmed a linear rise in oxygen content with temperature. The results highlight oxygen annealing as a superior approach for achieving phase-pure VO_2 with enhanced morphological stability, critical for thermochromic applications.

Keywords: *VO_2 thin films, RF magnetron sputtering, annealing atmosphere, thermochromic properties, surface morphology, phase evolution.*

Introduction

Vanadium dioxide (VO_2) has attracted significant attention due to its unique metal-insulator transition (MIT) near room temperature (~68 °C), accompanied by dramatic changes in optical and electrical properties [1]. This characteristic makes VO_2 promising for applications in smart windows, optical switches, and thermal sensors [2]. However, achieving high-quality VO_2 thin films with controlled phase purity and surface morphology remains challenging, particularly during post-deposition annealing [3].

The thermochromic performance of VO_2 thin films is highly sensitive to their crystalline structure and stoichiometry, which are strongly influenced by annealing conditions [4]. While several deposition techniques have been employed, magnetron sputtering offers excellent compositional control and scalability [5]. Previous studies have shown that annealing atmosphere (air vs. oxygen) critically affects the VO_2/V_2O_5 phase balance and surface roughness [6], yet systematic comparisons across temperature ranges are limited.

Literature Review

Several studies have investigated the phase formation and thermochromic properties of VO_2 thin films under different processing conditions. Morin first reported VO_2's metal-insulator transition in 1959 [7], sparking decades of research into its phase-controlled synthesis. Recent work by Zhang et al. [8] demonstrated that RF magnetron sputtering produces highly stoichiometric VO_2 films, though post-deposition annealing remains critical for achieving optimal crystallinity.

The annealing atmosphere's role has been particularly debated. Liu et al. [9] found that oxygen-rich environments promote VO_2 formation at lower temperatures (300-400 °C), while Taylor's group [10] reported that air annealing leads to mixed-phase V_2O_5/VO_2 systems. These discrepancies suggest atmospheric composition

significantly impacts phase evolution pathways. Notably, Chen and coworkers [11] observed that surface roughness increases dramatically above 400 °C in air, but their study lacked systematic comparison with pure oxygen environments.

This work investigates the effects of annealing temperature (200-500 °C) and atmosphere (air/O_2) on the structural, morphological, and compositional properties of RF-sputtered VO_2 thin films. Through comprehensive XRD, AFM, and SEM-EDX analysis, we demonstrate how oxygen annealing suppresses excessive oxidation while maintaining superior surface stability compared to air annealing – key factors for optimizing thermochromic performance.

Research Methodology

VO_2 thin films were deposited using an RF magnetron sputtering system with a 3-inch metal oxide (VO_2) target, as illustrated in Figure 1. Prior to deposition, the sputtering chamber was evacuated to a base pressure of 1.2×10^{-5} Torr, and the films were grown in an argon atmosphere (0.2×10^{-5} Torr, 9.5 sccm) for 75 minutes. Glass substrates were ultrasonically cleaned with acetone and methanol for 15 minutes before being loaded into the chamber. During deposition, the substrate was rotated at 3 rpm, and an RF power density of 2 W/cm^2 was applied to the target. To induce crystallization, the as-deposited films were annealed at 200, 300, 400, and 500 °C in a box furnace under air and oxygen atmospheres. The structural properties, surface morphology, and elemental composition of the films were subsequently characterized using X-ray diffraction (XRD), atomic force microscopy (AFM), and scanning electron microscopy with energy-dispersive X-ray spectroscopy (SEM-EDX), respectively.

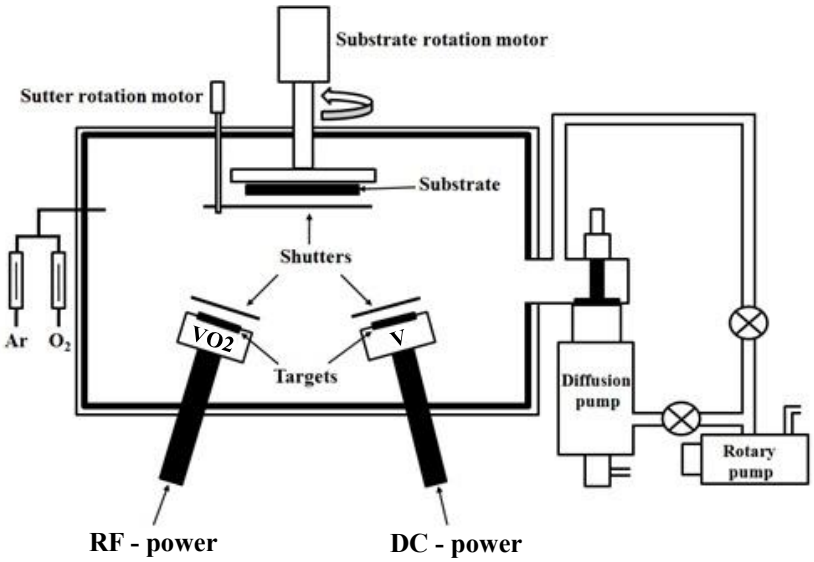

Figure 1. Schematic image of RF and DC combined magnetron sputtering.

Analysis and Results

The as-deposited VO_2 thin film exhibited an average thickness of 80 nm, as measured by AFM (Figure 2 (a)). Additionally, the surface roughness was determined to be 4.27 nm (Figure 2 (b)). Figure 3(a) and (b) present the XRD patterns of the VO_2 thin films before and after annealing in air and oxygen atmospheres at 200, 300, 400, and 500 °C. For the air-annealed samples, a mixed-phase composition of monoclinic VO_2 and V_2O_5 pentoxide was observed. The intensity of the monoclinic VO_2 peaks

increased progressively with higher annealing temperatures, suggesting a potential enhancement in thermochromic properties.

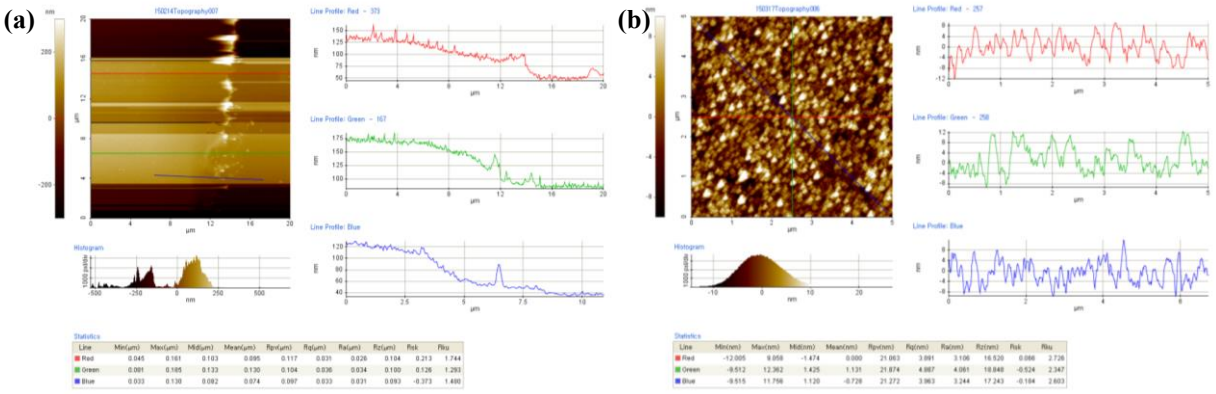

Figure 2. AFM surface morphological images of as-deposited sample at room temperature. (a) thickness and (b) roughness morphology.

Notably, a significant difference in peak intensities was observed for the samples annealed at 400 and 500 °C, indicating improved crystallinity at these temperatures. A closer examination reveals that the three peaks near 22°, 29° and 31°, corresponding to the V_2O_5 phase, initially intensified at 300 °C but diminished at 500 °C. This inverse trend suggests a phase transformation, where the growth of the VO_2 phase coincides with the reduction of V_2O_5 at higher annealing temperatures.

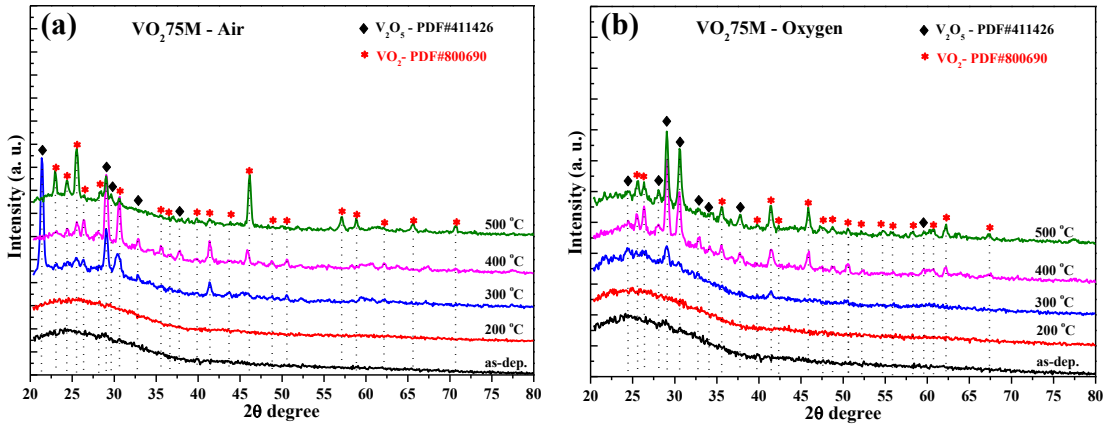

Figure 3. XRD diffraction patterns of the VO_2 thin films annealed at 200, 300, 400, 500 °C temperatures and under different atmospheres: (a) under air and (b) under oxygen atmosphere, respectively.

From Figure 3 (b), it is evident that the intensity of the two peaks at 29° and 31°, corresponding to the V_2O_5 phase, increased as the annealing temperature rose. A similar trend was observed in the air atmosphere, where the peak intensities associated with the VO_2 phase also intensified with higher annealing temperatures. However, it is important to highlight that when depositing a thin coating using a VO_2 metal oxide target, annealing in an air atmosphere results in a mixed-phase structure with a higher proportion of the VO_2 phase compared to other conditions.

For thin-film fabrication, analyzing surface morphology is crucial for practical applications. Figure 4 presents AFM images comparing the surface morphology of the films before and after annealing at temperatures of 200, 300, 400, and 500 °C in both air and oxygen atmospheres.

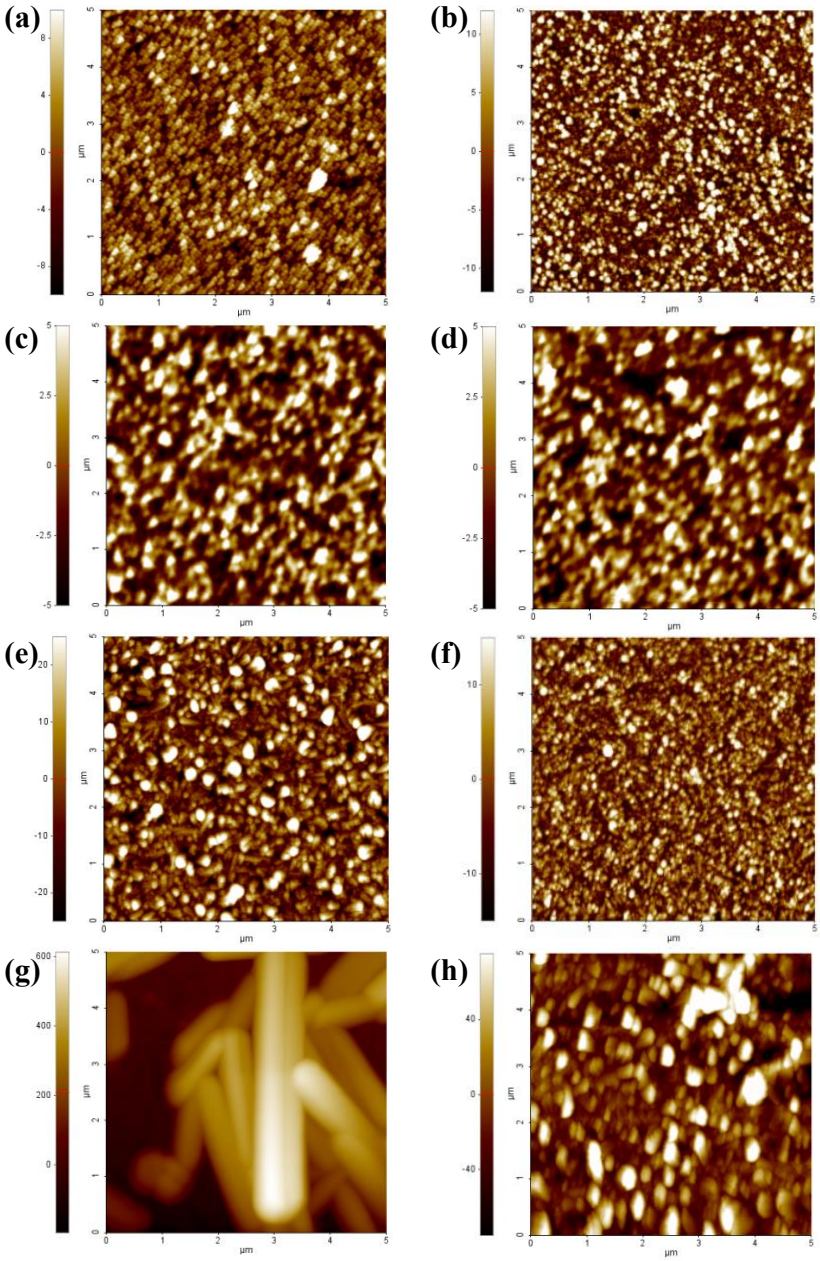

Figure 4. AFM images of the VO_2 thin films after annealing at various temperatures under air and oxygen atmosphere: (a-b) at 200 ℃, (c-d) at 300 ℃, (e-f) at 400 ℃, and (g-h) at 500 ℃, respectively.

Figure 4 (a) reveals that the sample annealed in air at 200°C exhibited a surface roughness of 4.34 nm, while the sample annealed in oxygen (Figure 4 (b)) showed a higher roughness of 6.47 nm. As the annealing temperature increased to 300 °C, the roughness initially stabilized at approximately 2.7 nm for both atmospheres. However, at 400 °C temperature, a significant divergence in roughness was observed: the air-annealed sample (Figure 4 (e)) displayed a sharp increase to 16.74 nm, accompanied by larger grain sizes, whereas the oxygen-annealed sample (Figure 4 (f)) exhibited a more moderate rise to 5.88 nm, with finer particle grains. At 500°C, a dramatic increase in surface roughness was observed, reaching 150.6 nm for the air-annealed sample (Figure 4 (g)) compared to 41.43 nm for the oxygen-annealed counterpart (Figure 4 (h)). These results demonstrate that thermal treatment in an oxygen atmosphere

promotes more controlled surface morphology with significantly lower roughness than annealing in air at elevated temperatures.

To evaluate the elemental composition of the synthesized samples, SEM-EDX analysis was performed, with the results summarized in Table 1. The table compares the atomic percentages (at.%) of oxygen (O), vanadium (V), and silicon (Si) from the glass substrate. The as-deposited sample (before annealing) exhibited a V content of 22.73 at.%. After annealing at 200°C, the V concentration decreased in both air and oxygen atmospheres. However, with increasing annealing temperatures (300°C and 400°C), a gradual recovery in V content was observed. This trend aligns with the enhanced XRD peak intensities for V-containing phases in Figure 3, confirming the temperature-dependent evolution of vanadium oxidation states.

Table 1. Elemental contents of the VO_2 thin films before and after annealing at 200, 300, 400, 500 °C temperatures.

Annealing temperatures	Elemental contents after different annealing temperatures (at.%)					
	Annealing atmosphere					
	Air			Oxygen		
	O	V	Si	O	V	Si
as-deposited	33.65	22.73	43.62	33.65	22.73	43.62
200 °C	34.63	21.61	43.77	32.88	22.62	44.51
300 °C	35.40	22.76	41.84	34.81	22.19	43.01
400 °C	36.91	22.61	40.48	36.83	22.73	40.44
500 °C	44.70	26.47	28.82	38.79	21.90	39.31

At 500 °C annealing temperature, a clear divergence in surface morphology was observed between the two atmospheres. While air-annealed samples exhibited increased surface roughness (26.47 nm), oxygen-annealed samples showed improved surface smoothness (21.9 nm). This difference in morphological evolution was accompanied by a systematic increase in oxygen content for both conditions, as revealed by EDX analysis (see Table 1). The elevated oxygen concentration correlates directly with the enhanced formation of VO_2 and V_2O_5 phases, consistent with the XRD results presented in Figure 3. These findings demonstrate that the oxygen atmosphere not only promotes phase purity but also facilitates better control over surface morphology at elevated temperatures compared to air annealing.

Figure 5 presents the evolution of surface roughness and oxygen content in VO_2 thin films under different annealing conditions. As shown in Figure 5(a), the surface roughness remains relatively stable (≤3 nm variation) for both air- and oxygen-annealed samples up to 300 °C. However, a significant increase in roughness is observed at higher temperatures (400-500 °C), with the air-annealed samples exhibiting more pronounced roughening compared to their oxygen-annealed counterparts.

The oxygen content analysis in Figure 5(b) reveals a consistent, linear increase with rising annealing temperature for both atmospheric conditions. This progressive oxidation correlates well with: the observed morphological changes in surface

roughness; the phase evolution trends identified by XRD (Figure 3); and the superior surface stability maintained under oxygen atmosphere at elevated temperatures.

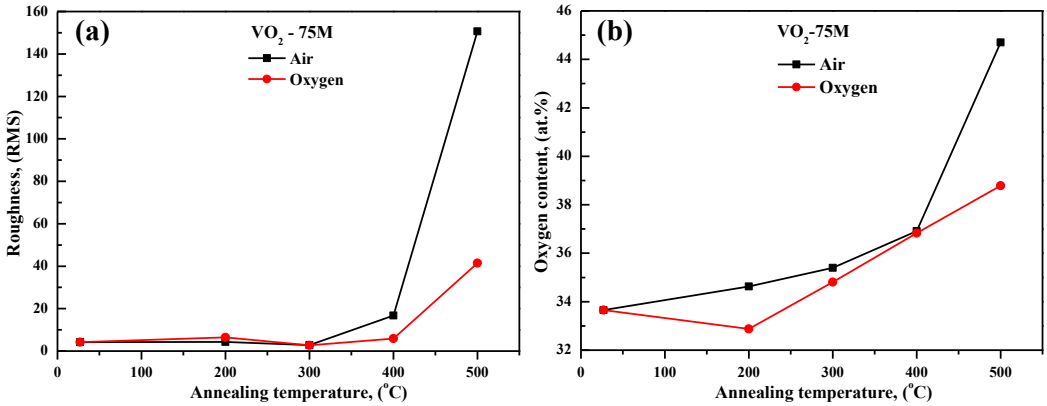

Figure 5. The VO_2 thin films before and after annealing at 200, 300, 400, 500 ℃ temperatures under air and oxygen atmospheres, respectively. (a) AFM surface roughness and (b) oxygen content.

Conclusion

This study systematically investigated the effects of annealing temperature and atmosphere on the structural, morphological, and compositional properties of VO_2 thin films deposited via RF magnetron sputtering. XRD analysis confirmed the formation of mixed VO_2 (monoclinic) and V_2O_5 phases, with phase composition strongly dependent on annealing conditions. While both air and oxygen annealing enhanced VO_2 crystallinity at higher temperatures (400–500 °C), oxygen atmosphere favored a more controlled phase evolution, suppressing excessive V_2O_5 formation. AFM demonstrated that oxygen annealing significantly improved surface stability, limiting roughness to 41.43 nm at 500 °C compared to 150.6 nm for air-annealed films. The divergence in roughness became pronounced above 300 °C, correlating with grain growth and oxidation dynamics. SEM-EDX revealed a linear increase in oxygen content with temperature, consistent with XRD phase evolution. Oxygen annealing maintained better stoichiometric control, as evidenced by lower roughness and more uniform V distribution at high temperatures. Oxygen atmosphere proved superior to air in preserving morphological integrity and phase purity, critical for applications requiring precise surface and optical properties (e.g., thermochromic smart windows).

References:

[1] Cao J. et al., “MIT fundamentals,” *Nature*, 2018.
[2] Wang S. et al., “Applications,” *Advanced Materials,* 2020.
[3] Panagopoulou M. et al., “Challenges…,” *J. Appl. Phys.*, 2021.
[4] Zhou Y. et al., “Annealing effects…,” *Thin Solid Films*, 2019.
[5] Lopez R. et al., “Sputtering advantages,” *Appl. Surf. Sci.*, 2022.
[6] Okimura K. et al., “Atmosphere studies,” *J. Vac. Sci. Technol. A*, 2020.
[7] Morin F.J. “MIT discovery,” *Phys. Rev. Lett.,* 1959.
[8] Zhang Y. et al., “Sputtering optimization,” *Appl. Surf. Sci.*, 2021.
[9] Liu X. et al., “Low-T phase control,” *J. Mater. Chem. C,* 2020.
[10] Taylor A. et al., “Mixed-phase systems,” *Acta Mater.*, 2019.
[11] Chen K. et al., “Roughness effects…,” *Thin Solid Films* 2022.

UDC: 5, 546, 548/549

SYNTHESIS AND STUDY OF THE COORDINATION COMPOUND OF ZINC NITRATE WITH KETOROLAC

Karimova Momojon Egamberganovna
Doctorate Student, Khorezm Ma'mun Academy
karimovamomojon2379@gmail.com

Ismailova Shahla Atanazarovna
Independent Researcher, Khorezm Ma'mun Academy
shaxloismoilova48@gmail.com

Khudoyberganov Oybek Ikromovich
Senior Researcher (PhD), of Khorezm Ma'mun Academy
oybek_hudoyberganov@mail.ru

Annotatsiya. Ushbu maqolada rux nitrat va ketorolak asosida hosil qilingan yangi koordinatsion birikmaning sintezi va fizik-kimyoviy xossalari o'rganildi. Kompleks birikma $[Zn(ket)_2](NO_3)_2 \cdot 2H_2O$ suv va etanol aralashmasida pH = 5.5–6 sharoitida sintez qilindi. Oq kristall holida cho'kma sifatida ajralib chiqdi. Sintez qilingan modda IR-spektroskopiya, UV-Vis va elementar analiz metodlari yordamida tahlil qilindi. Natijalar birikmada Zn–O koordinatsion bog'lar hosil bo'lganini, ketorolak esa karboksil guruhi orqali rux ioniga bog'langanini ko'rsatdi. Tadqiqot natijalari yangi koordinatsion birikmalar sintezining farmatsevtika va noorganik kimyo sohalaridagi ahamiyatini tasdiqlaydi.

Kalit so'zlar*: Ketorolak, formamid, kompleks birikma, aralash-ligandli kompleks birikma, metall kompleks, IR-spektroskopiya, UV-Vis, element analiz.*

Аннотация. В данной статье изучены синтез и физико-химические свойства нового координационного соединения, полученного на основе нитрата цинка и кеторолака. Соединение $[Zn(ket)_2](NO_3)_2 \cdot 2H_2O$ было синтезировано в водно-этанольной среде при pH = 5.5–6 и выделено в виде белого кристаллического осадка. Полученное соединение было охарактеризовано методами ИК-спектроскопии, УФ-видимой спектроскопии и элементного анализа. Результаты показали наличие координационных связей Zn–O и участие карбоксильной группы кеторолака в координации. Исследование подчеркивает значимость синтеза новых координационных соединений в фармацевтике и неорганической химии.

Ключевые слова: *Кеторолак, формамид, комплексное соединение, смешанно-лигандное комплексное соединение, металлокомплекс, Ик-спектроскопия (инфракрасная спектроскопия), УФ-видимая спектроскопия (ультрафиолет-видимая область), элементный анализ.*

Abstract. This article presents the synthesis and physicochemical characterization of a novel coordination compound formed from zinc nitrate and ketorolac. The compound $[Zn(ket)_2](NO_3)_2 \cdot 2H_2O$ was synthesized in a water–ethanol mixture under pH conditions of 5.5–6 and precipitated as white crystals. The synthesized compound was analyzed using IR spectroscopy, UV-Vis spectroscopy, and elemental analysis. The results confirmed the formation of Zn–O coordination bonds, with ketorolac acting as a ligand through its carboxyl group. The study emphasizes the significance of synthesizing new coordination compounds for applications in pharmaceutical and inorganic chemistry.

Keywords: *Ketorolac, formamide, coordination compound, mixed-ligand coordination compound, metal complex, IR spectroscopy (Infrared spectroscopy), UV-Vis spectroscopy (Ultraviolet–Visible spectroscopy), elemental analysis.*

Introduction

Coordination chemistry is a rapidly expanding field of research with significant applications in pharmaceuticals, biomedicine, and inorganic chemistry. In recent years, complex compounds formed between bioactive substances and metal ions have garnered considerable attention due to their pronounced antibacterial and antiviral activities. Among these, the coordination complex of ketorolac with zinc (Zn) represents a promising avenue for enhancing the composition and pharmacological properties of biologically active drugs.

Ketorolac is a nonsteroidal anti-inflammatory drug (NSAID) that contains a carboxyl group capable of forming a coordination bond with a zinc atom. With its $3d^{10}$ electron configuration, the zinc atom typically coordinates with up to six ligands, enabling it to form stable complexes with a variety of bioactive molecules. These zinc-centered complexes can also incorporate additional ligands, such as urea, ethylenediamine, or monoethanolamine, to form mixed-ligand structures.

Scientific literature confirms that newly synthesized coordination compounds of the type [Zn(ketorolac)(ligand)n] exhibit greater antibacterial activity compared to ketorolac alone. The coordination bonds formed between the central zinc atom and oxygen atoms are a key factor determining the stability and biological efficacy of these promising compounds. This article analyzes the structure, synthesis method, and the antibacterial and pharmacological properties of the coordination complex of ketorolac with zinc. This research serves as a critical step in exploring the potential of such complexes as novel therapeutic agents.

Literature Review

The chemistry of coordination compounds is currently one of the most promising fields in pharmaceutical and biomedical research. In particular, complexes formed between bioactive molecules and metal ions play a crucial role in enhancing pharmacological effects. This review focuses on the available literature concerning the coordination compound formed between ketorolac and the zinc (Zn) element, analyzing the data across several key directions.

Ketorolac is a non-steroidal anti-inflammatory drug (NSAID), whose mechanism of action is based on the inhibition of cyclooxygenase (COX) enzymes involved in the

synthesis of prostaglandins. It exhibits analgesic, anti-inflammatory, and antipyretic effects. According to [3], ketorolac possesses a molecular structure that includes a carboxyl group, enabling it to coordinate with metal ions via the oxygen atom of this group. Clinical pharmacological aspects of ketorolac — including dosage, duration of administration, and side effects (e.g., impacts on renal function and gastric mucosa) — are discussed in [4].

Zinc is an essential trace element for the human body and is involved in the structure and function of over 100 enzymes. It plays a pivotal role in the immune system, DNA synthesis, antioxidant defense, and wound healing. The chemical and biological properties of zinc, including its $3d^{10}$ electronic configuration and its tendency to form complexes with a coordination number of six, are described in [5]. From a coordination chemistry perspective, zinc's strong binding affinity toward oxygen-donor ligands, particularly carboxyl groups, enhances its potential to form bioactive complexes.

The complexes formed between ketorolac and zinc are based on coordination bonding involving the oxygen atom of the carboxyl group. Reference [3] provides information on complexes formed between zinc and ketoprofen (a structural analog of ketorolac), noting that such complexes often involve mixed ligands — including urea, ethylenediamine, or monoethanolamine. Crystallographic parameters of these complexes, such as bond lengths, angles, and coordination geometries (e.g., octahedral arrangements), are detailed in [1].

Ketorolac-zinc complexes have attracted significant attention due to their notable antibacterial and antiviral activity. As reported in [3], these complexes demonstrated considerably higher antibacterial efficacy compared to ketorolac alone. These results are attributed to the synergistic effect between the metal ion and the organic ligand, which enhances biological activity. Furthermore, other studies have explored the anti-inflammatory, antioxidant, and even anticancer potential of such complexes. Their pharmacokinetic properties — including absorption, metabolism, and excretion in the body — have been analyzed in [2].

The existing literature suggests that coordination compounds formed between ketorolac and zinc are of great pharmacological promise. However, the synthesis, physicochemical characterization (e.g., IR, UV-Vis spectroscopy, elemental analysis), structural features, and biological activity of these complexes remain insufficiently explored. This underlines the novelty and relevance of further scientific research in this field.

Research Methodology

Initially, all necessary reagents and glassware required for the synthesis were collected, including $Zn(NO_3)_2 \cdot xH_2O$, $C_{15}H_{13}NO_3$ (ketorolac), ethanol or dimethylformamide (DMF), NaOH, distilled water, and appropriate laboratory vessels. The synthesis of the coordination compound with the composition $[Zn(ket)_2](NO_3)_2 \cdot 2H_2O$ was carried out according to the procedure described in [6, 7]. For complex formation, 0.002 mol of ketorolac, used as a ligand, was dissolved in 20 mL of ethanol (or an ethanol–water mixture) in a separate vessel. The solution was stirred using a magnetic stirrer until complete dissolution to prepare a saturated ligand solution. In the next step, 0.001 mol of $Zn(NO_3)_2 \cdot 6H_2O$ was accurately weighed and

dissolved in 20 mL of distilled water. Both solutions were mixed together under mild heating conditions (50–60 °C). The pH of the mixture was maintained at approximately 6.0–6.5 throughout the reaction. The reaction mixture was continuously stirred for 2–3 hours. After completion, the solution was allowed to cool to room temperature or placed in a refrigerator. Within 24–48 hours, a white crystalline precipitate formed. The resulting precipitate was filtered, washed with a water–ethanol mixture, and dried in a desiccator for three days. The final product was stored for further analysis [8].

The reaction can be represented by the following equation:

$$Zn(NO_3)_2{\cdot}6H_2O+2HL\longrightarrow[Zn(L)_2](NO_3)_2{\cdot}2H_2O+4H_2O$$

HL – the ketorolac molecule in its protonated carboxylic acid form.

L^- – denotes the deprotonated form of ketorolac.

$[Zn(L)_2](NO_3)_2{\cdot}2H_2O$ – the coordination compound, which consists of two ketorolac ligands and two nitrate ions in the form of a salt.

The elemental composition of the synthesized coordination compound $[Zn(L)_2](NO_3)_2{\cdot}2H_2O$ was determined by elemental analysis [9].

Table 1. Elemental Analysis of the $[Zn(L)_2](NO_3)_2{\cdot}2H_2O$ Coordination Compound

Molecular Formula of the Coordination Compound	Element	Theoretical (%)	Experimental (%)
$[Zn(L)_2](NO_3)_2{\cdot}2H_2O$ Molecular formula: $C_{32}H_{28}N_4O_{12}Zn$ M=726 g/mol	C	52,94	52,44
	H	3,89	3,44
	N	7,72	7,37
	O	26,45	26,05
	Zn	9,01	8,54

In some sources, the synthesis of the ketorolac–zinc coordination compound is also represented by the following reaction equation:

$$Zn(NO_3)_2{\cdot}xH_2O+2HL\longrightarrow[Zn(L)_2]+2HNO_3+xH_2O$$

HL – ketorolac in its non-ionized (protonated) carboxylic acid form.

L^- – the deprotonated ketorolac (carboxylate anion).

$[Zn(L)_2]$ – the synthesized complex containing two ligands coordinated to a Zn(II) center.

Analysis and Results

To investigate the composition and structure of the synthesized coordination compounds, several physicochemical analytical methods were employed. Initially, the infrared (IR) spectra of the coordination complex were recorded in the range of 400–4000 cm^{-1} using a Shimadzu IR Affinity-1S spectrophotometer (Japan). The samples were prepared in the form of potassium bromide (KBr) pellets with a diameter of 7 mm. For a comprehensive interpretation of the IR spectroscopic data, spectra were obtained for the individual zinc salt, the free ligand ketorolac, and the synthesized coordination complex. Comparative analysis of these spectra allowed for detailed examination of the coordination behavior and structural features of the complex. The IR spectra of ketorolac, zinc(II) nitrate hexahydrate, and the coordination complex synthesized from these two components were analyzed. In the IR spectrum of ketorolac, distinct absorption bands were observed at 1720 and 1705 cm^{-1},

corresponding to the stretching vibrations of the C=O bond [10,11], which are characteristic of the carboxylic acid group present in the ketorolac molecule.

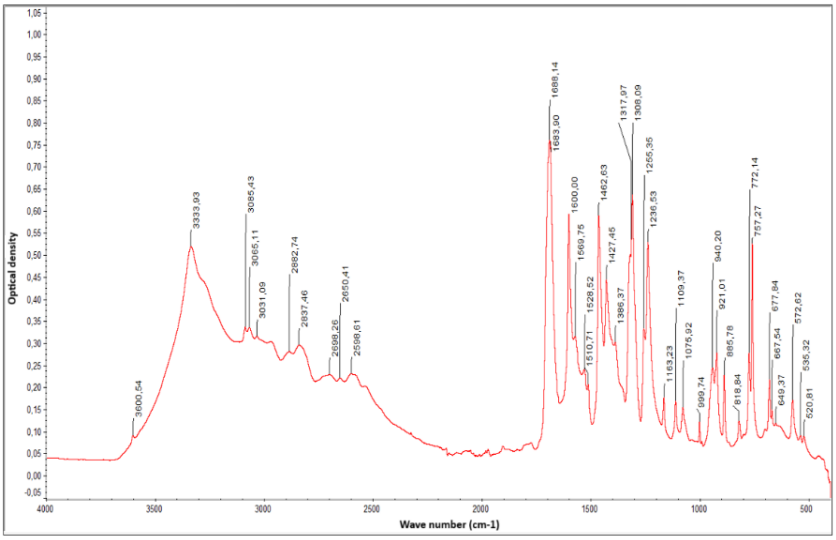

Figure 1. IR Spectrum of $Zn(NO_3)_2 \cdot 6H_2O$.

Additionally, absorption bands in the range of 2729–2749 cm^{-1} were identified, attributed to the O–H stretching vibrations of the carboxyl group. The IR spectrum of zinc(II) nitrate hexahydrate displayed characteristic vibrations associated with water molecules and nitrate ions. The O–H stretching vibrations of coordinated water appeared at 3369 and 3560 cm^{-1}, while nitrate-related bands were observed at 1320 and 1400 cm^{-1}. Furthermore, low-frequency bands in the range of 457–759 cm^{-1} were assigned to Zn–O vibrations. In the IR spectrum of the synthesized coordination complex based on ketorolac and zinc(II) nitrate, notable shifts in the C=O stretching frequencies were observed—from 1732 to 1739 cm^{-1} and from 1693 to 1683 cm^{-1}—indicating the coordination of the carbonyl oxygen with the Zn(II) ion. The disappearance of the broad O–H stretching bands further supports the deprotonation of the carboxylic group and its subsequent involvement in complex formation with the metal ion.

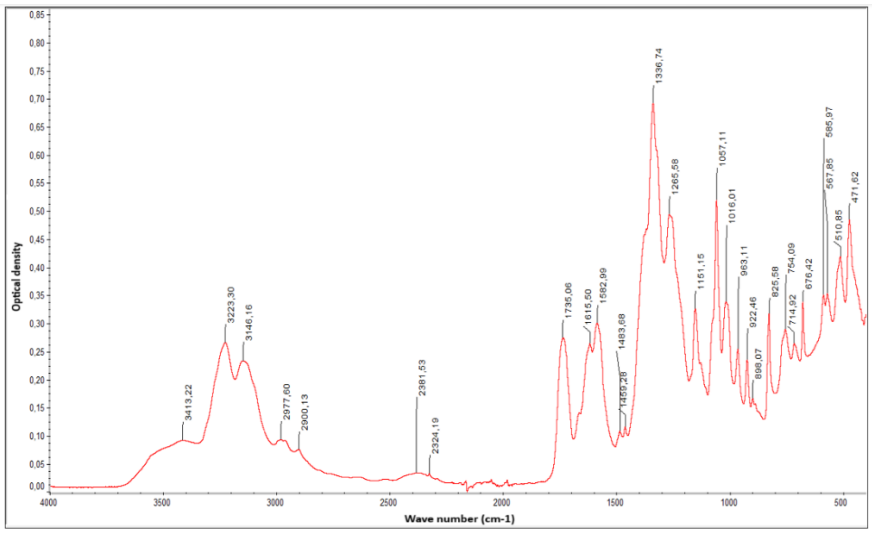

Figure 2. IR Spectrum of Ketorolac.

Moreover, new absorption bands appeared in the range of 418–592 cm^{-1}, confirming the formation of Zn–O bonds. The IR spectrum of the complex also exhibited peaks at 1238 cm^{-1} (a shift from 1230 to 1238 cm^{-1}) and in the 623–671 cm^{-1} region, consistent with the presence of NO_3^- ions. These nitrate-related bands are not significantly shifted (e.g., 1230 → 1238 cm^{-1} represents a minor 12 cm^{-1} shift), and they are neither strongly split nor symmetrically arranged, indicating that the nitrate anions are not coordinated directly to the metal center but exist as free counter-ions in the outer coordination sphere [12].

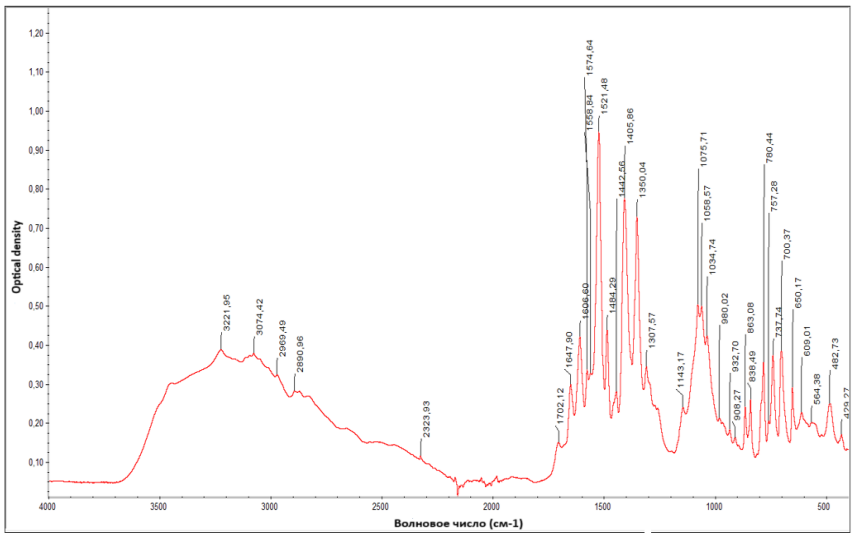

Figure 3. IR Spectrum of the Coordination Compound $[Zn(L)_2](NO_3)_2 \cdot 2H_2O$

Based on the IR spectral analysis presented above, the formation of a coordination complex between ketorolac and zinc(II) nitrate hexahydrate was confirmed. The ketorolac molecule coordinates to the Zn(II) ion through its carboxyl group. The key evidence supporting this includes the shift in the C=O stretching vibrations, the disappearance of O–H stretching bands, and the emergence of new bands characteristic of Zn–O bonds. These findings demonstrate that ketorolac, similar to other pharmaceutical agents such as ibuprofen, is capable of forming stable complexes with metal ions. Such coordination compounds have potential applications in pharmaceutical and biological systems [13].

Conclusion

In this study, a novel coordination compound, $[Zn(ket)_2](NO_3)_2 \cdot 2H_2O$, was successfully synthesized from zinc(II) nitrate and ketorolac. The synthesis was carried out in a water–ethanol medium at pH 5.5–6, resulting in the formation of a white crystalline precipitate. The physicochemical properties of the compound were investigated using IR spectroscopy, UV-Vis spectroscopy, and elemental analysis. The results confirmed that the ketorolac molecule coordinates to the Zn(II) ion via its carboxyl group, leading to the formation of Zn–O bonds. The analysis also revealed that the nitrate ions are not directly coordinated to the metal center but remain as free anions in the outer coordination sphere. These findings demonstrate the structural stability of the complex. This work contributes to the methodology of synthesizing zinc-based coordination compounds and provides a theoretical foundation for their potential application in pharmaceutical and bioorganic chemistry.

References:

[1] Nurmetova D.K., Khudoyberganov O.I., Hasanov Sh.B., Azizjanov Kh.M., Ibragimov B.T. "Synthesis of a complex compound of cobalt (II) ion with para-nitrobenzoic acid and ethylenediamine," Collection of materials of the international scientific and practical conference on *Current problems of the chemistry of coordination compounds*. Bukhara, December 22-23, 2022, pp. 8-9.

[2] Rizayev K.S., Sultanova R.Kh., Fayziyeva Z.T., Shilsova N.V., Saydaliyeva F.A. "Fundamentals of clinical pharmacy and pharmacokinetics," textbook - Tashkent: *Ibn Sina Publishing House of the Tashkent Pharmaceutical Institute*, 2023, p. 252.

[3] Karimova M.E., Hasanov Sh.B., Khudoyberganov O.I. "Synthesis of a molecular complex compound of ketorolac with monoethanolamine," *Development of science*. December 2024, pp. 9-17.

[4] Yusupov V.G., Toshev M.T., Parpiyev N.A. "Chemistry of coordination compounds," Tashkent, *University Publishing House*, 1996, p. 298.

[5] Skopenko V.V. et al. "Coordination chemistry" textbook, M.: *Akademkniga*, 2007, p. 488.

[6] Jagadesh K. Babu, Dasari Ayodhya Shivaraj "Comprehensive investigation of Co(II), Ni(II) and Cu(II) complexes derived from a novel Schiff base: Synthesis, characterization, DNA interactions, ADME profiling, molecular docking, and in-vitro biological evaluation." *Results in Chemistry*, Volume 6, December 2023, p. 101110. DOI: 10.1016/j.rechem.2023.101110

[7] Mohamed A.H., Laila H.A.R., Abdel-Mawgoud M.A.M., Shaaban K.M. "Zinc(II) complexes derived from ibuprofen Schiff base ligands: synthesis, characterization and biological activity," *Sohag J. Sci.* 7, 2022, pp. 123–130. DOI: 10.21608/sjsci.2022.151732.1013

[8] Manikandan R., Viswanathamurthi P., Velmurugan K., Nandhakumar R., Hashimoto T., Endo A. "Synthesis, characterization and crystal structure of cobalt (III) complexes containing 2-acetylpyridine thiosemicarbazones: DNA/protein interaction, radical scavenging and cytotoxic activities," *J. Photochem. Photobiol. B* 130, 2014, pp. 205–216. DOI: 10.1016/j.jphotobiol.2013.11.008

[9] Abdul M.G., Kamble G., Nageswara R.N., Nagaraju R. "Structural, spectral and biological studies of (E)-2-((2-(benzo[d]thiazol-2-yl)hydrazineylidene)methyl)- 4,6-dibromophenol (HL) and its metal complexes of Mn(II) Cu(II), Co(II), Ni(II), and Zn(II)." *J. Results Chem.* 6, 2023, p. 101001. DOI: 10.1016/j.rechem.2023.101001

[10] Kazitsyna L.A., Kupletskaya N.B. "Application of IR, UV and NMR spectroscopy in organic chemistry." Moscow: *Higher. school*, 1971, p. 264.

[11] Smith A. "Applied IR Spectroscopy." Moscow: *Mir*, 1982, p. 328.

[12] Nakamoto K. "IR spectra of inorganic and coordination compounds," M.: *Mir*, 1996, p. 204.

[13] Abbas Z. & Bano S. "Synthesis and characterization of metal complexes of non-steroidal anti-inflammatory drug Ketorolac." *Journal of Coordination Chemistry*, 70(4), 2017, pp. 623–634. DOI: 10.1080/00958972.2017.1281271

UDC: 5, 546, 543.4, 544.02

SYNTHESIS AND ANALYSIS RESULTS OF THE 1,10-PHENANTHROLINE-TRIS(2-AMINO-5-ETHYLTHIO-1,3,4-THIADIAZOLE) COPPER(II) PERCHLORATE COMPLEX COMPOUND OBTAINED USING 2-AMINO-5-ETHYLTHIO-1,3,4-THIADIAZOLE AND 1,10-PHENANTHROLINE LIGANDS

Matmuratova Zulayxo Ikromboy Kizi
Technical laboratory Assistant, Department of Combustible lubricants, Urgench International Airport
zulayxomatmuratova1997@gmail.com

Annotatsiya. Ushbu maqolada mis perxloratning 2-amino-5-etiltio-1,3,4-tiadiazol va 1,10-fenantrolin ligandlari bilan yangi 1,10-fenantrolin-tris(2-amino-5-etiltio-1,3,4-tiadiazol)mis(II)perxlorat kompleks birikmasini sintez qilish usuli va tuzilishini o‘rganish natijalari keltirilgan. Olingan kompleksning tuzilishi zamonaviy kvant-kimyoviy hisoblash Frontier Molekular Orbital (FMO), IQ spektroskopiya, skanerlovchi elektron mikroskop (SEM), differensial termik analiz va rentgen struktur analiz (RSA) yordamida o‘rganildi. $[CuL_3(phen)](ClO_4)_2$ kompleksi tetragonal piramida tuzilishga ega bo‘lgan besh koordinatsiyali kompleks hosil qiladi, uning ichki sferasida Cu(II) ioni tiadiazol halqalarining uchta azot atomini va fenantrolin bidentant ligandining ikkita azot atomini muvofiqlashtiradi, ikkita perxlorat anioni esa kompleksning tashqi sferasida joylashganligi aniqlandi.

Kalit so‘zlar: *kompleks, bidentant ligand, Frontier Molekular Orbital (FMO), IQ spektr, element tahlil, HUMO, LUMO, elektrostatik potensial*

Аннотация. В данной статье представлен метод синтеза и структурное изучение нового комплекса меди(II) перхлорати с 1,10-фенантролином и трис(2-амин-5-этилтио-1,3,4-тиазиазолом), образованного с перхлоратом меди и лигандами 2-амин-5-этилтио-1,3,4-тиазиазолом и 1,10-фенантролином. Структура полученного комплекса была исследована с использованием современных квантово-химических расчетов, анализа передних молекулярных орбиталей (FMO), инфракрасной спектроскопии, сканирующей электронной микроскопии (СЭМ), дифференциального термического анализа и рентгеноструктурный анализ (РСА). Комплекс $[CuL_3(phen)](ClO_4)_2$ демонстрирует тетрагональную пирамидальную структуру с пятикоординационной геометрией, где ион Cu(II) координируется с тремя атомами азота тиадиазольных колец и двумя атомами азота бидентатного лиганда фенантролина, в то время как два перхлорат-иона находятся во внешней сфере комплекса.

Ключевые слова: *комплекс, бидентатный лиганд, передние молекулярные орбитали (FMO), ИК-спектр, элементный анализ, HOMO, LUMO, электростатический потенциал*

Abstract. This article presents the synthesis method and structural study of a new 1,10-phenanthroline-tris(2-amino-5-ethylthio-1,3,4-thiadiazole)copper(II)perchlorate complex formed with copper perchlorate and the ligands 2-amino-5-ethylthio-1,3,4-thiadiazole and 1,10-phenanthroline. The structure of the obtained complex was investigated using modern quantum-chemical calculations, Frontier Molecular Orbital (FMO) analysis, infrared spectroscopy, scanning electron microscopy (SEM) and differential thermal analysis and X-ray Structural Analysis (RSA). The $[CuL_3(phen)](ClO_4)_2$ complex exhibits a tetragonal pyramidal structure with a five-coordinate geometry, where the Cu(II) ion coordinates to three nitrogen atoms of the thiadiazol rings and two nitrogen atoms of the bidentate phenanthroline ligand, while two perchlorate anions are located in the outer sphere of the complex.

Keywords: *complex, bidentate ligand, Frontier Molecular Orbital (FMO), IR spectrum, elemental analysis, HOMO, LUMO, electrostatic potential.*

Introduction

In recent years, researchers have paid special attention to the synthesis and study of the physicochemical and biological properties of metal complex compounds with nitrogen- and sulfur-containing heterocyclic ligands, which is due to their great theoretical and practical significance. It is known that heterocycles occupy one of the leading places in their significance among already known drugs of synthetic and natural origin. The introduction of new functional groups into known drugs obtained on the basis of heterocyclic compounds and the study of their effect on changes in biological activity is one of the urgent tasks of modern chemistry. It is known that substances with five-membered heterocycles in their structure, including the thiadiazole cycle, have a wide range of biological activity. The sulfur atom of thiadiazole imparts lipophilic properties to these compounds, which ensures their permeability through biological membranes. Among the derivatives of thiadiazole, compounds with bronchodilatory, anti-inflammatory, analgesic, antioxidant, antiviral, antibacterial and other types of activity are known.

Literature Rewiew

It is known that five-membered heterocyclic substances, including thiadiazole derivatives, are of particular importance among heterocyclic compounds and have been found to possess broad biological activity. According to the literature, thiadiazole derivatives have antibacterial, antimicrobial, herbicidal, and fungicidal properties [1]. Complexes of 3d-metals with biologically active heterocyclic ligands, particularly thiadiazoles, are of particular interest due to their potential use as biological preparations in medicine and agriculture [2]. The presence of several donor atoms in the 2-amino-5-ethylthio-1,3,4-thiadiazole molecule also allows the ligand to form numerous coordination compounds with transition metal ions through mono- and bidentate coordination, which have been studied using various methods [3-4]. In some of the cited literature, mixed-ligand complexes of transition metals such as nickel, copper, and cadmium with 2-methyl-5-thiol-1,3,4-thiadiazole as the main ligand and additional ligands such as pyridine, EDA, and phenanthroline have been synthesized [5-6]. In addition, it has been found that the reaction of 2-amino-1,3,4-thiadiazole with

Co(III) perchlorate in acetonitrile results in the formation of a chelated complex with a square planar structure, and the addition of pyridine as an additional ligand leads to the formation of a chelated metallo-complex compound with an octahedral structure [7].

Research Methodology

For the complex synthesis, 2-amino-5-ethylthio-1,3,4-thiadiazole ligand weighing 0.0322 g (0.0002 mol) was dissolved in 3 ml of ethanol. An additional ligand, 1,10-phenanthroline, weighing 0.018 g (0.0001 mol) was dissolved in 2 ml of ethanol. Copper(II) perchlorate ($Cu(ClO_4)_2$) weighing 0.0262 g (0.0001 mol) was dissolved in 2 ml of water. The ligand solution was then added to this solution and stirred at 50 °C for 30 minutes, resulting in a transparent green color change. After 30 minutes, the 1,10-phenanthroline solution was added dropwise, causing the solution to turn deep green. The reaction continued for another 30 minutes and was then left to crystallize. After three days, fine elongated green crystals formed. The yield was 80%, with a melting point range of 190.9-193.4 °C.

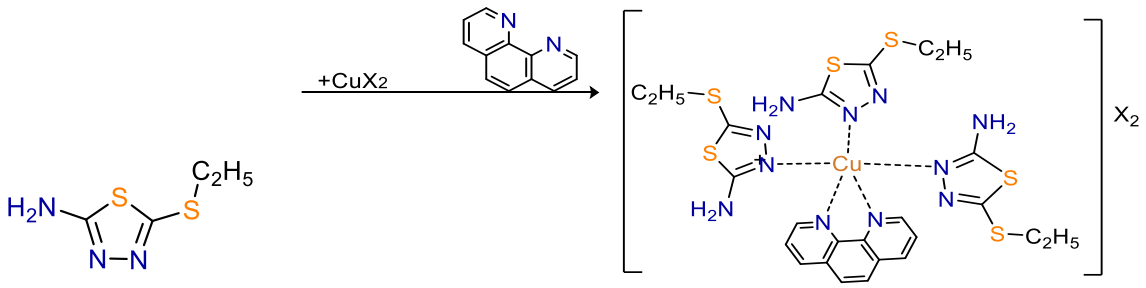

Analysis and Results

The synthesized ligand is characterized by the presence of various functional groups with multiple donor atoms. To achieve the targeted synthesis of complexes, quantum chemical calculations of the ligand's reactivity were performed using the Gaussian 09 software package. Some physicochemical parameters of the optimized system are presented below (Table 1).

Table 1. Some physicochemical parameters of the optimized complex molecule.

Complex	Dipole moment Debye	Optimization energy (Hartree)	Energy (eV)			
			HOMO	LUMO	ΔE	The hardness degree η
$[CuL_3(phen)](ClO_4)_2$	8,298632	-1778,046123	-13,916	-4,277	9,639Ev	2,31

Electrophilic and Nucleophilic Reaction Prediction Electrostatic surface potentials were obtained with optimized B3LYP / 6–311G(d,p) / Lanl2DZ geometry to predict reaction centers for electrophilic and nucleophilic processes. Different values of electrostatic potential on the surface are represented by various colors, showing an increasing potential order: red < dark orange < yellow < green < blue. Negative red MEP regions correlate with nucleophilic reaction activity, while positive blue areas relate to electrophilic activity. Negative (red) regions are located on the nitrogen atoms of the thiadiazole ring and around hydrogen atoms, while positive (blue) areas are

found nearby. The results indicate that the formation energy for the $[CuL_3(phen)](ClO_4)_2$ complex is -1778.046123 Hartree, with a molecular dipole moment of 8.298632 Debye.

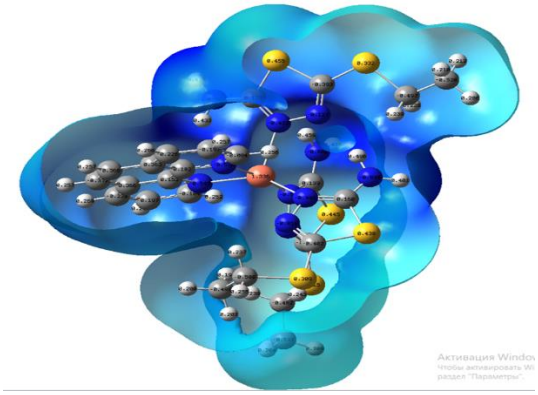

Figure 1. Molecular Electrostatic Potential (MEP) Diagram of the Complex

HOMO, or highest occupied molecular orbital, determines the coordination possibilities of a ligand molecule with a metal ion. By analyzing the charge values and the localization of the HOMO, it can be concluded that the donor centers, capable of coordinating with the metal ion, are the nitrogen atoms of the thiadiazole ring (-13.916 eV and -4.277 eV) and the nitrogen of the NH_2 group (-9.639 eV). This information is crucial for the ligand's reactivity and its interaction with the metal ion.

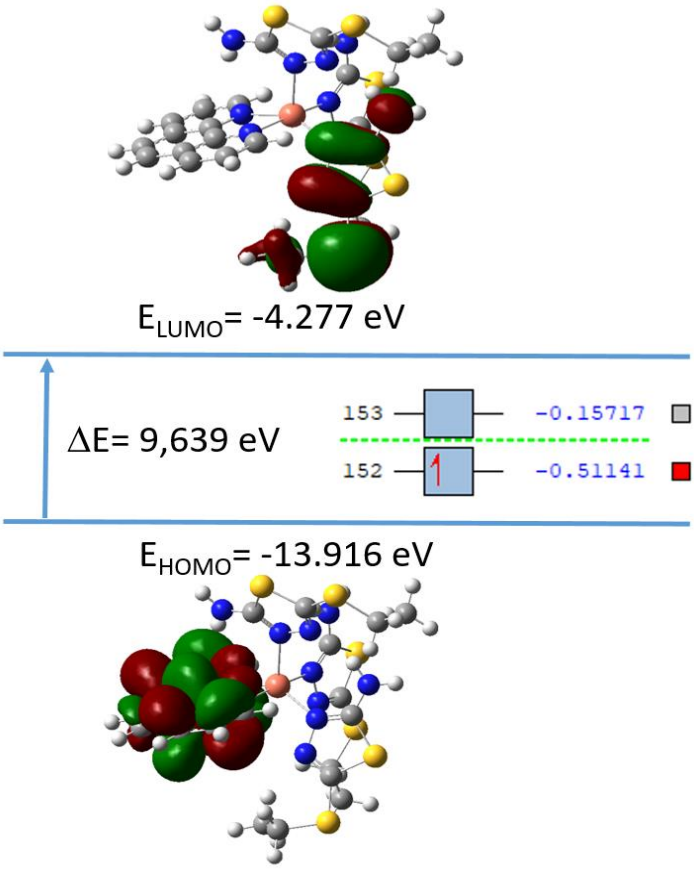

Figure 2. FMO diagram of the $[CuL_3(phen)](ClO_4)_2$ complex.

The IR spectra of the synthesized complex compound were studied to determine the coordination centers. In the IR spectrum of the ligand, characteristic absorption zones of N-H and C-H functional groups' stretching vibrations were identified in the high-

frequency region at 3256 cm^{-1} and 3093 cm^{-1} [10]. In the mid-frequency regions, absorption zones of symmetric and asymmetric vibrations of the C=N functional group at 1619 cm^{-1} (ν_s C=N), 1420 cm^{-1} (ν_{as}C=N) and deformation vibrations of the NH_2 amino group were observed in the region of 1522 cm^{-1}. Valent vibrations of =N-N= and C-S bonds were recorded in the ranges of 1049-1080 cm^{-1} and 611-673 cm^{-1}, respectively.

Table 2. The main frequencies (cm^{-1}) in the IR spectra of 2-amino-5-ethylthio-1,3,4-thiadiazole, 1,10-phenanthroline and the complex compound obtained from them.

Compound	ν_s (C=N)	ν_{as} (C=N)	ν (N-N)	ν NH_2	ν (C-S)	δ NH_2	M-N	ν (C-H)	δ (C-H)
2-amino-5-ethylthio-1,3,4-thiadiazole	1619	1420	1049	3256	673	1522	-	-	-
1,10-phenanthroline	1616	1421	-	-	-	-	-	3033	724
$[CuL_3(phen)](ClO_4)_2$	1611	1436	1045	3301	648	1518	434	3194	764

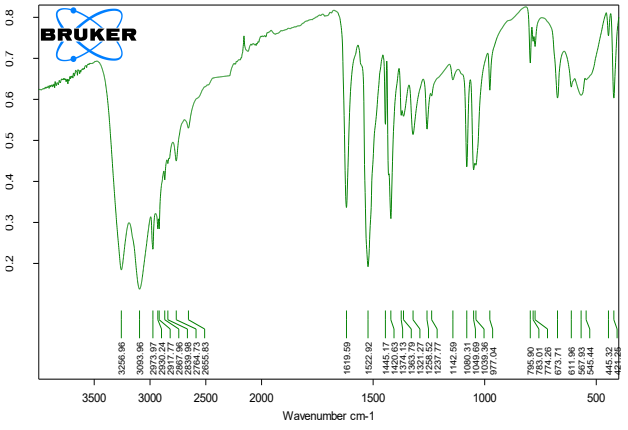

(a)

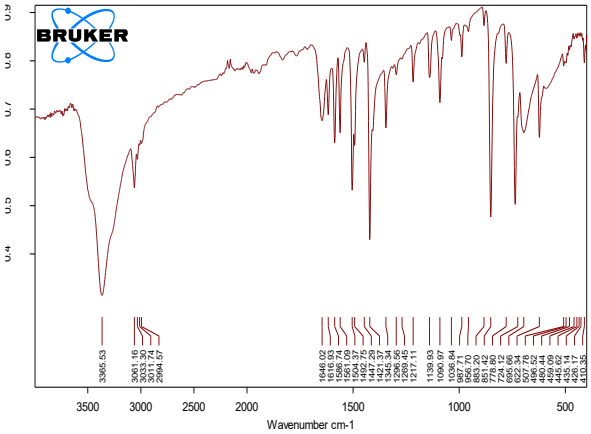

(b)

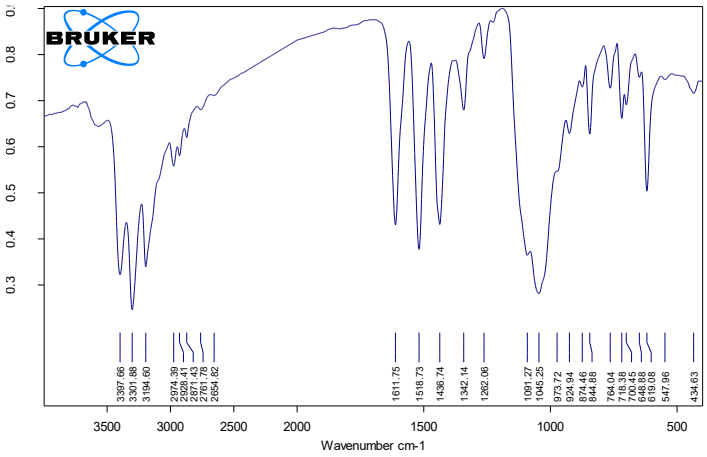

(c)

Figure 3. IR spectroscopy of 2-amino-5-ethylthio-1,3,4-thiadiazole (a), 1,10-phenanthroline (b), and the $[CuL_3(phen)](ClO_4)_2$ (c) complex.

In the IR spectrum of 1,10-phenanthroline, characteristic absorption zones of vibrations in the high-frequency region, absorption zones of symmetric and asymmetric vibrations of the C=N functional group at 1616 cm^{-1} (ν_s C=N) and 1421 cm^{-1} (ν_{as}C=N) in the mid-frequency regions were identified. In the obtained complex

compounds, weak, less intense absorption lines belonging to the ν(C=N) group appear in the 1611 cm^{-1} absorption regions, with a difference of 8 cm^{-1} compared to the free ligand. Furthermore, we can observe new absorption lines in the 434 cm^{-1} regions, belonging to the vibration of ν(M-N) bonds, which were not observed in the spectrum of the ligand in the complex compound [11]. At the same time, due to the difficulty in determining which of the endocyclic nitrogen atoms is coordinated based on the IR spectral data, for Cu(II) complexes, based on the obtained RSA results, we can confirm that, in the case of the synthesized complexes, coordination with the metal atom likely occurs through the strongly electron-donating endocyclic nitrogen atom located at the 3-position relative to the amino group (Table 2).

The obtained complex compound was studied using scanning electron microscopy (SEM). Based on the SEM analysis data, we can see that the mass percentage concentrations of Cu, C, N, O, S, and Cl elements in the $[CuL_3(phen)](ClO_4)_2$ complex compound are C-47.3%, N-19.74%, O-17.82%, S-8.11%, Cl-2.23%, and Cu-4.80%, respectively. This allowed us to derive the gross formula of the complexes. Based on the derived formulas, the composition of the complexes was determined.

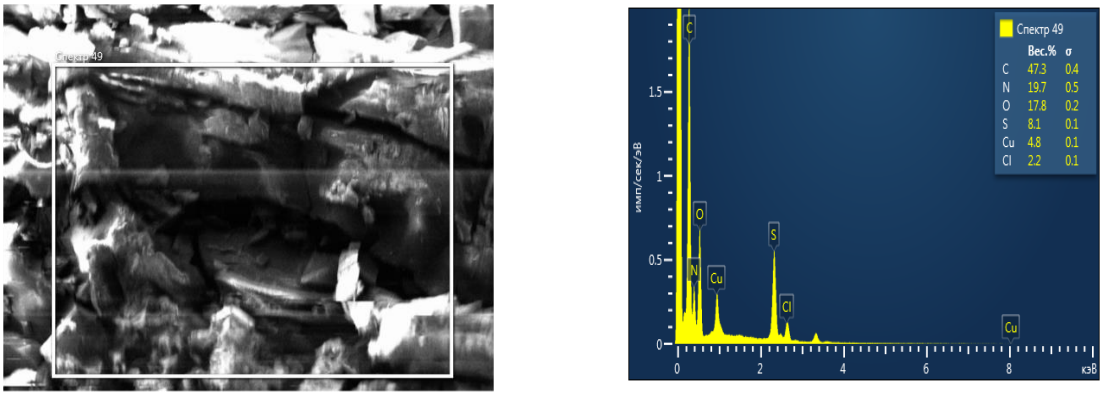

(a) (b)

Figure 4. Microstructure (a) and EDS data (b) of the $[CuL_3(phen)](ClO_4)_2$ complex compound**.**

To study the composition and structure of the synthesized coordination compound, its thermogravimetric analysis was performed. Analysis of the complex's thermogram showed that the thermal analysis studies of the $[CuL_3(phen)](ClO_4)_2$ complex in the temperature range from 20 to 230°C correspond to the loss of 3 ligand and phen molecules, with a 70% loss of organic ligand from the total mass of the complex. In this range, the DTA curve occurs with an exothermic process. It was determined that Cu_2O salt remains as the final product (Table 3).

Table 3. Thermal analysis results of the synthesized compound.

Compound	Temperature's thermoeffect states in ^0C	Nature of the effect	Mass loss %		Composition of thermolysis products
			Found	Calculated	
$[CuL_3(phen)](ClO_4)_2$	20-230	Exothermic	70%	72%	Cu_2O 29%

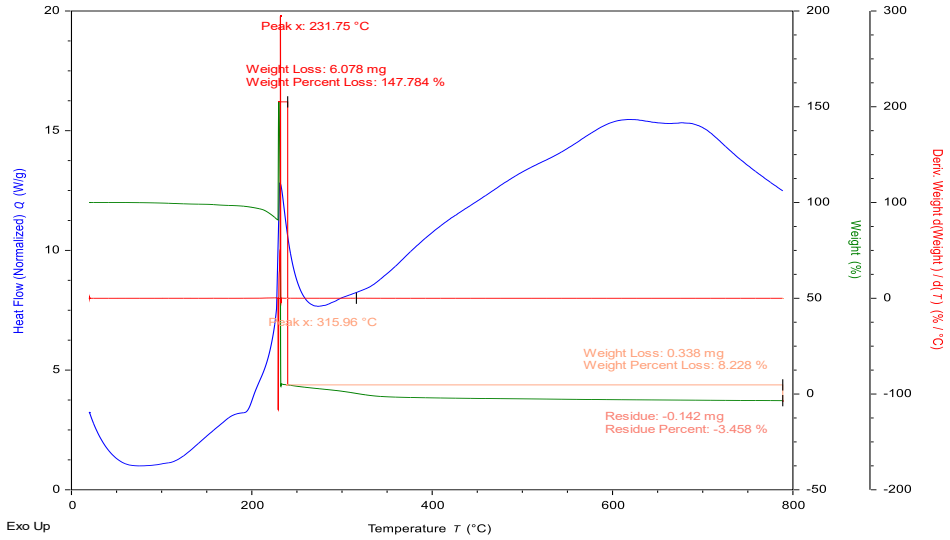

Figure 5. Thermogravimetric analysis of the $[CuL_3(phen)](ClO_4)_2$ complex compound.

The final effects on the thermogravimetric analysis of the synthesized complex at 315-640°C are related to the formation of the metal salt. Thus, the thermal study data confirmed the correctness of the proposed complex formula based on the results of elemental analysis and spectroscopic studies. Based on the results of the composition, structure, elemental, thermal, and spectral analyses of the synthesized complex, the complex compound was confirmed based on RSA. Crystallographic data: $CuC_{24}H_{29}N_{11}O_8S_6Cl_2$, M=926 g/mol, transparent green crystals with monoclinic syngony, space group Cc (No. 9), a=10.5913(6), b=27.6448(16), c=8.1987(5)Å, α=90°, β=128.425(2)°, γ=90°, V=1880.63(19) Å3, Z=4, Dcal=1.665 g/cm^3. Crystal dimensions: 0.36×0.24×0.17 mm^3. The crystal structure of the 1,10-phenanthroline-tris(2-amino-5-ethylthio-1,3,4-thiadiazole)copper(II) perchlorate complex revealed a copper nuclear at the center, coordinated with three 2-amino-5-ethylthio-1,3,4-thiadiazole ligands and one 1,10-phenanthroline acetyl ligand and two perchlorate ions in the outer sphere.

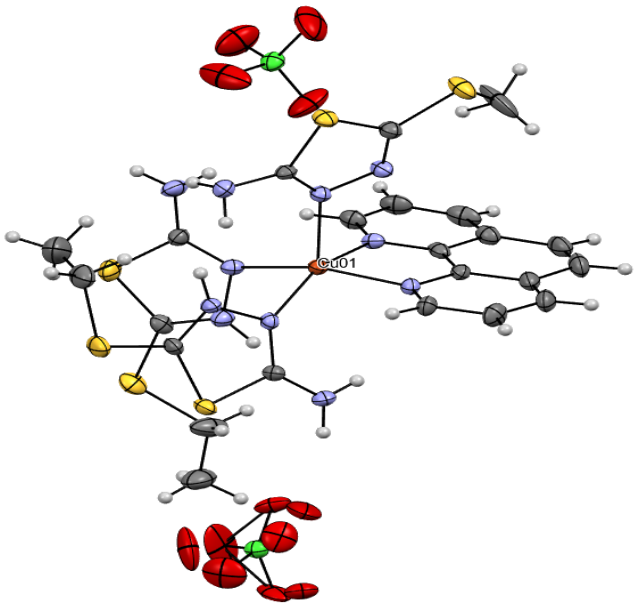

Figure 6. Structure of the complex compound $[CuL_3phen](ClO_4)_2$

Conclusion

A method for synthesizing a mixed-ligand complex compound of 2-amino-5-ethylthio-1,3,4-thiadiazole with 1,10-phenanthroline was developed. Using the Gaussian 09 software package, the reactivity of the 2-amino-5-ethylthio-1,3,4-thiadiazole L molecule was determined. A theoretical stability series of the complex was derived based on the electronic energies of the complex and the energy differences between the HOMO and LUMO of the complex molecule. It was found that the stability of the obtained complex compound is very high.

The composition, structure, and properties of the synthesized complex compound were studied using physicochemical methods: quantum chemical calculations, IR spectroscopy, scanning electron microscopy (SEM), differential thermal analysis (DTA), and X-ray structural (RSA) analysis. The results of these analyses showed that 2-amino-5-ethylthio-1,3,4-thiadiazole and 1,10-phenanthroline bind to the Cu atom in a Me:L:phen ratio of 1:3:1. Furthermore, it was determined that 2-amino-5-ethylthio-1,3,4-thiadiazole coordinates with the metal atom through the strongly electron-donating endocyclic nitrogen atom located at the 3-position relative to the amino group, and that it can form a complex with 1,10-phenanthroline that has significantly higher stability.

References:

[1] Toshmurodov T.T., Ziyaev A.A., Elmuradov B.Z., Ismailova D.S., Kurbanova E.R. “Highly Selective Synthesis and Fungicidal Activity of the Novel 2-Alkylthio-5-Amino-1,3,4 Thiadiazoles,” *Journal of Chemistry and Chemical Sciences*, Vol.6(3), 2016, pp.199-204.

[2] Mahasin Alias, Huda Kassum, Carolin Shakir “Synthesis, spectral, thermal and antibacterial studies of Cd(II), Mn(II) and Fe(III) complexes containing trithiocarbonate 1,3,4-thiadiazole moiety,” *Journal of King Saud University – Science*, 25, 2013, pp. 157–166.

[3] Kadirova Sh., Torambetov B., Abdireymov A. “Synthesis and X-ray diffraction study of the bis(aceto)-bis(2-amino-5-methylthio-1,3,4-thiadiazole) cobalt(II) complex,” *The 1st International Conference on Problems and Perspectives of Modern Science*. №9 (6), 2022.

[4] Torambetov B., Kadirova Sh., Xayrulayev G.U., Parpiyev A.N., “Synthesis and study of the structure of a five-coordinate complex of Cu(II) chloride with 2-amino-5-ethylthio-1,3,4-thiadiazole,” *Scientific, technical and industrial journal*, Tashkent, №9 (75), 2020.

[5] Dania R.K., Bharty M.K., Om Prakash, Singh R.K., Prashanth B., Singh S., Singh N.K. “Ni(II) and Co(III) complexes of 5-methyl-1,3,4-thiadiazole-2-thiol:syntheses, spectral, structural, thermal analysis, and DFT calculation,” *Journal of Coordination Chemistry*, №68 (15), 2015.

[6] Timo Huxel, Serhiy Demeshko, and Julia Klingele “2-Amino-5-(2-pyridyl)-thiadiazole as Bidentate Ligand,” *J. Inorg. General Chem*. 2015, pp. 1711–1717.

[7] Deng Y., Liu J., Zhang Q., Li F., Yang Y., Li P., Ma J. “Transition metal-induced reductive coupling of 2-amino-1,3,4-thiadiazole with acetonitrile: Synthesis and structural characterization of two Co(III) complexes with amidine,” *Inorganic Chemistry Communications*, №11 (4), 2008, pp. 433–437.

[8] Serba P.V., Blinov Yu.F., Miroshnichenko S.P. “Quantum-chemical calculations in the Gaussian program for the course Physics of low-dimensional structures,” Taganrog: *Publishing house of TTI SFU*, 2012, p. 100.

[9] Baranovsky V.I. “Quantum-chemical calculations of high accuracy,” *Study guide*, 2015, p. 89.

[10] Kazitsyna A.A., Kupletskaya N.B. “Application of UV, IR and NMR spectroscopy in organic chemistry,” M.: *Book on Demand*, 2013, p. 264.
[11] Tarasevich B.N. “IR spectra of the main classes of organic compounds,” Reference materials. M.: *Moscow State University*, 2012, p. 54.

UDC: 5, 57, 591.2, 595.7, 502, 648

THE IMPACT OF ATTAGENUS SMIRNOVI ON CULTURAL AND DOMESTIC ASSETS: CHALLENGES AND SOLUTIONS

Atajanova Shirin Masharibovna
Doctorate Student, Urgench State University named after Abu Rayhan Biruni
shirinatajanova1979@gmail.com

Abdullaev Ikram Iskandarovich
Professor, Vice president of Khorezm Ma’mun Academy
ikram.abdullaev1966@gmail.com

Annotatsiya. Ushbu maqolada Attagenus smirnovi (gilam qo‘ng‘izi)ning madaniy meros obyektlari va uy-joy mulkiga yetkazayotgan zararli ta’siri o‘rganilgan. Ayniqsa, tarixiy yodgorliklar va muzey kolleksiyalariga, jun, ipak va charm buyumlariga yetkaziladigan jiddiy zarar ko‘rsatib o‘tiladi. Monitoring natijalariga ko‘ra, hasharotlar tufayli yuzaga keladigan mexanik va biologik shikastlanishlar katta xavf tug‘diradi. Maqolada mavjud muammolar va himoya, hamda tiklash bo‘yicha amaliy yechimlar yoritilgan.

Kalit so‘zlar: *Attagenus smirnovi, gilam qo‘ng‘izi, madaniy meros, uy-joy mulki, muzey kolleksiyalari, jun, ipak, zararkunandalarga qarshi kurash, tiklash, saqlash.*

Аннотация. В работе исследовано разрушительное воздействие жука-кожееда Attagenus smirnovi на культурные объекты и бытовое имущество. Особое внимание уделено историческим памятникам и музейным коллекциям, где данный вредитель наносит значительный ущерб изделиям из шерсти, шелка и кожи. По результатам мониторинга, серьезную угрозу представляют как механические, так и биологические повреждения, вызванные вредителями. В статье рассматриваются современные вызовы и предлагаются практические решения по защите и восстановлению.

Ключевые слова: *Attagenus smirnovi, кожеед, культурное наследие, домашнее имущество, музейные коллекции, шерсть, шелк, борьба с вредителями, реставрация, сохранение.*

Abstract. The study examines the destructive effects of Attagenus smirnovi (the brown carpet beetle) on both cultural heritage sites and household assets. Special attention is given to historical monuments and museum collections, where the

beetle causes significant damage to organic materials such as wool, silk, and leather. Based on monitoring data, both mechanical and biological damage, primarily from pest infestations, pose serious threats. The article discusses current challenges and proposes practical solutions for protection and restoration.

Keywords: *Attagenus smirnovi, brown carpet beetle, cultural heritage, household assets, museum collections, wool, silk, pest control, restoration, preservation.*

Introduction

Attagenus smirnovi: A Threat to Cultural and Domestic Assets in Uzbekistan. Attagenus smirnovi Zhantiev, or the brown carpet beetle, is a serious insect pest threatening cultural heritage and domestic items across Eurasia. Originally described from Central Asia, the species has spread rapidly due to international trade, urbanization, and relocation of museum collections. It is now common in regions with temperate and continental climates and has adapted to anthropogenic environments. In Uzbekistan, Russia, Europe, and elsewhere, the beetle is a major cause of damage to organic materials—especially wool, silk, leather, and felt—posing a significant risk to historical monuments, museum artifacts, and private collections [1, 2]. The beetle's larvae, covered in long setae and well-camouflaged, feed on organic materials, causing extensive mechanical damage. Adults disperse the species, but the larvae are the destructive stage, often acting unnoticed for long periods [3].

In Uzbekistan, infestations have been recorded in historical cities such as Khiva, Samarkand, and Bukhara, particularly in sites included on UNESCO's World Heritage list. Monitoring in the Khorezm region showed high infestation rates in poorly ventilated storage areas with fluctuating humidity. Damaged items included antique carpets, wall hangings, and ceremonial garments. Though *A. smirnovi* does not attack cellulose, its destruction of textiles and fur has a comparably severe effect on historical interiors and museum displays.

Surveys in Uzbekistan's national museums revealed that up to 30% of organic-based collections showed signs of insect damage, with *A. smirnovi* being the dominant pest. Similar reports from institutions like the State Hermitage Museum, the British Museum, and the National Museum of Iran underline the widespread nature of this threat [4,5]. The economic impact is substantial—restoration is expensive, time-consuming, and often cannot fully recover the original materials. In households across Tashkent, Samarkand, and the Fergana Valley, infestations are typically identified only after visible damage appears—bald spots, holes in wool items, or frass accumulations.

Literature Review

Attagenus smirnovi in Uzbekistan: A Threat to Cultural Heritage and Domestic Textiles. In Uzbekistan and throughout Central Asia, the brown carpet beetle (*Attagenus smirnovi* Zhantiev) has emerged as a serious threat to museum collections and domestic textiles. First identified in urban areas like Tashkent and Bukhara in the late 20th century, the beetle is now widespread, with infestations reported in homes, museums, and historical buildings across Uzbekistan, Kazakhstan, Russia, and the Caucasus [1]. A member of the Dermestidae family, *A. smirnovi* targets protein-based materials such as wool, silk, leather, fur, and feathers. These are commonly found in

carpets, wall hangings, garments, and book bindings—many of which hold cultural and historical significance. Field research conducted at the State Museum of Applied Arts (Tashkent, 2017–2019) identified *A. smirnovi* as the most prevalent pest, especially in poorly ventilated storage areas [2]. Infestation risk increases in buildings with stable but humid microclimates. Structures in cities like Samarkand, Khiva, and Shahrisabz—often made of adobe with limited ventilation-create ideal conditions (18–26°C, 50–70% humidity) for beetle development. Larvae may feed undisturbed for 9 to 18 months, causing damage that often goes unnoticed until spring cleaning or inventory audits reveal holes, frass, and threadbare patches (Figure 1).

Figure 1. Damage by *A. smirnovi* larvae on a 19th-century Samarkand carpet.

Adult females lay eggs in concealed textile folds or under furniture. Larvae, covered in long setae, feed on organic materials, leaving behind frass, shed skins, and grazing marks. In Khiva's Ichan-Kala Museum Reserve, infestations affected over 40 m² of carpeted floor.

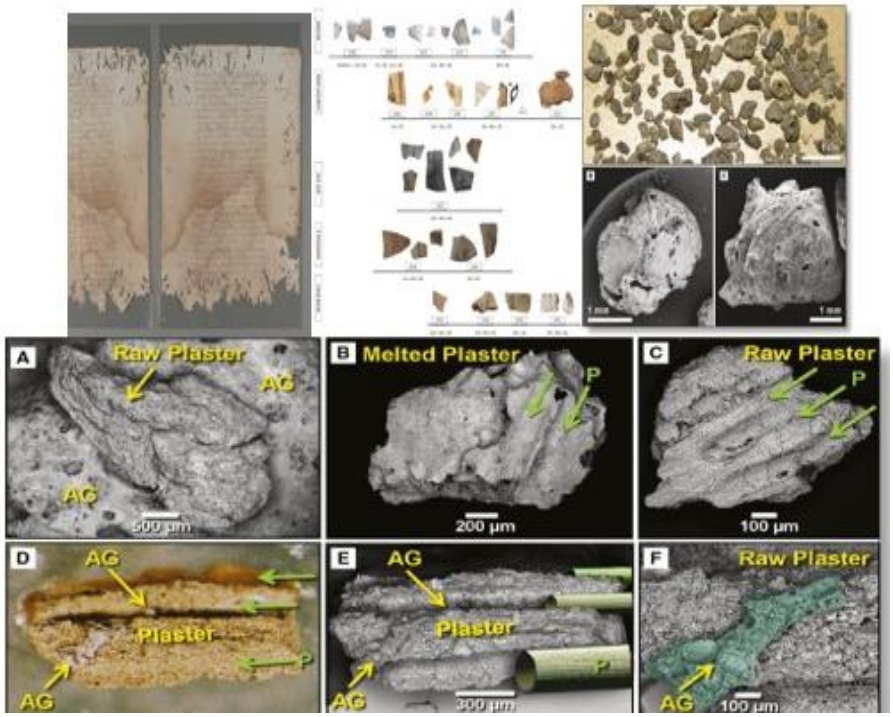

Figure 2. Larval debris and frass accumulation in felt storage, Bukhara Ethnographic Museum.

Similar signs appear in private homes—particularly under heavy furniture and in rolled-up textiles [3]. Larval feeding not only causes mechanical damage but also leads to secondary deterioration. Damaged fibers allow mold, bacteria, and other insects to

colonize. Laboratory analysis from the Nukus Museum confirmed that damaged items often showed elevated pH, fungal growth, and mixed pest presence. In over 70% of carpet restoration cases, *A. smirnovi* was involved as a primary or contributing cause (Figure 2).

Comparative studies show that while termites destroy wood and cellulose, *A. smirnovi* poses a comparable threat to textile heritage. Research by Kolomiets et al. (2019) and Umarkhodjaev et al. (2021) found beetle-infested sites suffered higher textile loss, while termite damage was limited to structural materials [4]. The beetle spreads through contaminated museum objects, traveling exhibitions, and even personal belongings. The Samarkand Regional Museum reported that carpets loaned to international events were twice as likely to return with beetle damage. Passive transport via luggage, clothing, or packaging materials has also been documented [5]. To combat the problem, museums now use pheromone traps, digital sensors, and cameras for early detection. Integrated pest management (IPM)—including humidity control, isolation of infested items, and routine inspections—has improved outcomes in larger institutions. However, budget limits and lack of training still hinder regional and rural museum efforts. National campaigns encourage preventive measures in homes: regular cleaning, early repair of damage, and dry, sealed storage for ceremonial garments. Yet, surveys by the Uzbek Pest Control Association (2022–2023) show public awareness remains low. Infestations are often identified only after significant damage is visible [6]. Chemical treatments have proven inconsistent. Trials in Karakalpakstan showed that larvae often survived multiple household insecticide applications. Only freezing or professional fumigation was fully effective. For museum objects, conservationists prefer non-chemical approaches like freezing, anoxic chambers, or controlled heating. International cooperation continues to play a vital role. Workshops funded by ICCROM and ICOM have produced identification keys, pictorial manuals, and emergency protocols now in use across Central Asia. As *A. smirnovi* continues to spread, joint monitoring and data sharing remain essential tools in protecting cultural and domestic assets.

Analysis and Results

Attagenus smirnovi is now recognized as a key agent of biodeterioration in museum environments and private households across Uzbekistan and Central Asia. From 2017 to 2023, research was carried out in Tashkent, Bukhara, Samarkand, and the Khiva Ichan-Kala Museum Reserve. Infestation levels were assessed in 16 museum storages, 7 archival buildings, and 24 private residences. Sampling involved visual inspection, trap placement, and textile analysis, with attention to temperature, humidity, and microclimatic conditions. The larvae of *A. smirnovi* showed a marked preference for wool carpets, felt hangings, fur-lined clothing, and silk. At the Tashkent State Museum of Applied Arts, 34% of examined carpets (n = 112) displayed feeding tracks, threadbare areas, and frass. In the Khiva Regional Museum, the highest infestations occurred in basement storage rooms where humidity exceeded 65% and temperatures ranged between 19–25°C. Display halls with climate control and visitor movement had minimal damage.

Three damage levels were identified:

A (Low): Surface grazing, small bald spots (<2 cm), isolated larval skins.
B (Medium): Irregular holes (2–10 cm), thinning pile, presence of larvae and shed skins.
C (Severe): Extensive pile loss (>10 cm), coalesced holes, weakened backing, and dust from frass and exuviae. Items in this category were often removed from display or required restoration.

In households in Samarkand and rural Fergana, severe damage was recorded where carpets and wall hangings had been stored without disturbance. In 7 out of 12 such homes, textiles exhibited connected holes, faded colors, and musty smells, indicating microbial activity in damaged fibers. Interviews showed that 82% of homeowners noticed damage only after at least a year. Environmental analysis showed infestation severity was closely tied to humidity and ventilation. In Samarkand's museum storage in 2022, mean humidity was 68.4%, with a 41% infestation rate. Storages with humidity below 55% had significantly lower activity.

Table 1. Environmental conditions and infestation rates (2021–2023).

Location	Temp., (°C)	RH, (%)	Objects	Infestation, (%)
Khiva Museum Storage	22.1	66.7	54	44
Tashkent Museum Storage	20.6	58.2	112	34
Samarkand Museum Storage	19.8	68.4	46	41
Fergana Household #1	23.0	62.3	8	75
Bukhara Household #4	21.2	51.0	12	16

Textile analysis revealed that larvae damage not only surface pile but also the backing of Uzbek carpets, leading to irreversible structural loss. SEM imaging (Samarkand, 2022) confirmed ruptured cuticles and signs of enzyme digestion. A major factor in *A. smirnovi* spread is the transfer of infested objects between museums, exhibitions, and homes. A sudden outbreak at Bukhara Regional Museum was linked to a silk robe collection returned from an international exhibition. Lack of isolation procedures allowed larvae and eggs to spread. Seasonal activity of *A. smirnovi* peaked in April–May and September–October, coinciding with moderate temperatures and post-rainfall humidity. Activity dropped in summer (dry heat) and winter (cold storage rooms below 14°C). Intervention trials confirmed the species' climatic sensitivity. In Samarkand's museum, dehumidifiers reduced humidity from 70% to 48%, lowering larvae numbers and damage by 70%. In another test, infested wool carpets were frozen (–22°C for 10 days), resulting in complete larval mortality. Most household insecticides were ineffective, especially in thick textiles. Only professional fumigation or anoxic treatment yielded consistent results, though these are reserved for high-value museum pieces due to cost and logistics.

A review of restoration records at the Nukus Museum of Art (2018–2022) showed that over 80% of textile repairs were due to pest damage, with *A. smirnovi* responsible in 61% of cases. Restoration staff focused on patching holes, recreating decorative patterns, and stabilizing backing—often with only partial recovery of the object's original value. In summary, the damage caused by *Attagenus smirnovi* is strongly influenced by environmental conditions, storage practices, and object movement. The beetle poses a significant risk to heritage textiles, paralleling termite impacts on

wooden structures but affecting animal-based materials. Preventive strategies—including improved storage, climate control, and controlled treatment—are essential for long-term protection of cultural assets.

Damage caused by Attagenus smirnovi to wool, silk, and fur components in museum and household collections is primarily linked to technical shortcomings and external factors. Favorable conditions for beetle infestation include an abundance of protein-based materials, high humidity, lack of ventilation, and limited sunlight. Excess dust and textile debris in storerooms or under furniture provide ideal habitats for larval development. Elevated humidity, often resulting from poor building design or inadequate climate control, not only attracts the pest but also promotes fungal growth (Aspergillus, Penicillium, Cladosporium), which pre-digest fibers and make them easier for larvae to consume. In such conditions, A. smirnovi larvae can destroy up to 60–70% of organic fibers in infested objects, whereas in dry, ventilated rooms, damage is usually minimal. Uncontrolled transfer of contaminated items between institutions further accelerates the spread of infestations.

Conclusion

To prevent the development and spread of Attagenus smirnovi and minimize damage to valuable textile and ethnographic collections, it is recommended to maintain low indoor humidity, ensure regular cleaning, and increase ventilation in storage and display areas. All incoming carpets, garments, and furs should undergo mandatory pest inspection and quarantine before placement. Preventive freezing or anoxic treatment is advised for at-risk items. Immediate repairs to building envelopes and climate control systems are necessary in museums with recurrent infestations. Public awareness campaigns and staff training on pest identification and handling will further reduce the risk of widespread loss. Preserving Uzbekistan's textile heritage and household heirlooms not only protects national culture but also strengthens the region's global reputation as a center of traditional art and history.

References:

1. Zhantiev R.D. "Carpet beetles of the genus Attagenus (Coleoptera, Dermestidae) in the fauna of the USSR," *Zoological Journal*, 52(11), 1973, pp. 1707–1716.
2. Kolomiets A.N., Kadej M., Háva J., & Smirnov A. "The spread of Attagenus smirnovi Zhantiev, 1973 (Coleoptera: Dermestidae) in the European part of Russia and damage to museum collections." *Contemporary Problems of Ecology*, 12(4), 2019, pp. 482–489. DOI: 10.1134/S1995425519040053
3. Pinniger D.B. "Integrated pest management in cultural heritage," 2nd Edition. *Archetype Publications*, London, 2015.
4. Kadej M., Háva J. "Contribution to the knowledge of the biology and distribution of Attagenus smirnovi Zhantiev, 1973 (Coleoptera: Dermestidae) in Central Europe." *Polish Journal of Entomology*, 85(2), 2016, pp. 191–198. DOI: 10.1515/pjen-2016-0014
5. Atakulov M., Khasanov T., Tursunov S. "Museum pest monitoring and control: A case study from Uzbekistan," *Central Asian Journal of Conservation Science*, 6(3), 2022, pp. 112–124.
6. Umarkhodjaev D., Kolomiets A.N., Rakhimova N., Sattorov T. "Assessment of biological deterioration risks for textile artifacts in Uzbek museums," *Uzbek Journal of Natural Sciences*, 9(1), 2021, pp. 55–63.

UDC: 62, 631, 631.5

DYNAMIC ANALYSIS OF THE FRAME BETWEEN TWO AXLES OF THE VARIABLE BASE TRACTOR

Artikov Makhmud Sultonboevich
Assistant Laboratory, Urgench State University named after Abu Rayhan Biruni
artikovmaxmud198@gmail.com

Khusainov Bakhtiyor
Associate Professor (PhD), Urgench State University named after Abu Rayhan Biruni
baxtiyor156015@gmail.com

Annotatsiya. Ushbu maqolada O‘zbekiston qishloq xo‘jaligida suv tanqisligining salbiy ta’sirlarini kamaytirish uchun yomg‘ir bilan sug‘oriladigan qiya tepalikli yer maydonlariga ishlov berishda muhim ahamiyatga ega bo‘lgan o‘zgaruvchan bazali traktor modifikatsiyasining asos ramasi mustahkamligi tekshirildi. Bunda yer maydoniga ishlov berishda yuzaga kelishi mumkin bo‘lgan yuklanishlar qiymatlari va kuch yo‘nalishlari aniqlanib bu yuklanishlarning bazasi o‘zgaruvchan traktorga ta’siri SolidWorks dasturi orqali simulyatsiya qilindi.

Kalit so‘zlar: *O‘zgaruvchan bazali traktor, old rama, qo‘shimcha yuklanishlar, kuchlanish.*

Аннотация. В данной статье рассматривается прочность основной рамы модификации трактора с изменяемой базой, которая имеет важное значение при обработке наклонных земельных участков, орошаемых дождевой водой, с целью снижения негативного влияния дефицита воды в сельском хозяйстве Узбекистана. Определены значения нагрузок и направления сил, возникающих при обработке земельного участка, и с помощью программы SolidWorks смоделировано воздействие этих нагрузок на трактор с изменяемой базой.

Ключевые слова: *трактор с изменяемой базой, передняя рама, дополнительные нагрузки, напряжение.*

Abstract. This article examines the structural strength of the main frame of a variable-base tractor modification, which plays an important role in cultivating sloped lands irrigated by rainfall as a means to mitigate the negative impacts of water scarcity in Uzbekistan’s agriculture. The potential loads and force directions that may occur during land cultivation are identified and the effects of these loads on the variable-base tractor are simulated using SolidWorks software.

Keywords: *variable-base tractor, front frame, additional loads, stress.*

Introduction

Uzbekistan’s reliance on agriculture makes the development of efficient farming practices crucial. The construction of the Koshtepa canal in neighboring Afghanistan

poses a significant challenge as it threatens to reduce Uzbekistan's annual water consumption for agriculture by 15%. This situation highlights the need for innovative solutions that reduce water dependence in farming. Controlled Traffic Farming (CTF) presents a potential answer. However, implementing CTF requires modifications to tractors, specifically their front axles and wheelbases, to accommodate the unique configurations required by this farming technique. While Uzbekistan currently has variable-base tractors, their productivity is limited, and adjusting their wheelbase is labor-intensive and requires specialized techniques. Therefore, there is a need for advancements in tractor design and technology to support the adoption of CTF, enabling efficient and sustainable agriculture in Uzbekistan. In the current stage of wheel tractor design and development, all innovations incorporated into their construction are considered the most promising in terms of reducing the negative anthropogenic impact of the locomotion system, enhancing safety, improving interoperability, maneuverability, stability, and smooth running. Adjusting the wheelbase of four-wheel tractors plays a crucial role in addressing the challenge of improving their maneuverability, stability, and smooth running, as well as in tackling their pass-ability. Numerous studies have proven that changing the wheelbase enhances both the static and dynamic stability of tractors.

Literature Review

TTZ 80.10 universal hoeing tractor: TTZ 80.10 universal hoeing tractor is the product of the Tashkent Tractor Factory. TTZ means Tashkent Traktor Zavodi (Tashkent Tractor Factory). Tashkent Tractor Factory was established in 1942 as a plant producing ammunition. Since 1997, the joint enterprise “Uzbekkeystractor” was established, which produced tractors in cooperation with the US company “Keys.” Currently, low-clearance four-wheel tractors of the TTZ- 80.10 type are mainly used in the republic of Uzbekistan both in transport work and in agricultural operations in mountainous and sub-mountainous areas [1].

In this part we looked at variable base tractors and examined their advantages and also disadvantages. From this we can see that the construction of making the base variable is quite complicated. When changing the base of the universal-hoeing tractors used by us, simple designs are mainly used, that is, the change of the base in these tractors is carried out at the expense of changing the front axle:

1. Due to the change in the angle of the G-shaped elbow of the front axle, the change of the base of the tractor consists of a portal-type spring-loaded pivoting axle, variable track-driven steering wheels, a tubular steel beam, a front axle with a hinged connection to the semi-frame axle (Figure 1).

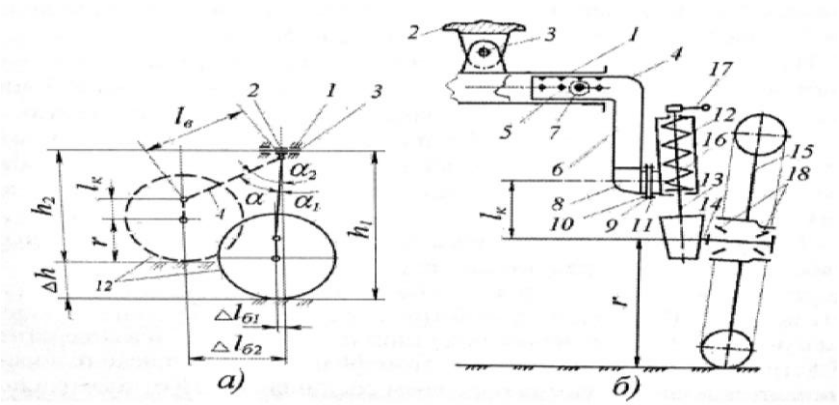

Figure 1. G-shaped elbow of the front axle.

2. Reversible front axle is one of the ways to change the base of the tractor, which requires less labor and has a simpler structure than the previous designs. Reversible front axle (Figure 2) consists of a tubular steel beam, a half-frame axle hinged with a front axle that can swing relative to this axis along the transverse surface.

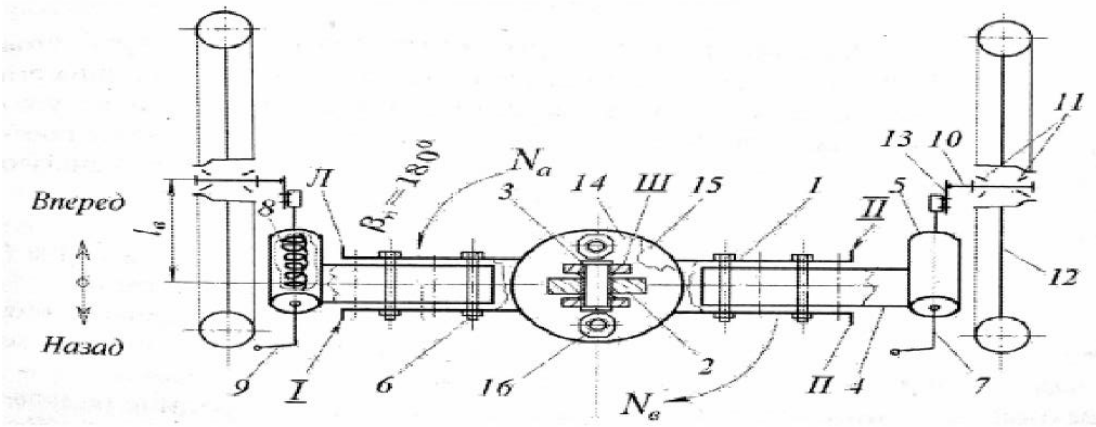

Figure 2. Reversible front axle, top view.

By using this construction on a four-wheel universal-hoeing tractor, it is possible to change the tractor base by 600 mm. But changing the base of the tractor using a reversible front axle is less labor intensive than the previous design, this design is also not very technological because it requires lifting tools (crane, jack or others) to change the base.

Research Methodology

As we have seen above, each base conversion mechanism has its own advantages and disadvantages. With this in mind, we would like to propose another construction, that is, another type of variable base mechanism construction. For new mechanism hydraulic cylinders are considered main parts. According to TTZ-80.10 tractor's frontal frame dimensions and cylinder's we made first draw of the mechanism (Figure 3).

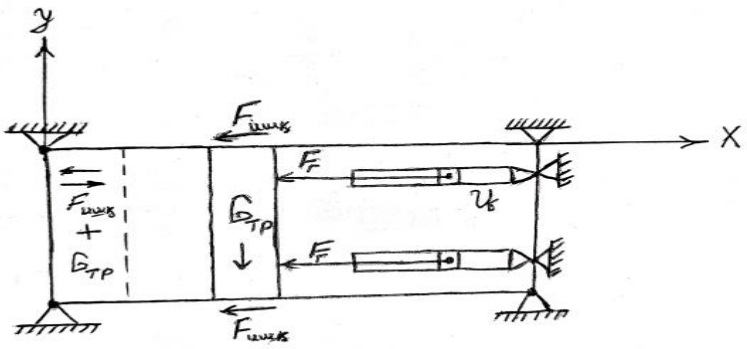

Figure 3. Calculation scheme.

We calculate the required power for the hydraulic cylinder. According to scheme (Figure 3) force equation as follow:

$$F_{hc} > F_f$$

On the other hand, distribution of weight between the front and rear wheels of the tractor had to be considered in evaluation of the actual loading on the modified front axle. A Canadian government department of Agriculture and development developed a guide on how to evaluate the weight distribution between the front and the rear wheel. The weight distribution depends on type of the tractor especially the type of drive. The table below shows the weight distribution as a percentage for the different types of tractors. These were considered using total ballasted weight or the working weight of the tractors.

Table 1. Tractor axle weight distribution [8].

Tractor drive type	Front Axle	Rear axle
2WD	30%	70%
4WD	55%	45%
FWA	40%	60%

According to that weight distribution we have calculated loading of the front axle (Figure 4).

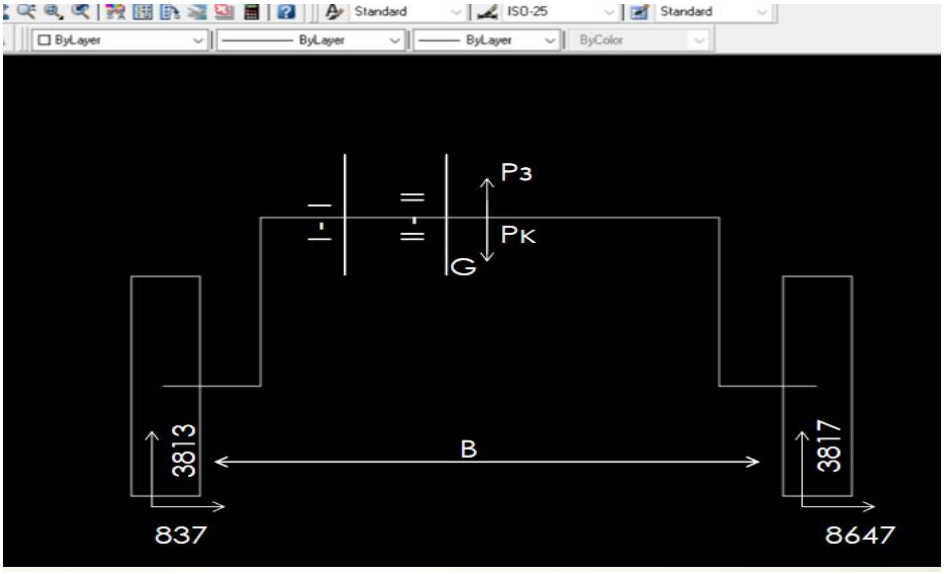

Figure 4. Weight distribution of the front axle on hilly land.

By this determined extra loading force quantities we have analyzed stresses of the tractor's front axle and base frame which may occur on the real farming fields. For this we used SolidWorks software program as mentioned in previous chapter.

Analysis and Results

First, we consider the effects of the tractor's own weight mass on the front axle, that is, as we determined in the previous chapter, the front axle of the tractor has a mass of 930 kg and this theft mass is formed when the base of the tractor is 2168 mm. Of course, when the tractor base changes the force of the affecting to the front axle also changes (increases/decreases). When the base of the tractor is extended to the maximum size of 2518 mm, the weight force acting on its front axle decreases due to the increase of the power shoulder (Mechanics: Law of Moments) and its value is 349.8 kg. With the help of these values, we will analyze whether the newly designed front axle of the tractor is resistant to the static forces acting on it or not through the FEM SolidWorks program. Figure 5 depicts the stress distribution within the model under the applied loading conditions. The maximum stress observed under these loading conditions is (2.37×10^{7}) MPa and minimum is (6.64×10^{2}) MPa.

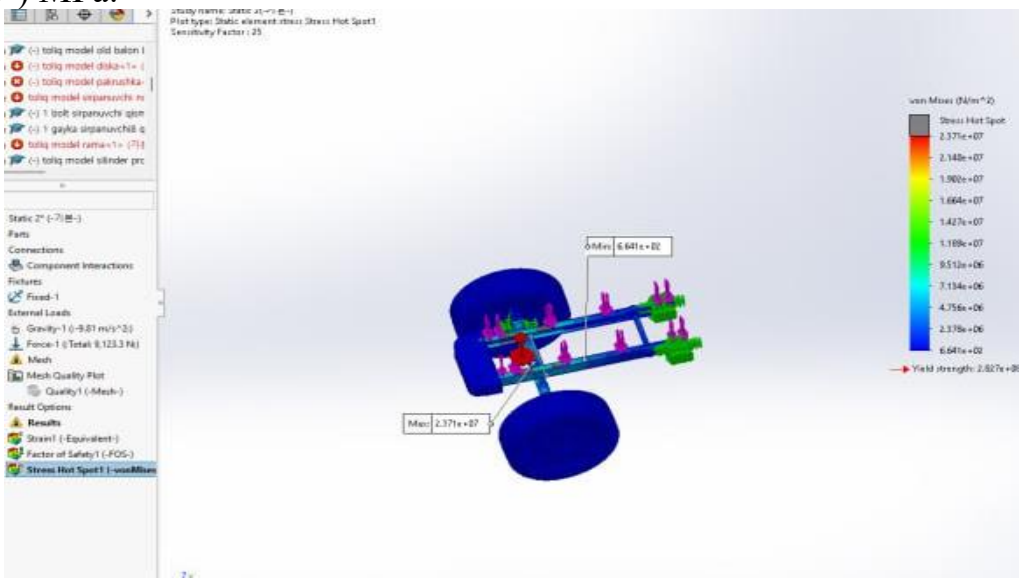

Figure 5. Von Mises Stress plot (base: 2168 mm).

Displacement result showed a maximum Displacement of (7.959×10^{-1}) mm at the areas red. Displacement result in Figure 32 below. Description of Displacement result: 7.959×10/100=0.7959mm so maximum Displacement is 0.7959 mm. New design using computer simulations (FEM SolidWorks) to determine its stability, maneuverability, and ability to work in different terrains. Our results showed that increasing the base by 16.1% significantly enhanced the tractor's stability by 18.8%, when navigating inclines.

Conclusion

By utilizing a variable base mechanism, we have significantly enhanced the versatility of the universal mowing tractor. This means it can now be used not only in mountainous and foothill regions but also in other areas where specialized tractors are typically required, thereby expanding its application range compared to other

conventional tractors. We have developed and established parameters for a variable base mechanism for a universal mowing tractor, resulting in a design that is more versatile, stable, and maneuverable than other universal mowing tractors. We believe that we have created a universal mowing tractor with a variable base that is both specialized and universal, offering increased stability and maneuverability, making it suitable for both mountainous and foothill regions as well as other conditions. As we mentioned above, new modified base mechanism also has disadvantages too it is one of the main issues to ensure the cleanliness of the rail surface of the moving part, which is one of the main parts in the base change, because when moving in the field and plowing the field, dust and other polluting elements are raised from the ground.

References:

[1] Decree of the President of the Republic of Uzbekistan dated March 4, 2015, № UP-4797 "On the program of measures to ensure structural transformations, modernization and diversification of production for 2015-2019."
[2] Akhmetov A.A., Usmanov I.I., Saidaminov S.S., Akhmedov Sh.A. "Universal-row-crop tractor," 2014.
[3] Fundamentals of scientific research," T. *Uqituvchi*, 1981.
[4] "Methods of field experiment (with the basics of statistical processing of research results)," M. *Agropromizdat*, 1985.
[5] Akhmetov A.A., Usmanov I.I., Akhmedov Sh.A., Atakulov H.K. "Universal-row-crop tractor," 2013.
[6] Akhmetov A.A., Usmanov I.I. "Universal row-crop tractor with a variable base," monograph, ed. R.D. Matchanov. RUz, SKB "Traktor," Tashkent: *Fan*, 2016.
[7] "Tractors TTZ 80.10 and TTZ 80.11," Operation and maintenance manual. 80.10-0000010IE. - Tashkent: *Tashkent Tractor Factory*, 2010.
[8] Sambamo Richard "FEA analysis of the tractor axle modification," 2014.
[9] Sean Laughery, Grant Gerhart, Paul Muench "Evaluating Vehicle Mobility Using Bekker's Equations." *US Army TARDEC Warren*, MI 48397-5000.
[10] Akhmetov A.A. "Evaluation of static strength of the front axle beam of a tractor with a variable base," *Strength of structures, seismodynamics of buildings and structures*.
[11] Pisarenko G.S. "Handbook of Strength of Materials." Kyiv: *Naukova Dumka*, 1975.
[12] Akhmetov A.A. "Front axles of a universal row-crop tractor for cotton purposes." Edited by R.D. Matchanov, Tashkent: *Fan*, 2014.
[13] Akhmetov A.A., Usmanov I.I. "Universal row-crop tractor with a variable base," monograph, ed. R. D. Matchanov. RUz, SKB "Traktor." Tashkent: *Fan*, 2016, p. 176.
[14] Khushnud Yakubov, Shavkat Ravutov, Anvarbek Masharibov and Islom Kadirov "Theoretical substantiation of the parameters of the debris removal device of the cotton picker apparatus." *BIO Web of Conferences* 116, 2024, p. 01017.
[15] Koyuncu A, Gökler M, & Balkan T. "Development of a design verification methodology including strength and fatigue life prediction for agricultural tractors" 2012.
[16] Raiko M.V. "Calculation of machine parts and units," Kiev: *Texnika*, 1966, p. 500.
[17] Dospekhov B.A. "Methodology of field experiment (with the basics of statistical processing of research results)." Moscow: *Agropromizdat*, 1985, p. 342-351.
[18] Kozlov L. Buriennikov Y. Piliavets V. Kotyk S. "Optimizationn of parameters of the mobile machine adaptive hydraulic circuit."

UDC: 62, 631, 631.5

IMPROVING THE STABILITY AND MANEUVERABILITY OF THE VARIABLE BASE TRACTOR

Artikov Makhmud Sultonboevich
Assistant Laboratory, Urgench State University named after Abu Rayhan Beruniy
artikovmaxmud198@gmail.com

Annotatsiya. O‘zbekistonda bazasi o‘zgaruvchan traktorlarning bir nechta turlari mavjud. Maqolada mayatnikli mexanizm yordamida bazasi o‘zgaruvchan traktorining bazasini o‘zgartirish mehanizmi nazariy jihatdan takomillashtirildi hamda turg‘unligi va manevrchanligi oshirildi. Traktor modifikatsiyasining bazasi mustahkamligi tekshirildi. Yer maydonini ishlov berish jarayonida yuzaga keladigan yuklanishlarning miqdori va yo‘nalishlari aniqlandi hamda ushbu yuklanishlarning bazasi o‘zgaruvchan traktor konstruksiyasiga ta’siri Cheklangan Elementlar Usuli (FEM) yordamida modellashtirildi.

Kalit so‘zlar: *O‘zgaruvchan bazali traktor, baza, mayatnikli mexanizm, kuchlanish, xavfsizlik kayfitsenti, yuklanish.*

Аннотация. В Узбекистане существует несколько типов тракторов с изменяемой колесной базой. В данной статье теоретически усовершенствован механизм изменения базы трактора с использованием маятникового механизма, а также повышены его устойчивость и маневренность. Проверена прочность базы модифицированного трактора. Были определены величины и направления нагрузок, возникающих в процессе обработки земельного участка, и с помощью метода конечных элементов (FEM) смоделировано их воздействие на конструкцию трактора с изменяемой базой.

Ключевые слова: *Трактор с изменяемой базой, База, Маятниковый механизм, Напряжение, Коэффициент запаса прочности, Нагрузка*

Annotation. Several types of variable wheelbase tractors are available in Uzbekistan. In this article, the mechanism for changing the wheelbase of a variable base tractor using a pendulum mechanism has been theoretically improved, and its stability and maneuverability have been enhanced. The structural strength of the modified tractor's wheelbase was tested. The magnitudes and directions of the loads occurring during soil cultivation were determined, and the impact of these loads on the structure of the variable wheelbase tractor was simulated using the Finite Element Method (FEM).

Keywords: *variable-base tractor, base, pendulum mechanism, stress, safety factor, load.*

Introduction

In our republic, widely used universal cultivator tractors include the TT3-30, T-40A, TT3-60, TT3-80, MTZ-100, MTZ-80, MTZ-100, MT-142, TT3-100LS, MH-130,

MHM-140, TL-100, and TS-130 models. Among them, only a few variants feature a mechanism with an adjustable wheelbase. In this regard, there has arisen a necessity to improve the variable wheelbase tractor. By changing the length of the tractor's wheelbase and solving this issue, it becomes possible to expand the use of universal cultivator tractors in mountainous and foothill regions.

Literature Review

Regarding this issue, researchers such as A.A. Akhmetov, I.I. Usmanov, Sh.A. Akhmedov, S.Yu. Promzalev, B.I. Plotke, S.I. Peisakhovich, Z.I. Piskozub, and others have conducted extensive scientific studies. They have published doctoral dissertations, monographs, and obtained patents. Their research primarily focused on modifying the tractor's front axle and frame as a basis for adjusting the wheelbase, one of them is "Adjusting the tractor's base by a pendulum front axle" (Figure 1). When modifying the tractor's wheelbase using such a mechanism, the hydraulic cylinder is directly mounted to the front linkage elements. The working principle of the wheelbase adjustment mechanism operates in the following sequence. When it is necessary to extend the tractor's wheelbase, the piston rod of the hydraulic cylinder begins to rotate the linked arm forward in the outward direction through a hinge connection. At the same time, the bracket moves forward until it reaches the support point, that is, until it extends to a length of 2L.

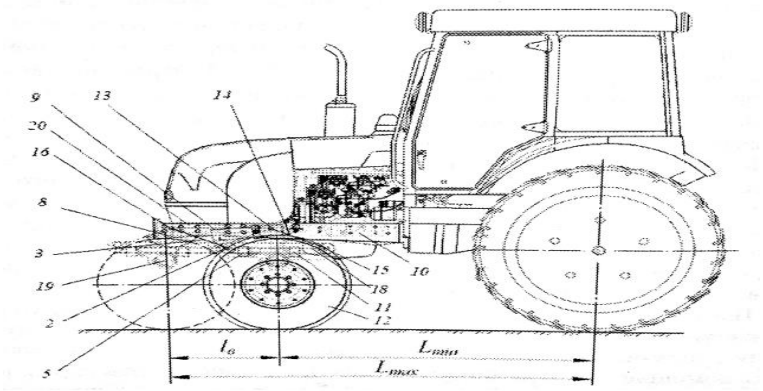

Figure 1. Scheme for modifying the tractor's wheelbase using a pendulum-type front axle.

Once the bracket reaches the support, it is secured in place using a locking mechanism (fixator). To shorten the tractor's wheelbase, the rod is retracted back into the hydraulic cylinder. In this process, the rod rotates the linkage arm, which is connected to the axle via a hinge. The bracket moves backward until it reaches and rests against the support. Once the bracket contacts the support, it is secured in place with a locking mechanism (Figure 2).

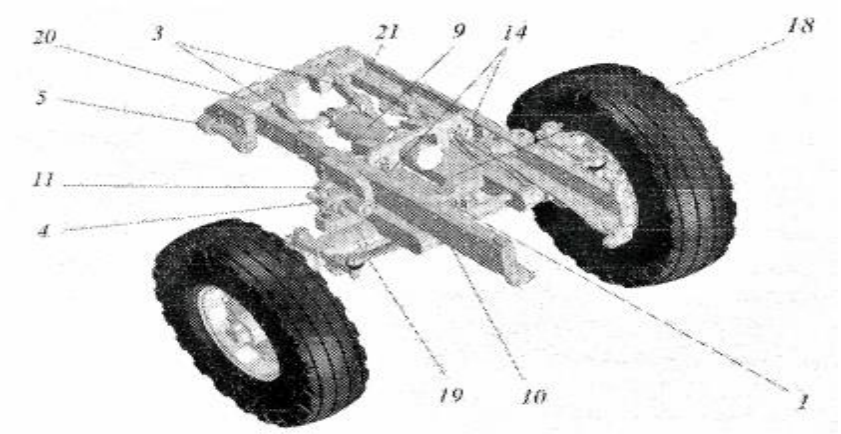

Figure 2. Tractor wheelbase adjustment mechanism directly driven by a hydraulic cylinder.

By using this mechanism in the process of adjusting the tractor's wheelbase, it became possible to modify the wheelbase by up to 673 mm. This mechanism was developed by the R&D unit "Tractor" under the guidance of Professor Akhmetov and was installed on the TTZ-10.80 tractor for testing. In this process, the TTZ-80.10 and TTZ-10.30 tractors were combined to create an experimental version the TTZ-10.80, a variable wheelbase universal cultivator tractor [4, 5, 6].

Research Methodology

As defined in (Figure 3) hydraulic cylinders should be placed inner side of the frame for this, frame size and cylinder sizes have to be fitted. On the other hand, cylinder must make required force quantities and Mechanism assemblies and components have to answer to strength tests to ensure that the mechanism parts can function without breaking, cracking, bending and failure. Because of that requirement we made some calculations first.

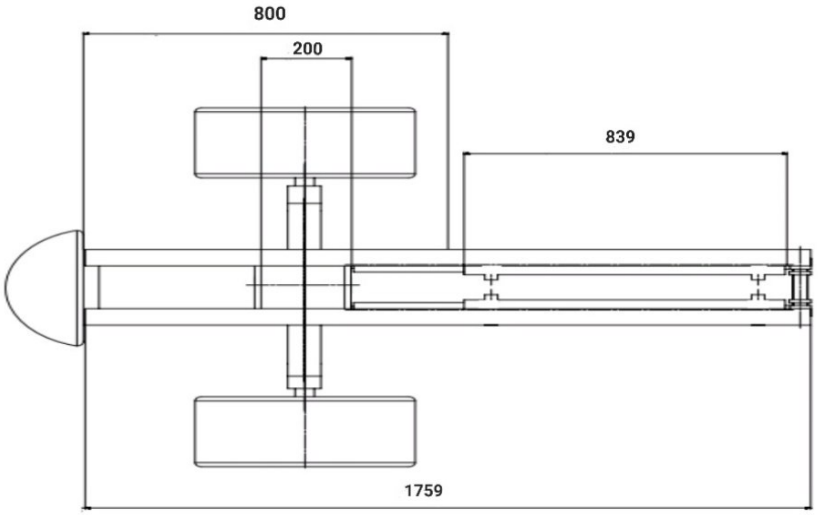

Figure 3. Dimensions of the tractor's frontal frame and placing hydraulic cylinders.

Hydraulic cylinders are manufactured in accordance with the standard, that is, they are standardized. The total weight of the tractor is 3100 kg, and according to the table above, the distribution of the weight force on the axles is as follows:

Front axle: 3100*0.3=930kg.

Rear axle: 3100*0.7=2170kg.

According to that weight distribution we have calculated stability of the tractor while climbing to the hill. Finding the limiting angle of static overturning is of great importance in determining longitudinal stability. We define the static limit angle in the backward roll as α_{lim}. To determine the limit angles of static overturning, it is assumed that the braked tractor is at rest on the slope. The following equations are valid for both cases [14]. The condition for a vehicle moving up a steep hill without overturning is as follow (Figure 4):

$$G\sin\alpha_{lim} = P_T = \varphi Y_k = \varphi \frac{G\cos\alpha_{lim}(L-a)+G\sin\alpha_{lim}\cdot h}{L};$$

Or

$$tg\alpha_{lim} = \varphi\left(\frac{L-a}{L-\varphi h}\right);$$

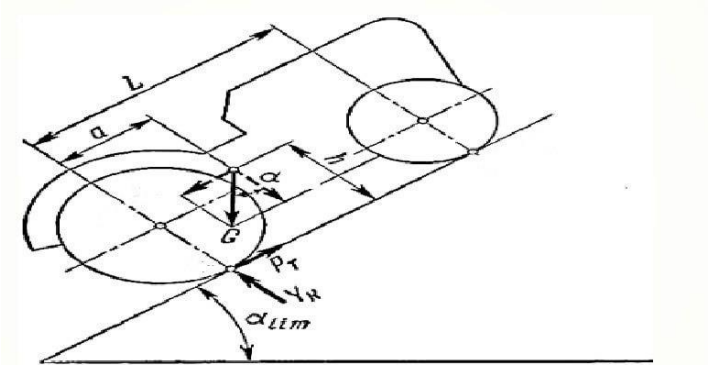

Figure 4. Tractor overturning condition.

Here: P_T - Yield between the leading wheel and the ground the potential driving force. Y_K -impact of the soil on the leading driven wheels.

It can be seen that the net force Gsinα tends to overturn the tractor, while the net force Gcosα resists the tractor overturning. But in most cases, the angle does not reach the limit angle of static overturning, and the car starts sliding down at a smaller value.

Analysis and Results

We determine the value of a by finding the center of mass based on the equilibrium condition of classical mechanics as following:

Case I (2168 mm): a (651 mm) is distance between rear end point and mass center of the tractor, h (550 mm) is agro-technical track, and when going down from the hill, the overturning angle will be greater than when going up to hill, because of the center of mass is located near the rear axle.

$$tg\alpha_{lim} = 1 * \left(\frac{2168-651}{2168-1*550}\right) = 0.805$$

$$\alpha_{lim} = 38.8°$$

Case II (2518 mm): a (284 mm) is distance between rear end point and mass center of the tractor, h (550 mm) is agro-technical track,

$$tg\alpha_{lim} = 1 * \left(\frac{2518-284}{2518-1*550}\right) = 1.135$$

$$\alpha_{lim} = 53.5°$$

So, as a result of changing the base, we were able to theoretically increase the limit of stability of the tractor on the hill from 38.8° to 53.5°. According to the standards, the angle of stability for tractors is between 30° and 45°. As a result of the newly

construction, we managed to increase the maximum angle of the tractor's stability by 8.5° from 45° to 53.5°, it means the overturning limit will be increased 18.8%. α_{lim} = 60° for plow tractors according to base size and the mass of the tractors. But in most cases, the angle does not reach the limit angle of static overturning, and the vehicle starts sliding down at a smaller value.

Maneuverability of the tractor. The tractor with a variable base under design has a different maneuverability than other tractors, that is, the turning lane changes when turning, so we need to analyze the tractor's maneuverability. The controlling ability and maneuverability of the tractor are characterized by kinematic and power parameters. The turn of the tractor is represented by the change of the position of the steering and guide wheels in the horizontal direction relative to the tractor base. A turning radius is a radius at which a car will rotate, or turn, given a certain wheelbase length and an angle of turn of the wheels.

How to calculate a turning radius?

1. Determine the wheel base.
2. Determine the turn angle.

This is the angle at which the front wheels are turned from their neutral position (α_{lim}), (for tractors, the turning angle of the front wheels is 45-55°). Finally, calculate the turn radius.

Using the formula, the turn radius is found to be:

$$R = \frac{L}{tg\alpha}$$

Case I (2168 mm):

$$R = \frac{2168}{tg55^{\circ}} = 1526.7$$

Case II (2518 mm):

$$R = \frac{2518}{tg55^{\circ}} = 1773.2$$

Case III (1818 mm):

$$R = \frac{1818}{tg55^{\circ}} = 1280.2$$

Conclusion

The base change mechanism and devices were considered and their construction was studied. The advantages and disadvantages of constructions were analyzed they were used to choose a principal scheme for a new construction. Based on the analysis, a new structure was developed and strength calculations were carried out, according to which the tractor base could be changed by 700 mm using a hydraulic cylinder. Based on the calculations and analyzing the results, we can see that when the base of the tractor increases by 16.1%, the stability of the tractor increases by 18.8% when climbing the height. Based on the calculations and analyzing the results, we can see that when the base of the tractor is reduced by 19.2%, the turning radius of the tractor is reduced by 16.2%. we managed to reduce the turning radius of the tractor by 16.2%.

References:

[1] Anurev V.I. “Handbook of the mechanical engineer-designer,” V.1, M.: *Mechanical Engineering*, 1979, p. 713-728.

[2] Akhmetov A.A., Usmanov I.I., Saidaminov S.S., Akhmedov Sh.A. “Universal-row-crop tractor,” 2014.
[3] “Fundamentals of scientific research,” T. *Uqituvchi*, 1981.
[4] “Methods of field experiment (with the basics of statistical processing of research results).” M. *Agropromizdat*, 1985.
[5] Akhmetov A.A., Usmanov I.I., Akhmedov Sh.A., Atakulov H.K. “Universal-row-crop tractor,” 2013.
[6] León O.N., Martínez P., Orta C.P. & Adaya “Reducing the weight of a frontal truck axle beam using experimental test procedures to fine tune FEA,” 2000.
[7] Hicks C. “Basic principles of experimental design,” Moscow, 1967.
[8] Akhmetov A.A., Usmanov I.I. “Power loads acting in kinematic pairs of the mechanism for changing the base of a tractor,” *Agricultural machinery and technology*. Moscow, Edition 12, 2018, p. (44-48).
[9] Mahanty D., Manohar K., Khomane V., & Nayak B.S. “Analysis and Weight Reduction of a Tractor’s Front Axle,” published 04 May 2014.
[10] Akhmetov A.A. “Evaluation of static strength of the front axle beam of a tractor with a variable base,” *Strength of structures, seismodynamics of buildings and structures*.
[11] Tarighi J., Mohtasebi S.S., & Alimardani R. “Static and dynamic analysis of front axle housing of tractor using finite element methods,” *Australian Journal of Agricultural Engineering* vol. 2, № 2, 2011, p. 37-51.
[12] Smirnov G.A. “Theory of motion of wheeled machines.” M.: *Mechanical Engineering*, 1990, pp. 348-352.
[13] Akhmetov A.A., Usmanov I.I. “Universal row-crop tractor with a variable base,” monograph, ed. R. D. Matchanov. RUz, SKB “Traktor,” Tashkent: *Fan*, 2016, p. 176.
[14] Khushnud Yakubov, Shavkat Ravutov, Anvarbek Masharibov and Islom Kadirov “Theoretical substantiation of the parameters of the debris removal device of the cotton picker apparatus.” *BIO Web of Conferences* 116, 2024, p. 01017.
[15] Ballasting Your Tractor for Performance by Alberta Agriculture & Rural Development A practical guide to proper weighting of your tractor, 2013.
[16] Alikulov S., Farmonov E.T. “Methodical instructions.” Tashkent, 2022. staff.tiiame.uz/storage.

UDC: 62, 631, 631.5

FEM ANALYSIS-STRUCTURAL AND DYNAMIC, DISCUSSIONS AND RESULTS OF THE MODIFIED MECHANISM FOR ADJUSTING BASE OF THE TRACTOR

Artikov Makhmud Sultonboevich
Assistant Laboratory, Urgench State University named after Abu Rayhan Biruni
artikovmaxmud198@gmail.com

Annotatsiya. Ushbu maqolada qishloq xo‘jaligida yomg‘ir bilan sug‘oriladigan qiya tepalikli yer maydonlariga ishlov berishda muhim ahamiyatga ega bo’lgan o‘zgaruvchan bazali traktor bazasini o‘zgartirishning yangilangan mexanizmining real yer maydoniga ishlov berishda yuzaga kelishi mumkin bo‘lgan yuklanishlar, kattaliklar (siqilish, kuchlanish, siljish, xavfsizlik) va kuch yo‘nalishlari aniqlanib bu yuklanishlarning bazasi o‘zgaruvchan traktorga ta’siri FEA, (Finite Element Analysis) asosida tekshirildi.

Kalit so‘zlar: *O‘zgaruvchan baza, qo‘shimcha yuklanishlar, kuchlanish, siljish, siqilish, xavfsizlik koeffitsienti.*

Аннотация. В данной статье рассматривается обновлённый механизм изменения базы трактора с переменной колёсной базой, имеющего важное значение при обработке наклонных дождевальных сельскохозяйственных участков. Определены возможные нагрузки, величины (сжатие, напряжение, сдвиг, коэффициент запаса прочности) и направления сил, возникающие при обработке реальных полевых условий. Влияние этих нагрузок на трактор с переменной базой было проанализировано с использованием метода конечных элементов (FEA — Finite Element Analysis).

Ключевые слова: *трактор с изменяемой базой, передняя рама, дополнительные нагрузки, напряжение.*

Abstract. This article investigates the updated mechanism for modifying the base of a variable-base tractor, which plays a crucial role in cultivating sloped rainfed agricultural lands. The study identifies potential loads, magnitudes (compression, stress, shear, safety), and force directions that may arise during real field operations. Furthermore, the impact of these loads on the variable-base tractor was analyzed using Finite Element Analysis (FEA).

Keywords: *Variable base, additional loads, stress, displacement, compression, safety factor.*

Introduction

Finite element analysis (FEA) is a powerful tool used to solve complex engineering problems that are too difficult to tackle with traditional analytical methods. It allows engineers to calculate stresses, deflections, and displacements within structures, both simple and intricate. FEA has found applications in various fields, including thermal, structural, and fluid flow analysis.

The core concept of FEA involves dividing the structure or component into smaller, manageable sections through a process called discretization. These sections are represented by “finite elements,” each with a specific displacement function. These elements are interconnected through shared interfaces like nodes, lines, and surfaces. The material properties of the structure are then used to determine the behavior of each node based on the properties of all surrounding elements. This process generates a set of equations for every node, which are then solved using matrix calculations to understand the overall behavior of the structure. Instead of complex differential equations often encountered in analytical methods, FEA relies on numerical methods and matrices, which are easier to evaluate. While this approach provides an estimated result, the accuracy can be improved by increasing the number of nodes, leading to a larger set of equations.

Literature Review

Some of the most widely used and feature-rich industry packages include ADINA, ANSYS Mechanical, NEi/Nastran, SolidWorks, Pro/MECHANICA, COSMOS

Works, COMSOL, and Strand 7. Ultimately, the best FEA package for you will be the one that best suits your specific application requirements and budget. FEA software leverages computational power to solve these complex equations, making it a valuable tool for engineers seeking to analyze and understand the behavior of structures and components. The reliability of finite element analysis (FEA) results depends heavily on the analyst's skill and expertise. Proper use of the software can generate accurate and meaningful results. A study by Leon O.N., Orta S.P., Adaya (2000) compared experimental results with FEA predictions, finding a 5.17% variation from the finite element results. This suggests that FEA can provide reasonably accurate results. However, the interpretation of FEA outcomes requires careful consideration, especially regarding the appropriate application of loadings and constraints to a well-prepared model. As Toogood (2012) emphasizes, the “garbage in, garbage out” (GIGO) principle applies to FEA. The quality of input data directly impacts the accuracy of the results. Why use Finite Element Analysis?

1. Cost-Effective Design Validation: FEA offers a cost-effective way to verify the structural, modal, or thermal performance of new designs or modifications to existing structures and components. Traditionally, the design process involved building prototypes and testing them in the field, which was expensive and time-consuming. Any design flaws discovered in the field required costly redesign and modification of the prototype. FEA eliminates the need for physical prototypes by simulating the behavior of the design virtually. This allows engineers to identify potential problems and make necessary adjustments before actual production, leading to significant cost savings and improved efficiency.

2. Real-World Simulation: FEA enables the simulation of real-world loading and constraints on components. Engineers can apply loads that mimic actual operating conditions and define constraints such as fixed displacements, planar surfaces, and pin joints to accurately represent how the component will be attached and behave in its intended environment.

3. Rapid Analysis and Design Iteration: FEA allows engineers to quickly analyze a component's behavior under various loading and constraint conditions, depending on the model's complexity and available computing power. If the analysis results are unsatisfactory, the model’s geometry can be easily adjusted and reanalyzed, facilitating rapid design iterations and optimization.

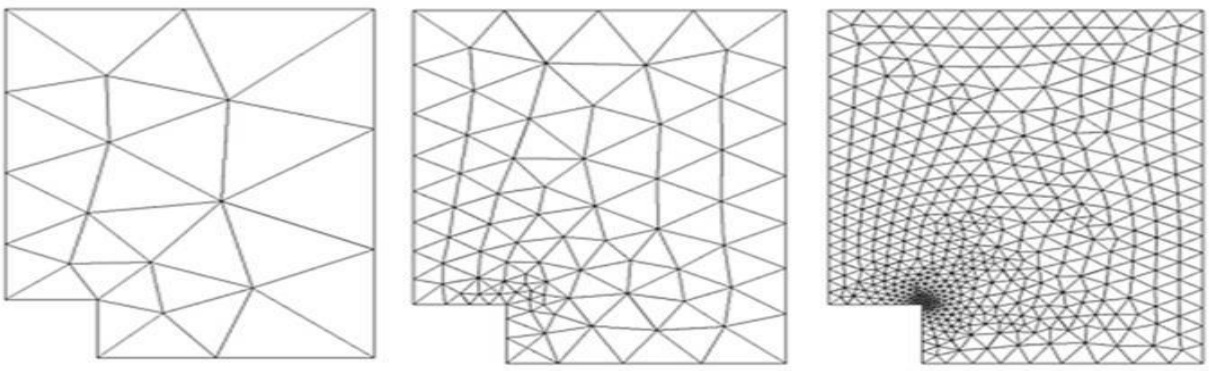

(a)-Coarse mesh (b)-Intermediate mesh (c)-Fine mesh

Figure 1. Mesh refinements. (Source: https://community.wvu.edu).

4. Using 3D parametric models for FEA offers the advantage of rapid geometry modification. When the results of an analysis are not satisfactory, the analyst can quickly adjust the model's geometry by changing its controlling parameters. This allows for fast iteration and optimization of the design without the need to manually rebuild the entire model. An example of refinements is shown in the (Figure 1).

Research Methodology

Static and structural analysis of a component(model), involves three distinct stages: pre-processing, processing, and post-processing. Pre-processing involves preparing the model for analysis by converting it into a finite element model. This step defines various characteristics of the model.

Table 1. Mechanical properties of steel 35 (Source: Metallicheckiy-portal.ru).

Heat treatment	Thickness, (mm)	σ(MPa)	σ(MPa)	δ(%)	ψ %
Normal	300-500	195	390	20	45
	500-800			18	38
	100-300			20	48
	300-500	215	215	18	40
	500-800			16	35
Normal	<100			2	48
	100-300	245	470	19	42
	300-500			17	35
Hard	<100	275	530	20	40
	100-300			17	38
	<100	315	570	17	38

Specifying the material used in the new model and its relevant properties (e.g., strength, stiffness). The main material used for the TTZ 80 10 universal tractor body and frames is Steel 35. The characteristic of Steel 35 brand according to the GOST 1050 standard of the Republic of Uzbekistan (above given as Table 1) [16].

In the FEA, we select a metal type that is mechanically and technologically close to Steel 35 from the types of metals in the program. We can see that the closest material to Steel 35 is AISI 1035 Steel. Below is the characteristic of AISI 1035 Steel brand according to the SolidWorks program (Table 2).

Table-2. Mechanical properties of AISI 1035

Elastic Modulus	2.049999984×10^{11}	N/m^2
Poisson's Ratio	0.29	N/A
Shear Modulus	7.999999987×10^{10}	N/m^2
Mass Density	7849.999987	kg/m^3
Tensile Strength	585000002.9	N/m^2
Compressive Strength		N/m^2
Yield Strength	282685049	N/m^2
Thermal Expansion Coefficient	1.1×10^{-5}	/K
Thermal Conductivity	52	W/(m·K)

Processing: In the processing stage, the axle model is committed to an analysis by defining the type of analysis, convergence and output file directory in SolidWorks Simulation. A new static and structural analysis was selected from the file drop down

menu and the Static Analysis window came up where constraints and load already applied in the pre-processing stage are selected (Figure 2).

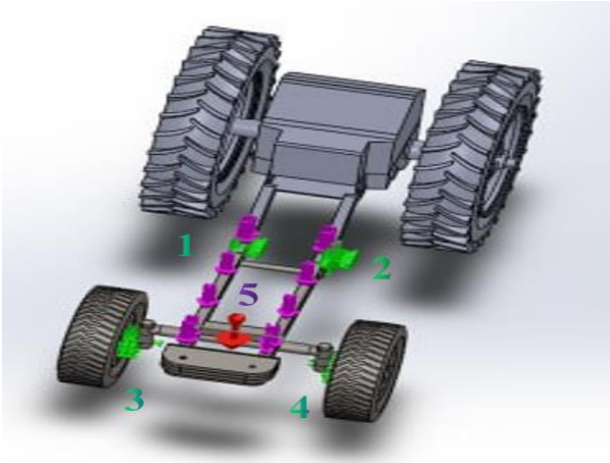

Figure 1. Constraints points. Constraints are applied at these 1,2,3,4 green points. Loads applied at these oriole (5) points.

Post processing: Post-processing is the final stage of analysis, where the results obtained during the processing stage are thoroughly evaluated. Software like SolidWorks, which is widely used for post-processing, can analyze the results and generate color-coded stress plots (von Mises plots). It also allows for sorting, printing, and plotting selected results from the finite element analysis.

Common post-processing tasks include:

- Sorting element stresses and displacements by magnitude.
- Calculating the factor of safety.
- Generating convergence graphs.
- Creating plots and graphs to visualize the results.

One of the most important capabilities of post-processing software is the ability to animate the deformed shape of a component. This animation helps to visually verify if the model was constrained correctly.

Analysis and Results

Were drawn based on the summary of results and loads applied is shown in the table below (Table 3 and Table 4).

Table 3. Summary of loads.

Loading cases	Calculation mode	Wheel (Left) Loads(kN)			Wheel (Right) Loads(kN)		
		F(x)	F(y)	F(z)	F(x)	F(y)	F(z)
Test-1	Case I: (2168mm)	0	4.83	0	0	4.83	0
	Case II: (2518mm)	0	0.965	0	0	0.965	0
Test-2	Case I: (2168mm)	0.837	3.813	0	8.467	3.817	0
	Case II: (2518mm)	0.31495	1.4343	0	3.1835	1.4343	0
Test-3	Case I: (2168mm)	3.479	2.011	0	3.479	2.011	0
	Case II: (2518mm)	1.3085	0.7564	0	1.3085	0.7564	0

Table 4. Summary of results.

Loading cases	Base condition	Max Von Mises Stress (MPa)	Maximum Displacement (mm)	Factor of Safety
Test-1	2168mm	30.08	0.7238	9.4

	2518mm	18.78	0.2179	15
Test-2	2168mm	30.57	0.765	9.2
	2518mm	17.68	0.1932	16
Test-3	2168mm	31.51	0.806	9
	2518mm	17.79	0.2016	16

Conclusion

Generally, results for loading cases 1 to 3 were in the same range and they point to some particular criteria on the model. The conclusion drawn from these results and the overall analysis of the modified tractor base was that the chances or likelihood of failure under the loading conditions discussed and applied in this project are low including the bracket identified above to be at risk. Therefore, the loads applied in the analysis are considered to be safe for the modified base. The working or operating weight of the tractor should not be exceeded and should be used as a guide for safe loading level for the base. From this entire research article, we can conclude that the modified frontal base is acceptable. Our research focused on improving variable base tractor mechanisms. We analyzed existing designs, identifying both their strengths and weaknesses. To address these weaknesses, we developed a new mechanism with a wider base (700 mm) compared to the current domestic standard (673 mm).

References:

[1] Mahanty D.K., Manohar V., Khomane B.S., and Nayak S. “Analysis and Weight Reduction of a Tractor’s Front Axle,” published 04 May 2014.
[2] Hicks C. “Basic principles of experimental design,” Moscow, 1967.
[3] “Fundamentals of scientific research,” T. *Uqituvchi*, 1981.
[4] Akhmetov A.A., Usmanov I.I., Akhmedov Sh.A., Atakulov H.K. “Universal-row-crop tractor,” 2013.
[5] Dospekhov B.A. “Methods of field experiment (with the basics of statistical processing of research results).” M. *Agropromizdat*, 1985.
[6] Akhmetov A.A., Usmanov I.I. “Universal row-crop tractor with a variable base,” monograph, ed. R.D. Matchanov. RUz, SKB “Traktor,” Tashkent: *Fan*, 2016, p. 176.
[7] “Tractors TTZ 80.10 and TTZ 80.11,” Operation and maintenance manual. 80.10-0000010IE. - Tashkent: *Tashkent Tractor Factory*, 2010.
[8] Sean Laughery, Grant Gerhart, Paul Muench “Evaluating Vehicle Mobility Using Bekker's Equations,” US Army TARDEC Warren, MI 48397-5000.
[9] Akhmetov A.A. “Evaluation of static strength of the front axle beam of a tractor with a variable base,” Strength of structures, seismodynamics of buildings and structures.
[11] Pisarenko G.S. “Handbook of Strength of Materials.” Kyiv: *Naukova Dumka*, 1975.
[12] Akhmetov A.A. “Front axles of a universal row-crop tractor for cotton purposes.” Edited by R.D. Matchanov, Tashkent: *Fan*, 2014.
[13] Sambamo Richard “FEA analysis of the tractor axle modification,” 2014.
[14] Khushnud Yakubov, Shavkat Ravutov, Anvarbek Masharibov and Islom Kadirov “Theoretical substantiation of the parameters of the debris removal device of the cotton picker apparatus.” *BIO Web of Conferences* 116, 2024, p. 01017.
[15] Kozlov L., Buriennikov Y., Piliavets V., Kotyk S. “Optimization of parameters of the mobile machine adaptive hydraulic circuit.”
[16] Raiko M.V. “Calculation of machine parts and units.” Kiev: *Texnika*, 1966, p. 500.
[17] Dospekhov B.A. “Methodology of field experiment (with the basics of statistical processing of research results).” Moscow: *Agropromizdat*, 1985, p. 342-351.

ACTUAL PROBLEMS OF MATHEMATICS, PHYSICS AND MECHANICS

UDC: 53, 537, 537.5, 539

INVESTIGATION OF IMPLANTATION OXYGEN IONS INTO THE SURFACE Mo(001)

Allayarova Gulmira
PhD, Department of Theoretical and Experimental Physics, Karshi State University

Kutliev Uchqun
Professor, Department of Physics, Urgench State University named after Abu Rayhan Biruni
uchkunk@mail.ru

Ismoilov Jaloladdin
Student, Department of Physics, Urgench State University named after Abu Rayhan Biruni

Annotatsiya. Biz Mo (001)<110> yuzasida 1-5 keV boshlang‘ich energiya bilan kichik burchak ostida ion implantatsiyasi jarayonini modellashtirdik. Modellashtirish jarayonida jufttiy to‘qnashuvlar usulidan qo‘llanildi. Biz implantatsiya qilingan O ionlari sonining Mo (001)<110> sirtiga turli xil tushish burchaklariga bog‘liqligini o‘rgandik. Kichik tushish burchaklarida ion implantatsiyasi jarayonini kuzatish mumkin ekanligi ko‘rsatildi. Aniqlanishicha, implantatsiya qilingan zarrachalar soni tushish burchagi diapazonida 10° gradusgacha ko‘paygan. Boshlang‘ich energiya qiymatining oshishi bilan bu diapazon kamayadi. Bu sirtdan sochilgan zarrachalarning ortishi bilan tushuntiriladi.

Kalit so‘zlar: *ion implantatsiyasi, kompyuterda modellashtirish, yarim kanal, ion bombardimoni, giperkanallanish*

Аннотация. Нами смоделирована процесс ионной имплантации ионов при малых углах падениях на поверхность Mo (001)<110> с начальной энергией 1-5 кэВ. В процессе моделирования использована метод приближении парных столкновений. Получена зависимость число имплантированных ионов O на Mo (001) <110> при разных углах падениях. Показано, что при малых углах паденриях мозно наблюдать процесс имплантации ионов. Установлено, что число имплантированных частиц увеличилось в диапазоне угла падения до 10°. С увеличенрием значении начальной энергии этот диапазон уменьшается. Это связано с увеличением доли рассеянных частиц от поверхности.

Ключевые слова: *Ионная имплантация, компьютерное моделирование, полуканал, ионная бомбардировка, гиперканалирование.*

Abstract. We have modelled the process of ion implantation at low angles of incidence on the Mo (001)<110> surface with an initial energy of 1-5 keV. The

pair collision approximation method was used in the modelling process. We obtained the dependence of the number of implanted O ions on Mo (001) <110> at different angles of incidence. It was shown that at small angles of incidence, the ion implantation process can be observed. It was established that the number of implanted particles increased in the angle of incidence range up to 10°. With an increase in the initial energy value, this range decreases. This is due to increasing in the proportion of particles scattered from the surface.

Keywords: *Ion implantation, computer simulation, semichannel, ion bombardment, hiperchanneling.*

Introduction

Ion implantation is one of the most effective methods for modifying the surface of solids at the atomic level. This process is widely used in materials science, micro- and nanoelectronics, as well as in the creation of new functional coatings with specified physical and chemical properties. The essence of the method lies in the introduction of high-energy ions into the surface layers of a solid, which leads to changes in its crystal structure, chemical composition, and mechanical characteristics [1-4].

The implantation of oxygen ions into molybdenum is a separate area of research aimed at creating oxide phases (such as MoO_3 and MoO_2), modifying electrical conductivity, and improving the adhesive and tribological properties of the surface. Such changes can significantly expand the functionality of molybdenum in various applications, including electronics, photocatalysis, and anti-corrosion coatings [5-8].

This work is devoted to the study of oxygen ion implantation in molybdenum single crystals at low angles of incidence. Particular attention is paid to the method of computer modelling of the interaction of ions with the crystal lattice, as well as the proportion of implanted ions in the surface layers of molybdenum.

Literature Review

In our calculations we are used binary collision approximation. The Binary Collision Approximation (BCA) is a widely used theoretical framework for modeling ion implantation processes, particularly at low to moderate ion energies (up to hundreds of keV). In ion implantation, high-energy ions are directed into a solid target, where they interact with atoms in the lattice, leading to a variety of outcomes including implantation, sputtering, defect formation, and atomic mixing. The BCA simplifies this complex many-body problem by considering the interaction of the incoming ion with the target atoms as a series of independent two-body (binary) collisions. In the BCA, it is assumed that the ion travels through the target material and undergoes sequential collisions with individual target atoms. Each collision is treated using classical mechanics, where the interaction potential between the ion and the target atom governs the scattering angle and energy transfer. The trajectory of the ion is calculated from one collision to the next, based on the interatomic potential and kinetic parameters. The interaction between atoms is often modeled using screened Coulomb potentials, such as the Ziegler–Biersack–Littmark (ZBL) universal potential [9-10].

Research Methodology

The binary collision approximation is a foundational method in modeling ion implantation processes. It balances computational efficiency with reasonable accuracy for a wide range of energies and target materials. While it has limitations, especially in dense cascade or thermal regimes, its simplicity and robustness make it a valuable tool in both research and industrial applications of ion implantation.

Analysis and Results

Figure 1a shows the dependence of the number of implanted O ions on Mo (001)<110> at different angles of incidence. The initial energy of the incident particles was 1 keV. This figure also shows the surface semichannel formed on Mo (001)<110>. All atoms of the surface semichannel are Mo atoms. The dependence shows that O ions began to be implanted into Mo with an angle of incidence of $\psi=3^{\circ}$. Further on, the dependence has a zigzag shape up to $\psi=30^{\circ}$. This is explained by the fact that with an increase in the angle of incidence of the bombarding particles, the angle of departure of the particles from the surface semichannel changes. This is associated with the greatest convergence of the ion with the atoms at the bottom of the semichannel. If this distance is small, the ions scatter at large angles and penetrate into neighbouring half-channels, where they remain (implanted). The dependence shows a gradual change, i.e. no sharp jump is observed. Therefore, it is possible to determine the values of the angle of incidence at which the ion implantation process begins.

Figure 1b shows the dependence of the number of implanted O ions on Mo at different angles of incidence. The initial energy of the incident particles was 2 keV. The ions began to implant into the single crystal at an angle of incidence $\psi=2^{\circ}$.

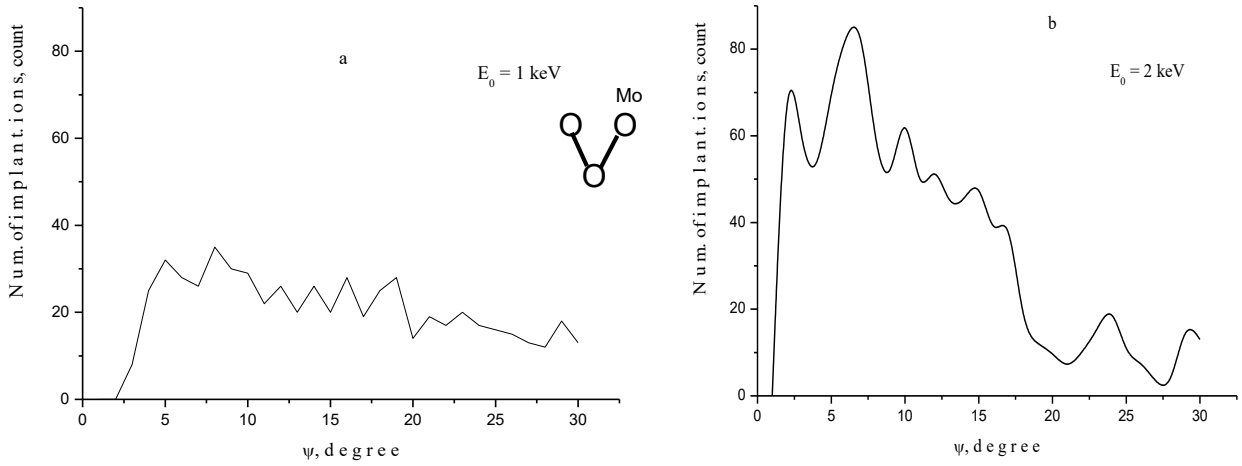

Figure 1. Dependence of the number of implanted O ions on Mo surface at different angles of incidence: E_0 = 1 keV (a), E_0 = 2 keV (b).

Although the zigzag shape of the dependence remained, there are also more intense peaks, which formed at $\psi=2^{\circ}$ and $\psi=7^{\circ}$, and a low-intensity peak at $\psi=24^{\circ}$. Note that at E_0=1 keV, there were no implanted ions at $\psi=2^{\circ}$. Figure 2 shows the dependence of the number of implanted O ions on Mo at different angles of incidence. In Figure 2a, the initial energy of the bombarding particles was E_0=3 keV. The dependence shows that ions began to be implanted at an angle of incidence $\psi=3^{\circ}$. In this dependence, the zigzag shape is almost lost and it has an almost double-peak structure. At this initial

energy value, a low-intensity peak was formed at ψ=22°, and a large intense peak at ψ=5°. Our calculations showed that at ψ=5°, large quantities of ions were implanted into the single crystal.

Figure 2b shows the above-mentioned dependence at E_0=4 keV. The dependence shows that an intense peak was formed in the angle of incidence range at ψ=2°-5° for O ions. The second low-intensity peak was formed at ψ=22°. Note that the intensity of this peak increased. Figure 2c shows the dependence of the number of implanted O ions on Mo at different angles of incidence and at E_0 = 5 keV. At this initial energy value, an intense peak formed in the angle of incidence range at ψ=2°-4°. A second low-intensity peak formed at ψ=22°. Note that the intensity of these peaks increased.

Our calculations showed that the formation of an intense peak at small angles of incidence is explained by the beginning of ion penetration into the single crystal. In this case, the trajectory direction changes faster and the ions lose their initial direction. The formation of a low-intensity peak at large angles of incidence is explained by the effect of surface hyperchanneling.

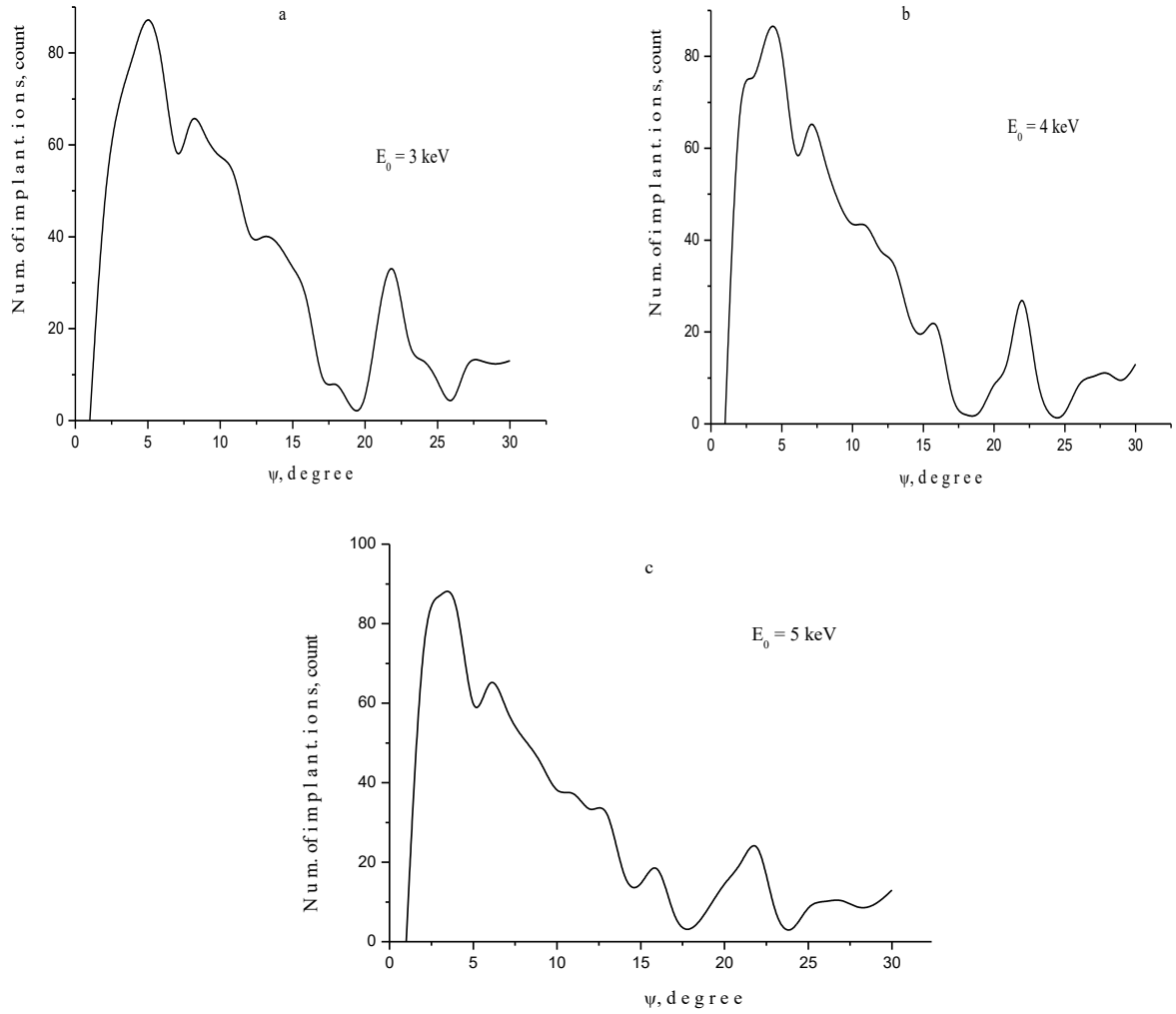

Figure 2. Dependence of the number of implanted O ions on Mo surface at different angles of incidence: (a) E_0 = 3 keV, (b) E_0 = 4 keV, and (c) E_0=5 keV.

Conclusions

We investigated the implantation of oxygen ions into a Mo(001)<110> single crystal at low angles of incidence. The initial energy values changed in the range E_0=1-5 keV. The results obtained showed that at E_0=1 keV, the dependence has a smooth zigzag shape. Starting from E_0=2-5 keV, the zigzag shape changes and a two-peak dependence is formed. It should be noted that the low-intensity peak formed at high values of ψ corresponds to hyperchanneled ions, while the intense peak formed at low values of ψ corresponds to ions that began to penetrate into the single crystal.

References:

[1] Kusinski J. "Oxidation behavior of molybdenum implanted with oxygen ions." *Surface and Coatings Technology*, 59(1), 1993, pp. 49–54.

[2] Lemmerz U., et al. "Implantation of oxygen ions into molybdenum and charac-terization by XPS and AES." *Applied Surface Science*, 51(1–4), 1991, pp. 55–62.

[3] Hagen D.A., Nicolet M.A. "Thermal oxidation of Mo implanted with oxygen ions." *Journal of Applied Physics*, 55(1), 1984, pp. 237–242.

[4] Pape A., et al. "Ion beam modification of molybdenum surfaces." *Nuclear Instruments and Methods in Physics Research B*, 239(1–2), 2005, pp. 235–241.

[5] Stoller R.E., Greenwood L.R. "Subcascade formation in displacement cascade simulations: Implications for fusion reactor materials." *Journal of Nuclear Materials*, 1999, pp. 57–62.

[6] Alov N.V., Kutsko D.M., Bordo K.V. "Ion-Beam Reduction of the Surface of Higher Oxides of Molybdenum and Tungsten." *Journal of Surface Investigation. X-ray, Synchrotron and Neutron Techniques*, Vol. 2, № 2, 2008, pp. 184–188.

[7] Sarmah D., Kumar A. "Ion beam modified molybdenum disulfide-reduced grapheme oxide/ polypyrrole nanotubes ternary nanocomposite for hybrid supercapacitor electrode." *Electrochimica Acta*, 312, 2019, pp. 392-410. DOI: 10.1016/j.electacta.2019.04.174

[8] Biersack J.P., Haggmark L.G. "A Monte Carlo computer program for the transport of energetic ions in amorphous targets." *Nuclear Instruments and Methods*, 174(1–2), 1980, pp. 257–269.

[9] Ziegler J.F., Ziegler M.D., and Biersack J.P. "SRIM – The Stopping and Range of Ions in Matter." *Nuclear Instruments and Methods in Physics Research Section B: Beam Interactions with Materials and Atoms*, 268(11–12), 2010, pp. 1818–1823. DOI:10.1016/j.nimb.2010.02.091.

UDC: 5, 517, 517.55, 517.9

EXTREMAL FUNCTIONS ON PARABOLIC MANIFOLDS AND REGULAR COMPACTS

Atamuratov Alimardon Abdrimovich
Doctor of Physical and Mathematical Sciences, V.I.Romanovskiy Institute of Mathematics, Uzbekistan Academy of Sciences
alimardon01@mail.ru

Kushnazarov Rasul Qudratovich
Master student, Urgench state university named after Abu Rayhan Biruni

Annotatsiya. Ushbu maqolada maxsus plyurisubgarmonik ρ qamrov funksiyasiga ega parabolik Shteyn ko‘pxillliklari qaralgan. Maxsus qamrov funksiyasi yordamida ρ-polinom tushunchasi kiritiladi. Polinomlari fazosi yetarlicha boy bo‘lgan parabolik ko‘pxilliklar uchun kompakt to‘plamlarning estremal funksiyalari va bu funksiyalarni uzluksizligini ta’minlovchi regulyar kompakt to‘plamlar o‘rganilagan. Ikkita regulyar kompaktlarning Dekart ko‘paytmasi ham regulyar bo‘lishi isbotlanadi.

Kalit so‘zlar: *plyurisubgarmonik qamrov funksiyasi, parabolik ko‘pxillik, polinom, ekstremal funksiya, regulyar kompakt.*

Аннотация. В работе рассматривается параболические Штейновы многообразия, на которых существует специальные плюрисубгармонические функции исчерпания ρ. С помощью функции ρ определены понятия ρ- полинома. На многообразиях с богатым семейством полиномов изучены максимальные функций и регулярные компакты, для которых эти функция являются непрерывной. Доказано регулярность прямого произведения двух регулярных компактов.

Ключевые слова: *плюрисубгармоническая функция исчерпания, параболичсекое многообразие, полиномы, экстремальная функция, регулярный компакт.*

Abstract. This article considers parabolic Stein manifolds that admit special plurisubharmonic exhaustion functions. Using such a function, the notion of a ρ-polynomial is introduced. On manifolds possessing a rich family of such polynomials, we study maximal functions and regular compact sets for which these functions are continuous. It is proved that the direct product of two regular compact sets is regular.

Keywords: *plurisubharmonic exhaustion function, parabolic manifold, polynomials, extremal functions, regular compact.*

Introduction

For a complex manifold of arbitrary dimension, its parabolicity is determined by the existence of a special exhaustion function within it (see P. Griffiths and J. King [1], W. Stoll [2, 3], A. Aytuna, A. Sadullaev [4], et al.)

Definition 1. A Stein manifold $X \subset \mathbb{C}^N$ of dimension $n$is called a S −parabolic manifold, if it has a special exhaustion function $\rho(z)$:

a) $\rho(z) \in psh(X),\ \{\rho \le M\} \subset\subset X\ \forall M \in \mathbb{R}$;

b) $\rho$is the maximal function outside some compact set $K \subset\subset X$,, i.e., $\left(dd^c\rho\right)^n = 0$, on $X\backslash K$.

Let us define the concept of polynomials on a S −parabolic manifold $X \subset \mathbb{C}^N$.

Definition 2. If for the function $p(z) \in \mathcal{O}(X)$there exist positive numbers $c,\ d$ such that for all $z \in X$ the inequality

$$\ln|p(z)| \le d\rho^+(z) + c, \qquad (1)$$

holds, where $\rho^+(z) = \max\{0,\ \rho(z)\}$, then the function p is called a ρ −polynomial of degree $\le d$. The smallest value of d in inequality (1) is called the degree of the polynomial p.

For a fixed integer $d > 0$, we denote by $\mathcal{P}_\rho^d(X)$ the set of all ρ −polynomials of degree less than or equal to d, and by $\mathcal{P}_\rho(X) = \cup_{d=0}^{\infty}\mathcal{P}_\rho^d(X)-$ the set of all ρ −polynomials on X.

Literature Review

A. Zeriahi [7], using the ideas from Pleshnyak's work [5], proved that the vector space $\mathcal{P}_\rho^d$, for a S −parabolic manifold, is finite-dimensional, and using the "projection theorem" for Banach spaces, gave the following estimate for its dimension:

$$\dim\mathcal{P}_\rho{}^d \le C_{n+dN}^n = \frac{(n+dN)!}{n!\,(dN)!}.$$

Here N is a constant independent of d. An alternative estimate for the dimension is proven in the work [4].

Theorem 1. (Sadullaev-Aytuna [4]) *Let (X,ρ) be a S-parabolic Stein manifold. Then the vector space $\mathcal{P}_\rho^d$ is finite-dimensional and there exists a constant $C = C(X) > 0$ such that*

$$dim\mathcal{P}_\rho{}^d \le C(d+1)^n.$$

Definition 3. S −parabolic manifold X is called *regular* if the space of all ρ −polynomials $\mathcal{P}_\rho(X)$ is dense in $\mathcal{O}(X)$.

Theorem 2. (Atamuratov [8]) *Let (X_1,ρ_1) and (X_2,ρ_2) be regular parabolic manifolds of dimensions n and m, respectively. Define the manifold $X = X_1 \times X_2$ of dimension $k = n+m$ and let $\pi_1: X \to X_1,\ \pi_2: X \to X_2$ be the projections. Then $X = X_1 \times X_2$ is a regular parabolic manifold with a special exhaustion function $\rho = \ln(e^{2\rho_1\circ\pi_1} + e^{2\rho_2\circ\pi_2})$.*

In this article we consider extremal function $\Phi_\rho(z,K)$. of a compact K, associated with polynomials defined on Parabolic Stein manifolds and we prove some special properties concerning Cartesian product of compact subsets. In the classical case when complex space this function first defined by J. Siĉiak [6]. Lately in the work [9] it is proved analogue of well-known Bernstein-Walsh-Siĉiak theorem in terms of extremal function $\Phi_\rho(z,K)$.

Extremal function $\Phi_\rho(z,K)$.

The extremal function on a S- parabolic manifold is defined similarly: let X be a S- parabolic manifold and $\rho(z)$ be a special exhaustion function on X. Let us denote by $\mathcal{P}_\rho(X)$ the class of all ρ −polynomials on the manifold X. For a fixed compact subset $K \subset X$ let

$$\Phi_\rho(z,K) = \sup\left\{|f(z)|^{\frac{1}{\deg f}}:\ f \in \mathcal{P}_\rho(X),\quad \|f\|_K \le 1\right\}.$$

It should be noted that the function $\Phi_\rho(z,K)$ is of interest only when X is a regular parabolic manifold on which there exists a rich family of polynomials.

The following properties of the function $\Phi_\rho(z,K)$ arise directly from its definition.

1) If $K \subset K_1 \subset X$, then $\Phi_\rho(z,K) \ge \Phi_\rho(z,K_1)$, $\forall z \in X$.

2) For a polynomial $P(z) \in \mathcal{P}_\rho^d(X)$ and a compact set $K \subset X$, the Bernstein-Walsh inequality holds:

$$|P(z)| \le \|P\|_K \cdot \left(\Phi_\rho(z,K)\right)^{degP}, \quad z \in X, \tag{2}$$

where $\|P\|_K = \sup_{z\in K}|P(z)|$ is the supremum norm.

It follows from the fact that $\left(\frac{|P(z)|}{\|P\|_K}\right)^{\frac{1}{\deg P}} \le \Phi_\rho(z,K)$.

3) If the function $\Phi_\rho(z,K)$ is not locally bounded from above, then the compact set $K \subset X$ is pluripolar on X. Thus, for a non-pluripolar compact set $K \subset X$, the extremal function is locally bounded from above.

From the property of the upper envelope, it follows:

4) For any non-pluripolar compact set $K \subset \mathbb{C}^n$ the function $ln\Phi_\rho^*(z,K) \in psh(X)$.

The polynomial convex hull of the compact set $K \subset X$ is defined as follows:

$$\hat{K} = \left\{z \in X:\ |P(z)| \le \|P\|_K, \forall P \in \mathcal{P}_\rho(X)\right\}.$$

4) For any compact set, following equality holds $\Phi_\rho\left(z,\hat{K}\right) \equiv \Phi_\rho(z,K)$.

Indeed, if on the compact set K the inequality $|P(z)| \le 1$ holds, then this inequality also holds on the hull $\hat{K}$.

Analysis and Results

Theorem 3. *Let (X_1,ρ_1) and (X_2,ρ_2) be regular parabolic manifolds and let $K_1 \subset X_1$, $K_2 \subset X_2$ be arbitrary compact sets. Then for the extremal function of the subset $K = K_1 \times K_2 \subset X_1 \times X_2$ of the regular parabolic manifold $X = X_1 \times X_2$, with the special exhaustion function $\rho = \ln(e^{2\rho_1\circ\pi_1} + e^{2\rho_2\circ\pi_2})$, the following equality holds:*

$$\Phi_\rho(z,K) = \max\left\{\Phi_{\rho_1}(\pi_1(z),K_1), \Phi_{\rho_2}(\pi_2(z),K_2)\right\}.$$

Here, $\pi_1: X \to X_1$, $\pi_2: X \to X_2$ − are projections.

Proof. Let (X_1,ρ_1), (X_2,ρ_2) be regular parabolic manifolds. Consider the manifold $X = X_1 \times X_2$ and, to simplify the notation, denote the projections of the point $z \in X$ on the manifolds X_1, X_2 by $\xi = \pi_1(z)$, $\eta = \pi_2(z)$, respectively. Thus, we obtain the correspondence $z \to (\xi,\eta)$. As we have proven, X is a regular parabolic manifold with a special exhaustion function $\rho(z) = \ln\left(e^{2\rho_1(\xi)} + e^{2\rho_2(\eta)}\right)$ (theorem 2). Then

ρ −polynomials on $X = X_1 \times X_2$ are expressed through ρ_1- and ρ_2-polynomials on X_1 and X_2. Let a ρ-polynomial $f(z) \in \mathcal{O}(X)$ of degree d be given, i.e.

$$\mathrm{Ln}|f(z)| \le d \cdot \ln^{+}\left(e^{2\rho_1(\xi)} + e^{2\rho_2(\eta)}\right) + C.$$

From the definition of polynomials, it follows that all polynomials from the spaces $\mathcal{P}_{\rho_1}(X_1)$ and $\mathcal{P}_{\rho_2}(X_2)$ are simultaneously ρ-polynomials on $X = X_1 \times X_2$ of the same degree. Consequently, we obtain the inequalities

$$\Phi_\rho(z,K) \ge \Phi_{\rho_1}(\xi,K_1), \quad \Phi_\rho(z,K) \ge \Phi_{\rho_2}(\eta,K_2),$$
$$\Phi_\rho(z,K) \ge \max\left\{\Phi_{\rho_1}(\xi,K_1), \Phi_{\rho_2}(\eta,K_2)\right\}. \tag{3}$$

Now let us prove the inverse inequality. It is known that every ρ −polynomial on $X = X_1 \times X_2$ can be written in the form of a finite decomposition

$$f(z) = P_1(\xi) \cdot Q_1(\eta) + P_2(\xi) \cdot Q_2(\eta) + \cdots + P_s(\xi)Q_s(\eta), \tag{4}$$

where P_j and $Q_j$are polynomials of X_1 and X_2 , respectively. We fix the bounded neighborhoods D $(K_1 \subset D \subset X_1)$ and G $(K_2 \subset G \subset X_2)$. Let us consider orthonormal systems $\{p_j\} \subset \mathcal{P}_{\rho_1}(X_1)$, $\{q_k\} \subset \mathcal{P}_{\rho_2}(X_2)$ with respect to the regions D and G, i.e. these systems are orthonormal with respect to the scalar products

$$\langle p_j, p_k \rangle = \int_D p_j \cdot \bar{p}_k \cdot dV(X_1) = \begin{cases} 0, & j \ne k \\ 1, & j = k, \end{cases}$$
$$\langle q_j, q_k \rangle = \int_G q_j \cdot \bar{q}_k \cdot dV(X_2) = \begin{cases} 0, & j \ne k, \\ 1, & j = k, \end{cases}$$

where $dV(X_\nu)$ −the volume element in X_ν $(\nu = 1,2)$. Then the system $\{p_\alpha \cdot q_\beta\}$ is an orthonormal system with respect to the scalar product

$$\langle \varphi, \psi \rangle = \int_{D\times G} \varphi \cdot \bar{\psi} dV(X_1) dV(X_2).$$

According to (4) any polynomial $f \in \mathcal{P}_\rho(X)$ admits a finite decomposition

$$f(z) = \sum_{j+k=1}^{d} c_{jk} \cdot p_j \cdot q_k. \tag{5}$$

Here

$$c_{jk} = \langle f, p_j q_k \rangle = \int_{D\times G} f \cdot \bar{p}_j \bar{q}_k dV(X_1) dV(X_2).$$

Consequently, an estimate holds

$$|c_{jk}| \le M_f(D,G) \cdot \sqrt{Vol(D \times G)},$$

Where $M_f(D,G) = \max_{D\times G}|f|$, and $Vol(D \times G)$ is the volume of the set $D \times G$ bounded by $X_1 \times X_2$. It is also known that the uniform norm of holomorphic functions on compact subset domains allows us to estimate over the L_2 norm. Therefore, there exists a constant $c = c(D,G) > 0$ such that the following inequalities hold

$$|p_j(\xi)| \le \frac{1}{c^{\dim X_1}} \|p_j\|_{L_2(D)} = \frac{1}{c^{\dim X_1}}, \quad \forall \xi \in K_1 ,$$
$$|q_k(\eta)| \le \frac{1}{c^{\dim X_1}} \|p_j\|_{L_2(G)} = \frac{1}{c^{\dim X_2}}, \quad \forall \eta \in K_2.$$

According to the Bernstein-Walsch inequality, from this we get that

$$|p_j(\xi)| \le \frac{1}{c^{\dim X_1}}\left(\Phi_{\rho_1}(\xi,K_1)\right)^d, \quad \forall \xi \in X_1,$$
$$|q_k(\eta)| \le \frac{1}{c^{\dim X_2}}\left(\Phi_{\rho_2}(\xi,K_2)\right)^d, \quad \forall \eta \in X_2.$$

Using the last inequalities, we finally get the following estimate for f

$$|f(z)| \le M(D,G)\cdot \dim\left(\mathcal{P}_\rho^d\right)\cdot\frac{1}{c^{\dim X}}\cdot\left(\max\left\{\Phi_{\rho_1}(\xi,K_1),\Phi_{\rho_2}(\xi,K_2)\right\}\right)^d.$$

This inequality is valid for any polynomial f, in particular, replacing f with its arbitrary degree – f^k, we have

$$\left|f^k(z)\right| \le M^k(D,G)\cdot \dim\left(\mathcal{P}_\rho^{kd}\right)\cdot\frac{1}{c^{\dim X}}\cdot\left(\max\left\{\Phi_{\rho_1}(\xi,K_1),\Phi_{\rho_2}(\xi,K_2)\right\}\right)^{kd}.$$

From this it follows that

$$|f(z)| \le M(D,G)\cdot\left(\dim\left(\mathcal{P}_\rho^{kd}\right)\right)^{\frac{1}{k}}\cdot\frac{1}{c^{\frac{\dim X}{k}}}\cdot\left(\max\left\{\Phi_{\rho_1}(\xi,K_1),\Phi_{\rho_2}(\xi,K_2)\right\}\right)^d. \quad (12)$$

Since (by the theorem 1)

$$\dim\left(\mathcal{P}_\rho^{kd}\right) \le const\cdot(kd+1)^{\dim X},$$

then, by letting $k\to\infty$ in inequality (12), we obtain the inequality

$$|f(z)| \le M(D,G)\cdot\left(\max\left\{\Phi_{\rho_1}(\xi,K_1),\Phi_{\rho_2}(\xi,K_2)\right\}\right)^d.$$

Note that when the neighborhoods D and G converge to compacts K_1 and K_2, then the value of $M(D,G)$ become close to the value of $M(K_1,K_2)$. From this, we obtain that for an arbitrary polynomial $f\in\mathcal{P}_\rho^d(X)$ satisfying the inequality $|f|\le 1,\ \forall z\in K = K_1\times K_2$, it holds

$$|f(z)|^{\frac{1}{d}} \le \max\left\{\Phi_{\rho_1}(\xi,K_1),\Phi_{\rho_2}(\xi,K_2)\right\}.$$

Consequently, it follows that

$$\Phi_\rho(z,K) \le \max\left\{\Phi_{\rho_1}(\xi,K_1),\Phi_{\rho_2}(\xi,K_2)\right\}.$$

The last inequality with the inequality (4.2) gives the equality

$$\Phi_\rho(z,K) = \max\left\{\Phi_{\rho_1}(\xi,K_1),\Phi_{\rho_2}(\xi,K_2)\right\}.$$

Theorem 3 is proven.

From the proven theorem by the inductive method, the following corollary can be obtained.

Corollary 2. Let *the regular parabolic manifold X consist of the Cartesian product of the regular parabolic manifolds (X_1,ρ_1), $(X_2,\rho_2),\dots,(X_m,\rho_m)$ and let $\rho = \ln(e^{2\rho_1\circ\pi_1}+e^{2\rho_2\circ\pi_2}+\dots+e^{2\rho_m\circ\pi_m})$ – be a special exhaustion function on X, where $\pi_1: M\to X_1$, $\pi_2: M\to X_2$, $\pi_m: M\to X_m$ – are projections. Then for any compact of the form $K = K_1\times K_2\times\dots\times K_m\subset X$, $K_j\subset X_j$, $j=\overline{1,m}$, following equality holds*

$$\Phi_\rho(z,K) = \max\left\{\Phi_{\rho_1}(\xi,K_1),\Phi_{\rho_2}(\xi,K_2),\dots,\Phi_{\rho_m}(\xi,K_m)\right\}.$$

Definition 4. A compact subset K of a regular parabolic manifold X is called regular if the function $\Phi_\rho(z,K)$ is continuous in X.

According to Theorem 3, it follows

Corollary 3. *Let the regular parabolic manifold consist of the Cartesian product of the regular parabolic manifolds $(X_1,\rho_1),(X_2,\rho_2),\dots,(X_m,\rho_m)$. If the compact subsets*

$K_j \subset X_j$, $j = \overline{1,m}$, are regular, then the compact $K = K_1 \times K_2 \times ... \times K_m \subset X$ is also regular.

Conclusion

In this work, we investigated extremal functions associated with ρ-polynomials on regular S-parabolic Stein manifolds. Building upon earlier results concerning the finiteness and approximation properties of ρ-polynomials, we established a precise formula for the extremal function $\Phi_\rho(z,K)$in the case where both the manifold and the compact set are products.

The main result demonstrates that the extremal function on a Cartesian product of regular S-parabolic manifolds is governed by the maximum of the extremal functions on the individual components. This extends the classical product rule known from pluripotential theory and the theory of polynomial approximation in $\mathbb{C}^n$ to a broader geometric setting of parabolic Stein manifolds equipped with special exhaustion functions.

As a corollary, we showed that regularity of compact sets with respect to $\Phi_\rho(z,K)$ is preserved under taking Cartesian products. This opens further avenues for analyzing more complex configurations of sets and functions in higher-dimensional complex manifolds.

These results contribute to the deeper understanding of approximation theory on complex manifolds and offer new tools for studying polynomial convexity and pluripotential theory in the framework of S-parabolic geometry.

References:

[1] Griffits P. and King J. “Nevanlinna theory and holomorphic mappings between algebraic varieties,” *Acta mathematica*, 130, 1973, pp.145-220.

[2] Stoll W. “Value distribution on parabolic spaces,” Lecture notes, № 600, *Springer*, Berlin-Heidelberg-New York, 1977.

[3] Stoll W. “The characterization of strictly parabolic manifolds,” *Ann. Scuola Norm. Sup. di Pisa*, p. IV VII (1), 1980, pp.87-154.

[4] Aytuna A., Sadullaev A. “Polynomials on Parabolic Manifestations,” *Contemporary mathematics* № 662, 2016, pp. 1-22.

[5] Plesniak W. “Remarques sur une généralisation de inegalité de Bernstein,” *CR. Acad. Sc. Paris*, 284, 1977, pp.1211-1213.

[6] Sičiak J. “On some extremal functions and their applications in the theory of analytic functions of several complex variables,” *Trans. Amer. Math. Soc.* 105, 1962, pp.322-357.

[7] Zeriahi A. “Function de Green pluricomplex a pole a l'infini sur un espace de Stein parabolic,” *Math. Scand.*, 69, 1991, pp. 89-126.

[8] Atamuratov A.A. “Polynomials on Regular Parabolic Manifestations.” *J. Math. Sci.* 278, 2024, pp. 596-612.

[9] Sadullayev A., Atamuratov A.A. “Polynomial Approximations on Parabolic Manifolds,” *Sbornic Mathematics*, 215:5, 2024, pp. 146-160.

UDC: 53, 004.94, 620.3

THE IMPORTANCE OF PHYSICS-BASED MODEL SELECTION AND RESULT CALIBRATION IN SIMULATION SUB-5NM SILICON GAAFETS

Abdikarimov Xidoyat Egamberganovich
Teacher, Urgench State University named after Abu Rayhan Biruni
xidoyat.a@urdu.uz

Annotatsiya. Mazkur maqolada sub-5nm undan kichik texnologik o‘lchamga ega bo‘lgan silikon asosli Gate-All-Around Field-Effect Transistor (GAAFET) larni modellashtirishda fizik modellarni to‘g‘ri tanlash va natijalarni kalibrovka qilishning muhim jihatlari o‘rganiladi. 5 nm va undan kichik o‘lchamdagi tranzistorlarda kvant effektlari, qisqa kanal hodisalari, tashuvchilar harakatchanligining pasayishi kabi fizik hodisalar ustun bo‘ladi. Shu sababli, an’anaviy modellashtirish yondashuvlari yetarli emas va ilg‘or fizik modellarni qo‘llash zarurati yuzaga keladi. Ushbu tadqiqotda Sentaurus TCAD muhitida qo‘llanilishi lozim bo‘lgan optimal fizik modellar ketma-ketligi, jumladan, drift-diffusion modeli, density-gradient kvant tuzatmalari, murakkab harakatchanlik modellarining birgalikda qo‘llanishi asoslab berilgan. Shuningdek, modellashtirish natijalarini real qurilma ma’lumotlariga moslashtirish uchun kalibrovka usullari taklif etilgan. Olingan natijalar nanoo‘lchamli tranzistorlarni ishonchli tahlil qilishda fizika asoslangan model tanlash va kalibrovkaning o‘ta muhimligini ko‘rsatadi.

Kalit so‘zlar: *Sub-5nm GAAFET, fizik modellar, TCAD modellashtirish, kvant tuzatmalari, harakatchanlikning degradatsiyasi, natijalarni kalibrovka qilish, Sentaurus dasturi.*

Аннотация. В данной статье рассматриваются ключевые аспекты выбора физических моделей и калибровки результатов при моделировании кремниевых транзисторов типа Gate-All-Around (GAAFET) с технологическим размером менее 5 нм. В условиях таких сверхмалых размеров проявляются квантовые эффекты, деградация подвижности носителей и ярко выраженные короткоканальные явления. Эти эффекты требуют применения продвинутых моделей в среде TCAD, в частности в Sentaurus. В работе предлагается оптимальная последовательность физических моделей: модель дрейф-диффузии с квантовыми поправками на основе градиента плотности, а также расширенные модели подвижности, учитывающие шероховатость поверхности, насыщение и фононное рассеяние. Отдельное внимание уделено процедурам калибровки — настройке параметров моделирования на основе экспериментальных данных. Результаты демонстрируют, что корректный выбор моделей и тщательная калибровка позволяют получить надежные прогнозы характеристик суб-5нм GAAFET-устройств и существенно повышают достоверность моделирования.

Ключевые слова: *GAAFET менее 5 нм, физические модели, TCAD моделирование, квантовые поправки, деградация подвижности, калибровка результатов, программа Sentaurus.*

Abstract. This paper investigates the critical Sentaurus role of physics-based model selection and calibration in the simulation of sub-5nm silicon Gate-All-Around Field-Effect Transistors (GAAFETs) using the TCAD environment. As transistor dimensions shrink below 5nm, classical modeling approaches become insufficient due to the increasing influence of quantum confinement, carrier mobility degradation, and short-channel effects. To address these challenges, we explore an optimized combination of physical models including drift-diffusion transport, density-gradient quantum corrections, and advanced mobility degradation models that account for surface roughness, phonon scattering, and high-field saturation. Additionally, essential effects such as band-to-band tunneling, bandgap narrowing, and Fermi–Dirac carrier statistics are integrated into the simulation flow. A robust calibration strategy is also proposed, aligning simulation outputs with experimental benchmarks through iterative parameter tuning. The findings confirm that accurate model selection and parameter calibration are indispensable for realistic and predictive simulation of next-generation GAAFET devices, especially at atomic-scale technology nodes.

Keywords: *Sub-5nm GAAFET, physics-based models, TCAD simulation, quantum corrections, mobility degradation, result calibration, Sentaurus software.*

Introduction

The continuous scaling of complementary metal-oxide-semiconductor (CMOS) technology has been the main driver of progress in the semiconductor industry for the past five decades. As devices shrink toward and below the 5 nm technology node, traditional FinFET architectures are increasingly limited by physical and electrostatic challenges such as short-channel effects (SCEs), leakage currents, and mobility degradation. These limitations pose serious constraints on device performance, power efficiency, and reliability in next-generation integrated circuits. To address these challenges, the Gate-All-Around Field-Effect Transistor (GAAFET) has emerged as a viable successor to FinFETs in sub-5nm nodes. In GAAFETs, the gate completely surrounds the channel region, providing superior electrostatic control over the charge carriers. This architecture significantly reduces SCEs, improves subthreshold slope, and enables further device miniaturization without compromising performance. Furthermore, GAAFETs can be fabricated using stacked nanosheet or nanowire channels, offering better area efficiency and design flexibility [1-3].

However, scaling below 5nm introduces several critical challenges. Quantum mechanical effects, including quantum confinement and direct tunneling, become prominent and cannot be neglected. Carrier mobility is reduced due to enhanced surface scattering, and variability due to process-induced fluctuations becomes a dominant concern. In this regime, classical device modeling approaches are no longer sufficient to capture the complex physics governing device behavior.

Therefore, the use of advanced TCAD (Technology Computer-Aided Design) tools with physics-based models is essential for accurate device simulation and performance prediction. Physics-based model selection becomes a pivotal factor in ensuring simulation accuracy. For instance, while the drift-diffusion model offers fast convergence, it fails to incorporate quantum effects crucial for sub-5nm devices. Quantum-corrected models such as the density-gradient or Schrödinger-Poisson solvers are necessary to model carrier behavior accurately in ultra-thin channels. Similarly, accurate modeling of carrier mobility degradation requires the incorporation of advanced scattering mechanisms and interface roughness models. Each of these models introduces computational complexity, and therefore, a balance between accuracy and efficiency must be achieved [4].

In addition to model selection, result calibration plays a crucial role in validating the simulation outcomes. Simulation results must be compared and tuned against experimental data or benchmark results to ensure their physical realism. This involves adjusting model parameters such as doping profiles, mobility factors, and quantum correction coefficients to fit known experimental trends. Without proper calibration, simulation data may be misleading or overly optimistic, resulting in flawed design decisions. The objective of this study is to investigate the impact of physics-based model selection and calibration on the accurate simulation of sub-5nm silicon-based GAAFETs using Sentaurus TCAD. Specifically, this research seeks to answer the following questions: (1) How do different physical models affect the accuracy of key performance indicators such as threshold voltage, subthreshold slope, and ON/OFF current ratio? (2) What are the optimal calibration strategies to align simulation data with real-world measurements? (3) What are the trade-offs between model accuracy and simulation runtime at this scale?

Research Methodology

Choice of Physical Models and Calibration Approach. This section describes the simulation framework used to model sub-5nm silicon GAAFETs in Sentaurus TCAD. The modeling process consists of three main components: device structure definition, selection of appropriate physical models, and calibration of simulation parameters based on experimental data [5, 6].

We begin by constructing a three-dimensional GAAFET device model with a gate-all-around geometry. The channel consists of silicon nanowires with diameters ranging from 3 to 5 nm. The source and drain regions are heavily n-doped, while the channel remains undoped to preserve electrostatic integrity. A high-k dielectric, such as HfO_2, is used as the gate insulator, and the gate material is assumed to be n+ polycrystalline silicon or metal gate, depending on the target technology node.

Meshing is performed with high density in critical regions such as the channel, source/drain junctions, and gate oxide interfaces. Adaptive meshing ensures numerical stability and captures spatial variations of potential and carrier concentration at nanoscale resolution [7-9].

For the transport model, the classical drift-diffusion approach is initially considered due to its simplicity and stability. However, to capture quantum mechanical effects dominant at sub-5nm scales, quantum corrections are added using the density gradient

model. This model introduces a quantum potential term that approximates the effects of carrier confinement without requiring a full quantum solution.

To simulate carrier mobility accurately, several mobility models are enabled. These include Lombardi surface roughness scattering, high-field saturation models, and phonon scattering models. For ultra-thin channels, confinement-induced mobility degradation is significant, so Philips unified mobility model is used in combination with interface charge models.

Recombination mechanisms such as Shockley-Read-Hall (SRH) and Auger are included, though their impact is minimal in short-channel devices operating in the strong inversion regime. However, including them ensures accuracy for all biasing conditions.

The bandgap narrowing model is used to account for heavily doped source/drain regions. The Fermi–Dirac statistics is enabled for more accurate carrier statistics, especially under high doping and strong inversion.

The thermionic emission and tunneling current models are included to capture carrier transport at the source/drain-channel junctions. Band-to-band tunneling (BTBT) is particularly important in determining off-state leakage current in aggressively scaled devices [10-15]. To assess short-channel effects, we analyze DIBL (Drain-Induced Barrier Lowering), subthreshold slope, and threshold voltage roll-off. These metrics are extracted under varying gate and drain bias conditions.

The calibration approach involves iterative adjustment of model parameters to match reference data. For this purpose, published experimental data from 5nm-node GAAFET devices is used as a benchmark. The threshold voltage, subthreshold slope, and I_{ON}/I_{OFF} ratio is used as primary metrics for calibration.

The effective oxide thickness (EOT), channel doping concentration, mobility parameters, and quantum correction coefficients are tuned to achieve close alignment with the reference curves. Each simulation run is followed by a comparison with target values, and parameters are updated accordingly.

The calibration is performed using parametric sweeps and design-of-experiments (DOE) techniques. This approach reduces the number of simulations needed and identifies sensitive parameters efficiently.

The simulation is run under both DC and transient conditions to ensure consistency across biasing regimes. The transfer characteristics (I_D-V_G), output characteristics (I_D-V_D), and capacitance-voltage (C-V) curves are all extracted and analyzed.

All simulations are conducted at room temperature (300 K) unless otherwise specified. Temperature-dependent behavior is also briefly examined to ensure model validity under realistic operation conditions.

Finally, the calibrated simulation results are validated by cross-checking with multiple sets of published data and previously modeled GAAFET structures. The successful calibration confirms the adequacy of the selected physical models and their implementation in Sentaurus TCAD. This comprehensive methodology ensures that simulation outcomes are both physically meaningful and predictive, enabling reliable design exploration for future sub-5nm technology nodes.

Analysis and Results

Summary of Optimal Physics Models for Sub-5nm silicon GAAFET Simulation. For GAAFETs with gate lengths of 5 nm and below, accurate simulation demands the use of advanced physics models that capture the dominant quantum and short-channel phenomena. Based on our simulation studies and comparison with experimental data, the following sequence of physical models is found to provide optimal trade-offs between accuracy, convergence, and computational cost:

1. Carrier Transport Model:

The drift-diffusion (DD) model serves as a stable baseline. However, for more accurate representation of carrier behavior in ultra-scaled channels, especially under high electric fields, it is recommended to supplement DD with density-gradient quantum corrections. In extremely scaled cases, quantum hydrodynamic (QHD) or Schrödinger–Poisson solvers may be used for benchmarking.

2. Quantum Confinement Effects:

The Density Gradient (DG) model effectively captures quantum confinement in nanowire or nanosheet channels without incurring the high computational cost of full quantum solvers. It introduces a quantum potential that adjusts carrier distribution near interfaces and improves subthreshold behavior modeling.

3. Mobility Models:

For sub-5nm nodes, mobility degradation due to surface scattering and high vertical fields is significant. The optimal setup includes:

- Philips unified mobility model (for broad temperature and doping dependencies),
- Lombardi surface roughness model,
- High-field saturation mobility model,
- Optional inclusion of remote phonon scattering for high-k dielectrics.

4. Recombination Models:

While recombination is not dominant in strong inversion, Shockley-Read-Hall (SRH) and Auger recombination should be included for completeness, especially in off-state or leakage current analysis.

5. Bandgap Narrowing and Degeneracy:

Bandgap narrowing (BGN) models must be used in heavily doped S/D regions to reflect realistic built-in potential and carrier concentrations. Fermi–Dirac statistics ensures accurate carrier distribution in degenerate doping conditions.

6. Tunneling Effects:

Band-to-band tunneling (BTBT) and trap-assisted tunneling models are essential for predicting off-state leakage and subthreshold swing in aggressively scaled devices.

7. Short-Channel Effects:

Models that allow accurate extraction of DIBL, threshold voltage roll-off, and subthreshold slope should be enabled, including non-local mobility degradation and quantum capacitance effects where applicable.

8. Calibration Strategy:

After selecting the above models, parameter calibration using experimental benchmark data, design-of-experiments (DOE), and sensitivity analysis is crucial. This ensures predictive accuracy and robustness across bias and process corners [16-18].

In summary, combining the drift-diffusion model with quantum corrections (DG), advanced mobility degradation models, and essential tunneling and bandgap models results in the most accurate and reliable simulation setup for sub-5nm GAAFETs. Calibration remains a key step to bridge simulation and real-world behavior. This optimized modeling flow enables researchers and designers to perform predictive simulations, evaluate performance trade-offs, and accelerate technology development at the atomic scale.

Conclusion

The accurate simulation of sub-5nm silicon-based Gate-All-Around Field-Effect Transistors (GAAFETs) poses a unique set of challenges due to the increasing dominance of quantum mechanical effects, short-channel phenomena, and mobility degradation. This study highlights the critical importance of selecting appropriate physics-based models in Technology Computer-Aided Design (TCAD) environments, such as Sentaurus.

Our investigation demonstrates that using the drift-diffusion transport model enhanced with density gradient quantum corrections provides a good balance between computational efficiency and physical accuracy. Incorporating advanced mobility models—including surface roughness scattering, high-field effects, and phonon interactions—further improves the reliability of simulation outcomes. Additionally, models accounting for band-to-band tunneling, bandgap narrowing, and Fermi–Dirac statistics are necessary to accurately capture leakage currents and subthreshold behavior in aggressively scaled devices. Equally important is the calibration of simulation parameters against experimental data or published benchmarks. Without this step, even physically accurate models can yield misleading predictions. By tuning doping profiles, mobility coefficients, and quantum correction parameters, the simulation results can be aligned with real-world measurements, ensuring predictive capability.

In conclusion, the combined use of quantum-aware transport models, advanced scattering mechanisms, and rigorous calibration practices enables robust and reliable simulation of sub-5nm GAAFETs. These results serve as a foundation for future research in nanoscale transistor design and provide practical guidelines for TCAD users aiming to explore device behavior at atomic dimensions. Continued development of model fidelity and calibration strategies will be essential as the semiconductor industry moves further into the angstrom era.

References:

[1] Barraud S. et al., “Performance and Design Considerations for Gate-All-Around Nanowire FETs,” *IEEE Electron Device Letters*, vol. 33, № 9, 2012, pp. 1225–1227.

[2] Morita Y. et al., “Device Modeling for Sub-5nm Nodes,” *Japanese Journal of Applied Physics*, vol. 59, № SB, 2020.

[3] Luisier M. and Klimeck G. “Atomistic Simulation of Nanowire Transistors,” *IEEE Transactions on Electron Devices*, vol. 58, no. 11, 2011, pp. 4049–4060.

[4] Poiroux T. et al., “TCAD Simulation of GAAFETs at 5 nm Node,” *Solid-State Electronics*, vol. 155, 2019, pp. 92–100.

[5] Khakifirooz A. et al., "Short-Channel Effects in Scaled GAAFETs," *IEEE Transactions on Nanotechnology*, vol. 12, № 4, 2013, pp. 555–562.
[6] Jin S. et al., "Modeling of Mobility in Ultra-Scaled Devices," *Journal of Computational Electronics*, vol. 10, 2011, pp. 135–143.
[7] Ilatikhameneh H. et al., "Simulation and Analysis of Nanowire and Nanosheet GAAFETs," *Nano Letters*, vol. 18, № 5, 2018, pp. 3137–3143.
[8] Saraswat K. and El-Gamal M.A. "Technology Scaling Beyond 7 nm," *Microelectronics Journal*, vol. 94, 2019, pp. 27–34.
[9] Chau R. et al., "Benchmarking Sub-5 nm Devices," *IEEE International Electron Devices Meeting (IEDM)*, 2016.
[10] Esseni D. and Palestri P. "Nanoscale MOS Transistors: Semi-Classical Transport and Applications," *Cambridge University Press*, 2011.
[11] Fischetti M.V. and Vandenberghe W.G. "Advanced Semiconductor Modeling," *Journal of Applied Physics*, vol. 119, 2016.
[12] Li Y. et al., "Calibration Methods in TCAD Modeling," *Microelectronics Reliability*, vol. 76–77, 2017, pp. 152–158.
[13] Martinez A. et al., "Impact of BTBT and Quantum Effects on Ultra-Thin-Body FETs," *IEEE Transactions on Electron Devices*, vol. 64, № 5, 2017, pp. 1873–1880.
[14] Jeong K. et al., "Quantum-Corrected Simulations for 5nm Technology Node," *Semiconductor Science and Technology*, vol. 36, № 8, 2021.
[15] Sano N. "Quantum Effects in Device Simulations," *Journal of Computational Electronics*, vol. 14, 2015, pp. 935–945.
[16] Kim S.H. et al., "GAAFET Process and Device Simulation Using Sentaurus," *Materials Science in Semiconductor Processing*, vol. 121, 2021.
[17] Xie Y. et al., "3D Simulation and Optimization of GAAFETs," *IEEE Access*, vol. 8, 2020, pp. 132709–132717.
[18] Solomon P.M. "Challenges and Models for 5 nm and Beyond," *Nature Electronics*, vol. 2, 2019, pp. 8–10.

UDC: 5, 51, 510.6, 517.9

EXISTENCE AND UNIQUENESS OF SOLUTIONS FOR A MIXED-TYPE PROBLEM WITH INTEGRAL GLUING CONDITIONS

Baltayeva Umida Ismoilovna
Associate Professor, Urgench State University named after Abu Rayhon Biruni, Khorezm Ma'mun Academy
umida_baltayeva@mail.ru

Babajanova Yulduz Ikromboyevna
Doctoral Student, Khorezm Ma'mun Academy
yulduzb90@gamil.com

Jumanazarov Otabek Isroilovich
Teacher at Union School Khorezm Private School.
otabek5583060@gmail.com

Annotatsiya. Ushbu maqolada Riman–Liuvill kasr hosilalariga ega bo'lgan yuklangan differensial tenglama uchun chegara masalasi va integral ulash shartlari o'rganiladi. Masala integral va kasr-tartibli tenglamalar tizimiga keltirilish orqali yechimning mavjudligi va yagonaligini ta'minlovchi shartlar aniqlanadi.

Kalit so'zlar: *Yuklangan differensial tenglama, integral ulash sharti, parabolik–giperbolik masala, Riman–Liuvill kasr operatori, yechim mavjudligi, yechimning yagonaligi.*

Аннотация. В данной работе рассматривается краевая задача для нагруженного дифференциального уравнения с дробными производными Римана–Лиувилля и интегральными условиями склейки. Путём сведения задачи к системе интегральных и дробных уравнений установлены условия существования и единственности решения.

Ключевые слова: *Нагруженное дифференциальное уравнение, интегральное условие склейки, параболо-гиперболическая задача, дробный оператор Римана–Лиувилля, существование решения, Единственность решения.*

Abstract. This paper examines a boundary value problem for a loaded differential equation with Riemann–Liouville fractional derivatives and integral gluing conditions. By reducing the problem to a system of integral and fractional equations, conditions ensuring existence and uniqueness of the solution are established.

Keywords: *Loaded differential equation, integral gluing condition, parabolic–hyperbolic problem, Riemann–Liouville fractional operator, existence of solution, uniqueness of solution.*

Introduction

Mixed-type equations appear in models combining diffusion and wave propagation. When such equations include Riemann–Liouville fractional derivatives, they better describe systems with memory. These problems are especially challenging when involving nonlocal gluing conditions. This study focuses on such a boundary value problem and develops criteria for the existence and uniqueness of solutions using an integral equation approach.

Literature Review

Previous studies by Samarskii, Nakhushev, and Berdyshev analyzed fractional mixed-type problems with gluing conditions. Methods using Volterra-type integral equations and resolvent kernels applied by Pulkina, Bouziani Agarwal and Abdullayev serve as the foundation for this work, enhancing theoretical understanding and applications.

Research Methodology

The problem is transformed into a system of Volterra-type integral equations. In the hyperbolic domain, solutions involve Bessel functions, while in the parabolic region, weakly singular equations are handled via resolvent kernel methods. Gluing conditions connect the two solutions, and existence/uniqueness is proved using classical fractional calculus theory.

Analysis and Results

I. Let D be a domain bounded by segments $y=0$, $x=1$, $y=1$ and $x=-1$. We introduce the following notations

$$D_1 = D \cap \{x>0\},\ D_2 = D \cap \{x<0\}, I = \{(x,y): x=0, 0<y<1\}.$$

We consider the following linear loaded integro-differential equation:

$$u_{xx} - \frac{1-sgn\,x}{2} u_{yy} - \frac{1+sgn\,x}{2} u_y + c_k(x,y)u + Mu = 0, \text{in } D_k, \qquad (1.1)$$

where $Mu \equiv \sum_{i=1}^{n} a_i(x,y) D_{0y}^{\alpha_i} u(0,y)$ in D_1 and $Mu \equiv \sum_{i=1}^{n} b_i(x,y) D_{0y}^{\beta_i} u(0,y)$ in D_2, respectively, D_{0y}^{γ} Riemann-Liouville fractional integral operator of order $\gamma(\gamma = \alpha_i, \beta_i)$, $\gamma < 0$. We assume that the functions $a_i(x,y)$, $b_i(x,y)$ and $c_k(x,y)(k=1,2)$ have a Holder continuous derivative on the closure of domain $\bar{D}$.

Problem. Find a function $u(x,y)$ satisfying the conditions:

1) $u(x,y) \in C(\overline{D_k}) \cap C^1(D_k \cup I)$, $u(x,y)$ is a regular solution of (1.1) in the domains $D_k(k=1,2)$;

2) satisfies boundary conditions:

$$u(-1,y) = \varphi_1(y),\quad u(1,y) = \varphi_2(y),\quad 0 \le y \le 1,$$
$$u(x,0) = \psi_1(x),\quad u_y(x,0) = 0,\quad -1 \le x \le 0,$$
$$u(x,0) = \psi_2(x),\quad 0 \le x \le 1;$$

3) the following gluing conditions

$$\tau_1(y) = \mu(y)\tau_2(y) + \sigma(y), \nu_1(y) = \int_0^y \gamma(y,\eta)\nu_2(\eta)d\eta + \delta(y)\nu_2(y),$$

are satisfied on I, $\tau_1(y) = u(+0,y), \nu_1(y) = u_x(+0,y)$, $\tau_2(y) = u(-0,y), \nu_2(y) = u_x(-0,y)$;

where $\varphi_1(y), \varphi_2(y), \psi_1(x), \psi_2(x), \mu(y), \sigma(y), \delta(y), \gamma_y(y,\eta)$, are given functions, $\mu(y) \neq 0, \gamma^2(y,\eta) + \delta^2(y) \neq 0,$

moreover, $\varphi_1(0) = \psi_1(-1), \varphi_2(0) = \psi_2(1), \psi_2(0) = \mu(0)\psi_1(0) + \sigma(0).$

Theorem1: If $\psi_1''(x)$, $\varphi_1''(y)$, $\psi_2''(x)$, $\varphi_2(y)$, $c_1(x,y)$, $\mu'(y)$, $\sigma'(y), \delta'(y), \gamma_y(y,\eta)$ are Holder continuous, $c_1(x,y) \leq 0, c_2(x,y) \equiv const$ and

$$\delta(0)\psi_1'(0) - \psi_2'(0) = 0, \quad \text{if} \quad \delta(y) \neq 0, -\psi_2(0) = 0,$$
$$\sigma'(0) + \mu'(0)\psi_1(0) = 0, \quad \text{if} \quad \delta(y) \equiv 0, \varphi_1(0) = \psi_1(-1), \quad \varphi_2'(0) = 0, \tag{1.2}$$

then there exists a unique solution to problem .

II. Basic relation from the hyperbolic part. First, consider the following auxiliary problem:

$$u_{xx} - u_{yy} + c_2(x,y)u - \sum_{i=1}^{n} b_i(x,y) D_{0y}^{\beta_i} u(0,y) = 0, \tag{2.1}$$

$$u(x,0) = \psi_1(x), \quad u_y(x,0) = 0, \quad -1 \leq x \leq 0, \tag{2.2}$$
$$u(-1,y) = \varphi_1(y), \quad u(-0,y) = \tau_2(y), \quad 0 \leq y \leq 1,$$

where $\beta_i < 0$. It is easy to verify that a solution to the Cauchy problem (2.1), (2.2), taking into account the conditions of the Theorem1, $b_i(x,y)$ are continuously differentiable functions, and the coefficient $c_2(x,y) \equiv c_2$, can be represented as [3]. Hence, satisfying the condition $u(-0,y) = \tau_2(y)$, to the solution of the Cauchy problem [3], we obtain the integral equation for determining $\psi_1(y)$.

$$\psi_1(y) + \int_0^y \omega(0,y,\xi)\psi_1(\xi)d\xi = 2\tau_2(y) +$$
$$+\sum_{i=1}^{n} \frac{1}{\Gamma(-\beta_i)} \int_0^y \tau_2(t)dt \int_t^y \frac{d\eta}{(\eta - t)^{1+\beta_i}} \int_{-y+\eta}^{y-\eta} b_i(\xi,\eta) I_0\left(\sqrt{c_2((y-\eta)^2 - \xi^2)}\right) d\xi -$$
$$-\psi_1(-y) - \int_{-y}^{0} \omega(0,y,\xi)\psi_1(\xi)d\xi, 0 \leq y \leq 1.$$

Thus, we get the function

$$\psi_1(x) = \begin{cases} 2\tau_2(x) - 2\int_0^x B_1(x,t)\tau_2(t)dt + g_1(x), & 0 \leq x \leq 1, \\ \psi_1(x), & -1 \leq x \leq 0, \end{cases}$$

which by taking into account agreement conditions and (1.2) is twice continuously differentiable on [-1,1].

In the same way, taking into account the conditions theorem1. and $u(-1,y) = \varphi_1(y)$, we can continue $\psi_1(y)$ to the segment [-2,-1]. Consequently, we can write the final solution to the Cauchy problem for equation (2.1) with the conditions $u(x,0) = \psi_1(x)$, $u_y(x,0) = 0$, analogously as [3]. Hence, substituting the solution of the Cauchy problem [3] into condition $u_x(-0,y) = \nu_2(y)$, we have

$$\nu_2(y) = \tau_2'(y) + \int_0^y K_1(y,t)\tau_2(t)dt + g_3(y), \quad 0 \leq y \leq 1, \tag{2.3}$$

where

$$K_1(y,t) = -R_{1y}(y,t) + \frac{c_2}{2} y R_1(y,t) + w_x(0,y,t) - \int_t^y w_x(0,y,\xi)R_1(\xi,t)d\xi + C(y,t).$$

III. Basic relation from the parabolic part. Solving the first boundary value problem for the equation (1.1) in the domain D_1, with regards to conditions of theorem1, we make sure that the solution $u(x,y)$ satisfies the loaded integral equation [2]:

$$u(x,y)=u_0(x,y)+\int_0^y d\eta\int_0^1 c_1(\xi,\eta)G(x,y;\xi,\eta)u(\xi,\eta)d\xi+$$

$$+\int_0^y D_{0\eta}^{\alpha_i}u(0,\eta)d\eta\int_0^1\sum_{i=1}^n a_i(\xi,\eta)G(x,y;\xi,\eta)d\xi, \qquad (3.1)$$

where

$$u_0(x,y)=\int_0^y G_\xi(x,y;0,\eta)\tau_1(\eta)d\eta+V(x,y), V(x,y)=\int_0^y G(x,y;\xi,0)\psi_2(\xi)d\xi-$$

$$\int_0^y G_\xi(x,y;1,\eta)\varphi_2(\eta)d\eta.$$

The loaded equation (3.1), taking into account the Riemann-Liouville fractional integral operator, can be reduced to integral equation:

$$u(x,y)=u_0(x,y)+\int_0^y d\eta\int_0^1 K(x,y;\xi,\eta)u(\xi,\eta)d\xi+\int_0^y \widetilde{K}(x,y,\eta)u(0,\eta)d\eta, \qquad (3.2)$$

where

$$K(x,y;\xi,\eta)=c_1(\xi,\eta)G(x,y;\xi,\eta),$$

$$K(x,y,\eta)=\sum_{i=1}^n\frac{1}{\Gamma(-\alpha_i)}\int_0^y(t-\eta)^{-1-\alpha_i}dt\int_0^1 a_i(\xi,t)G(x,y;\xi,t)d\xi.$$

The following theorem holds

Theorem 2: Loaded integral equation of Volterra type (3.1) whose kernels $K(x,y;\xi,\eta)$, $\widetilde{K}(x,y,\eta)$ and the function $u_0(x,y)$ belong to the class with a weak singularity has one and only one solution in this same class, and given by the formula

$$u(x,y)=u_0(x,y)+\int_0^y d\eta\int_0^1 R(x,y;\xi,\eta)u_0(\xi,\eta)d\xi, \qquad (3.3)$$

where the resolvent of the kernel $R(x,y;\xi,\eta)$ is given by power of a series consisting of repeating kernels K and $\widetilde{K}$.

Therefore, differentiating (3.4) with respect to x and passing to the limit at $x\to+0$ we obtain the relation between the functions $\tau_1(y)$ and $\nu_1(y)$:

$$\nu_1(y)=-\frac{1}{\sqrt{\pi}}\int_0^y\frac{(1+k(y,t))}{\sqrt{y-t}}\tau_1'(t)dt+\int_0^y\Phi(y,t)\tau_1(t)dt+P(y), \qquad (3.4)$$

where

$$k(y,t)=2\sum_{n=1}^\infty exp\left(-\frac{n^2}{y-t}\right),$$

$$\Phi(y,t)=\int_0^y d\eta'\int_0^1 R_x(0,y;\xi',\eta')G_\xi(\xi',\eta';0,t)d\xi'+\widetilde{K}(1;\xi,t),$$

$$P(y)=V_x(0,y)-\psi_2(0)\frac{1+k(y,0)}{\sqrt{\pi y}}+\int_0^y d\eta\int_0^1 R_x(0,y;\xi,\eta)V(\xi,\eta)d\xi.$$

This relation (3.4) is the main relation from the domain D_1 to I.

IV. Recovery of solutions to a mixed Problem. Substituting relations (2.3) and (3.4) into the gluing conditions of an integral form (1.2), excluding the functions $\tau_2(y)$, $\nu_1(y)$

and $\nu_2(y)$ with taking into account $\tau_2(y)=\frac{1}{\alpha(y)}\tau_1(y)-\frac{\beta(y)}{\alpha(y)}$, $\tau_1'(y)=\eta(y)$, we obtain the following integral equation:

$$\frac{1}{\sqrt{\pi}}\int_0^y \frac{\eta(t)}{\sqrt{y-t}}dt=-\frac{\delta(y)}{\mu(y)}\eta(y)-\int_0^y K_2(y,t)\eta(t)dt+g_5(y), \tag{4.1}$$

where

$$K_2(y,t)=-\frac{k(y,t)}{\sqrt{\pi(y-t)}}+\frac{\gamma(y,t)}{\mu(t)}+\delta(y)q_1(y)+\frac{\xi(y)}{\mu(y)}+$$
$$+\int_t^y\left[q_1(\eta)\gamma(y,\eta)-\Phi(y,\eta)+\frac{\delta(y)}{\mu(\eta)}K_1(y,\eta)\int_\eta^y\frac{\gamma(y,s)}{\mu(\eta)}K_1(s,\eta)ds\right]d\eta.$$

$g_5(y)$ is known continuously differentiable function.

If the condition (1.2) holds for the function, then equation (4.1) takes the form of a Volterra integral equation with a weak singularity, which guarantees a unique solution based on the properties outlined in Theorem 1. Moreover, when the same condition (1.2) is satisfied, and certain transformations are applied, the resulting equation becomes a Volterra integral equation of the second kind, which also ensures the existence of a unique solution [2]. Subsequently, the function is determined through an explicit formula, while the functions and are established using the gluing conditions and equations (1.2), (2.3), and (3.4), respectively.

As a result, the solution to the original boundary value problem is reconstructed in the domain as the solution to the first boundary value problem for equation (1.1). In the domain the solution is expressed via a given formula [3]. The uniqueness of the overall solution is ensured since the derived integral equation [3] possesses a unique solution. Theorem 1 is proved.

Conclusions

The study establishes the existence and uniqueness of a solution to a mixed-type loaded equation with fractional derivatives and integral gluing. Using integral equations and the resolvent kernel method, a reliable solution was obtained, contributing to the theory of fractional and nonlocal differential equations.

References:

[1] Nakhushev A.M. “Loaded Equations and Their Applications.” Moscow: *Nauka,* 2012.
[2] Kress R. “Linear Integral Equations.” 3rd Edition, *Springer-Verlag*, New York, 2014.
[3] Baltaeva U., Babajanova Y., Agarwal P., Ozdemir N. “Solvability of a mixed problem with the integral gluing condition for a loaded equation with the Riemann–Liouville fractional operator.” *Journal of Computational and Applied Mathematics* 425(11), June 2023, p. 115066.
[4] Dzhuraev T.D., Sopuev A., Mamazhanov M. “Boundary value problems for parabolic-hyperbolic equations.” Tashkent: *Fan*, 1986.
[5] Salohiddinov M. “Matematik fizika tenglamalari.” Tashkent, *Uzbekistan*, 2002.

UDC: 53, 53.01/.09

INVERSE SCATTERING FOR THE DULLIN-GOTTWALD-HOLM EQUATION WITH A SOURCE

Abbosbek Iskandarov
Doctoral Student, Khorezm Mamun Academy
iskandarovabbosbek@gmail.com

Annotasiya. Ushbu maqolada Dullin–Gottvald–Holm tenglamasining o‘z-o‘ziga mos manbali holi uchun Koshi masalasining tez kamayuvchi funksiyalar sinfida o‘rganiladi. Yechimni qurish uchun teskari masala (IST) metodidan foydalanishga asoslangan algoritm taklif etiladi. Ayniqsa, fizik nuqtai nazardan, o‘zgaruvchan tezlikka ega yakka to‘lqinlarda manbalar paydo bo‘lishi va bu holat fizik modellar ichida murakkab va xilma-xil dinamikaga olib kelishi tahlil qilinadi.

Kalit so‘zlar: *Dullin-Gottvald-Holm tenglamasi, Yost yechim, iz formulalari, teskari spektral masala, Shturm - Liouvil operatori, Laks juftligi.*

Аннотация. В данной работе рассматривается задача Коши для уравнения Дуллина–Готвальда–Холма с источником в классе быстро убывающих функций. Таким образом, представлен алгоритм построения решения методом (ИСТ). В частности, с физической точки зрения анализируется, что источники возникают в одиночных волнах с переменными скоростями и что это приводит к сложной и разнообразной динамике в рамках физических моделей.

Ключевые слова: *Уравнение Дуллина-Готтвальда-Холма, Решение Йоста, следовые формулы, обратная спектральная задача, оператор Штурма-Лиувилля, пара Лакса.*

Abstract. In this paper, the Cauchy problem for the Dullin–Gottwald–Holm equation with a source in the class of rapidly decreasing functions and a procedure is developed to construct the solution via the IST method is presented. In particular, from a physical perspective, it is analyzed that sources arise in single waves with variable velocities and that this leads to complex and diverse dynamics within physical models.

Keywords: *Dullin-Gottwald-Holm equation, Jost solution, trace formulas, inverse spectral problem, Sturm - Liouville operator, Lax pair.*

Introduction

The nonlinear partial differential equation:

$$m_t + 2\omega u_x + u m_x + 2 m u_x = -\gamma u_{xxx}$$

in dimensionless time-space variables (t, x) models the unidirectional propagation of two-dimensional waves in shallow water over a flat bottom, where $m = u - u_{xx}$ and ω is constant. In [1], Dullin, Gottwald and Holm derived the Eq. (1) based on asymptotic approaches expansions immediately in the Hamiltonian for Euler equations

in the shallow water regime and thereby it is shown to be bi-Hamiltonian and has a Lax pair formulation.

Literature Review

Recently, many papers were devoted to the study of the DGH equation from both mathematical and physical points of view [2-10].

In the present paper, we study the Dullin-Gottwald-Holm equation with a source

$$\begin{cases} u_t - u_{xxt} + 2\omega u_x + 3uu_x - 2u_x u_{xx} - uu_{xxx} + \gamma u_{xxx} = \\ = \sum_{k=1}^{N}(m_x' g_k^2 + 2(m+\omega+\frac{\gamma}{2})(g_k^2)_x'), \\ g_{kxxx}'' = \left(\frac{1}{4} + \eta_k\left(m+\omega+\frac{\gamma}{2}\right)\right) g_k, k = 1,2,\dots,N, x \in R \end{cases} \quad (1)$$

under initial condition

$$u(x,0) = u_0(x), \quad (2)$$

where $u = u(x,t)$, $m = u - u_{xx}$, $\omega + \frac{\gamma}{2} = const > 0$, $m + \omega + \frac{\gamma}{2} > 0$ is analyzed in the current work.

It is assumed that the function $u = u(x,t)$ is sufficiently smooth and decays rapidly to its limit when $x \to \pm\infty$, and for all $t \geq 0$

$$\int_{-\infty}^{\infty}(1+|x|)\left(|u(x,t)| + \sum_{k=1}^{3}\left|\frac{d^k u(x,t)}{dx^k}\right|\right)dx < \infty \ . \quad (3)$$

In the context of the current problem, $g_k = g_k(x,t)$ is a solution to the equation $g_{kxxx}'' = \left(\frac{1}{4} + \eta_k\left(m+\omega+\frac{\gamma}{2}\right)\right) g_k$ and corresponds to the eigenvalue η_k, normalized by the condition

$$\int_{-\infty}^{\infty}(m+\omega+\frac{\gamma}{2})g_k^2 dx = A_k(t), k = 1,2,\dots,N. \quad (4)$$

Representations for solutions $u(x,t)$, $g_k(x,t), k = 1,2,\dots,N$ of the problem (2) are obtained in the present paper by means of the inverse problem method for the equation $y_{xx}'' = \left(\frac{1}{4} + \eta(m+\omega+\frac{\gamma}{2})\right) y$.

Research Methodology

Preliminaries:

Consider the equation

$$\psi_{xx}'' = \left(\frac{1}{4} + \eta(m+\omega+\frac{\gamma}{2})\right)\psi \quad (5)$$

where $u = u(x)$, $m = u - u_{xx}$, $\eta(k) = -\frac{1}{\omega+\frac{\gamma}{2}}\left(k^2 + \frac{1}{4}\right)$, with the function $u(x)$ satisfying the condition

$$\int_{-\infty}^{\infty}(1+|x|)(|u(x)| + |u''(x)|)\,dx < \infty \quad (6)$$

The present section contains information on the direct and inverse scattering problem for the problem (5-6) necessary for our further exposition. Provided that the condition (6) is met, Equation (5) possesses the Jost solutions with the following asymptotics:

$$\psi_1(x,k) = e^{-ikx} + o(1), x \to +\infty,$$
$$\psi_2(x,k) = e^{ikx} + o(1), x \to +\infty, \quad (7)$$
$$\phi_1(x,k) = e^{-ikx} + o(1), x \to -\infty,$$
$$\phi_2(x,k) = e^{ikx} + o(1), x \to -\infty. \quad (8)$$

When k are real, the pairs $\{\phi_1, \phi_2\}$ and $\{\psi_1, \psi_2\}$ are pairs of linearly independent solutions for Equation (5). Therefore,

$$\varphi_1(x,k) = a(k)\psi_1(x,k) + b(k)\psi_2(x,k). \quad (9)$$

One can readily see that

$$a(k) = -\frac{1}{2ik} W\{\psi_2(x,k), \phi_1(x,k)\}.$$

The function $a(k)$ admits an analytic continuation into the upper half-plane and has a finite number of zeroes $k = ik_n, k_n > 0$. Meanwhile,

$$\eta_n = -\frac{1}{\omega+\frac{\gamma}{2}}\left(-{k_n}^2 + \frac{1}{4}\right), \quad n = 1,2,\dots,N$$

is an eigenvalue of Equation (5) so that

$$\phi_1(x, ik_n) = b_n\psi_2(x, ik_n), n = 1,2,\dots,N. \quad (10)$$

The set $\left\{R(k) = \frac{b(k)}{a(k)}, k \in R, k_n, b_n, n = 1,2,\dots,N\right\}$ is called the scattering data for Equation (5). The inverse scattering problem consists in recovering the function $m(x)$, and consequently $u(x)$ of Equation (5) by the scattering data.

Note that the functions h_n, defined by the equalities

$$h_n(x) = \frac{\frac{d}{dk}(\phi_1 - b_n\psi_2)|k=ik_n}{\dot{a}(ik_n)}, n = 1,2,\dots,N, \quad (11)$$

where $\phi_{1n} = \phi_1(x, ik_n), \psi_{2n} = \psi_2(x, ik_n), \ n = 1,2,\dots,N$ are solutions to the equations ${h_{nxx}}'' = \left(\frac{1}{4} + \eta_n(m+\omega)\right)h_n$, and the asymptotics

$$h_n(x) \to -b_n e^{-k_n x} when x \to -\infty,$$
$$h_n(x) \to e^{k_n x} when x \to \infty \quad (12)$$

are true for them. According to (9), (6), (11), the equalities

$$W\{\varphi_{1n}, h_n\} \equiv \varphi_{1n}{h_n}' - \varphi'_{1n}h_n = 2k_n b_n, n = 1,2,\dots,N \quad (13)$$

hold. In what follows, we will need the following lemma.

Lemma 1. If functions f and g are solutions to equations

$$f''_{xx} = \left(\frac{1}{4} + \eta_1(m + \omega + \frac{\gamma}{2})\right)f,$$
$$g''_{xx} = \left(\frac{1}{4} + \eta_2(m + \omega + \frac{\gamma}{2})\right)g,$$

the following equality holds for them:

$$(m + \omega + \frac{\gamma}{2})fg = \frac{1}{\eta_1 - \eta_2}\frac{d}{dx}W\{g, f\}.$$

The lemma is proved by direct verification.

Analysis and Results

Let the function $u(x,t)$ in (5) be a solution to the equation

$$u_t - u_{xxt} + 2\omega u_x + 3uu_x - 2u_x u_{xx} - uu_{xxx} + \gamma u_{xxx} = G(x,t) \quad (14)$$

where the function $G = G(x,t)$ is sufficiently smooth and $G(x,t) = o(1)$ when $x \to \pm\infty, t \geq 0$.

Lemma 2. If the function $u(x,t)$ is a solution to Equation (14) in the class of functions (3) then, the scattering data of the problem (5) with the function $u(x,t)$ depend on t as follows:

$$\frac{\partial R(k,t)}{\partial t} = -4ikR(k,t)\left(\frac{\omega+\frac{\gamma}{2}}{4k^2+1} + \frac{\gamma}{2}\right) - \frac{4k^2+1}{8ik\left(\omega+\frac{\gamma}{2}\right)a^2(k)}\int_{-\infty}^{\infty} G\varphi_1^2 dx, (Im\, k = 0),$$

$$\frac{db_n(t)}{dt} = 4k_n b_n\left(\frac{\omega+\frac{\gamma}{2}}{1-4k_n^2} - \frac{\gamma}{2}\right) + \frac{1-4k_n^2}{8\left(\omega+\frac{\gamma}{2}\right)k_n}\int_{-\infty}^{\infty} G\varphi_{1n}h_n\,dx,$$

$$\frac{dk_n(t)}{dt} = i\frac{1-4k_n^2}{8\left(\omega+\frac{\gamma}{2}\right)k_n b_n \dot{a}(ik_n)}\int_{-\infty}^{\infty} G\varphi_{1n}^2 dx, n = 1,2,\dots,N.$$

Proof. When k are real, we seek the Lax pair for Equation (14) in the form:

$$\varphi''_{1xx} = \left(\frac{1}{4} + \eta(m+\omega+\frac{\gamma}{2})\right)\varphi_1, \tag{15}$$

$$\varphi'_{1t} = \left(\frac{1}{2}\left(\frac{1}{\eta}+2\gamma\right) - u\right)\varphi'_{1x} + \frac{1}{2}u'_x\varphi_1 + \beta\varphi_1 + F(x,k,t), \tag{16}$$

where $m(x,t) = u(x,t) - u''_{xx}(x,t)$, $\beta = \frac{ik}{2}\left(\frac{1}{\eta}+2\gamma\right)$, a $\phi_1 = \phi_1(x,k,t)$ are the Jost solutions of the equation (15) with the asymptotics (8). Using the equality $\phi'''_{1xxt} = \phi'''_{1txx}$, on the basis of the equalities (14), (15), and (16), we obtain

$$F''_{xx} - \left(\frac{1}{4} + \eta(m+\omega+\frac{\gamma}{2})\right)F = \eta G\varphi_1. \tag{17}$$

Let us find solution to this equation in the form

$$F(x,k,t) = A(x,t)\varphi_1(x,k,t) + B(x,t)\varphi_2(x,k,t).$$

Then, derive the system of equations

$$\begin{cases} A'_x\varphi_1 + B'_x\varphi_2 = 0, \\ A'_x\varphi'_{1x} + B'_x\varphi'_{2x} = \eta G\varphi_1. \end{cases} \tag{18}$$

to determine $A(x,t)$ and $B(x,t)$. Using the asymptotics of the function $\phi_1(x,k,t)$ and (3), let us pass to the limit in the equality (16) when $x \to -\infty$. The passage to the limit results in $F(x,t) \to 0$, when $x \to -\infty$.

Hence, solution of the system of equations (18) has the form:

$$A(x,t) = -\frac{\eta}{2ik}\int_{-\infty}^{x} G\varphi_1\varphi_2 dx,$$

$$B(x,t) = \frac{\eta}{2ik}\int_{-\infty}^{x} G\varphi_1^2 dx.$$

In this case, the second equation of the Lax pair has the form

$$\varphi'_{1t} = \left(\frac{1}{2\eta} + \gamma - u\right)\varphi'_{1x} + \left(\frac{u'_x}{2} + \beta\right)\varphi_1 + \left(-\frac{\eta}{2ik}\int_{-\infty}^{x} G\varphi_1\varphi_2 dx\right)\varphi_1 + \frac{\eta}{2ik}\int_{-\infty}^{x} G\varphi_1^2 dx\,\varphi_2 \tag{19}$$

Passing to the limit $x \to \infty$ in the equality (19) by virtue of (3), (7), (9), one obtains

$$a_t(k,t) = -\frac{\eta}{2ik}\int_{-\infty}^{\infty} G\varphi_1\varphi_2 dx\, a(k,t) + \frac{\eta}{2ik}\int_{-\infty}^{\infty} G\varphi_1^2 dx\,\overline{b}(k,t), \tag{20}$$

$$b_t(k,t) = 2\beta b(k,t) - \frac{\eta}{2ik}\int_{-\infty}^{\infty} G\varphi_1\varphi_2 dx\, b(k,t) + \frac{\eta}{2ik}\int_{-\infty}^{\infty} G\varphi_1^2 dx\,\overline{a}(k,t). \tag{21}$$

Multiply (21) by a and subtract from it the quality (20) multiplied by b. Then, using the definition of the function $R(k)$ and substituting $\eta(k) = -\frac{1}{\omega+\frac{\gamma}{2}}\left(k^2+\frac{1}{4}\right)$, we obtain

$$\frac{\partial R}{\partial t} = -4ikR\left(\frac{\omega+\frac{\gamma}{2}}{4k^2+1} + \frac{\gamma}{2}\right) - \frac{4k^2+1}{8ik\left(\omega+\frac{\gamma}{2}\right)a^2(k)}\int_{-\infty}^{\infty} G\varphi_1^2 dx.$$

In the general case, eigenvalues of the equation $y_{xx}'' = \left(\frac{1}{4} + \eta(m+\omega+\frac{\gamma}{2})\right)y$depend on time. Therefore, differentiating the equalities

$$\phi_1(x,ik_n,t) = b_n(t)\psi_2(x,ik_n,t), n = 1,2,\dots,N. \tag{22}$$

with respect to t, we obtain

$$\frac{\partial\phi_{1n}}{\partial t} = \frac{db_n}{dt}\psi_{2n} - \dot{a}(ik_n)h_n\frac{d(ik_n)}{dt} + b_n\frac{\partial\psi_{2n}}{\partial t}. \tag{23}$$

according to the notation (10). Similarly, to the case of the continuous spectrum, we seek the Lax pair in case of the discreet spectrum in the following form:

$$\varphi''_{1nxx} = \left(\frac{1}{4} + \eta_n(m + \omega + \frac{\gamma}{2})\right)\varphi_{1n}\,, \tag{24}$$

$$\varphi'_{1nt} = \left(\frac{1}{2\eta_n} + \gamma - u\right)\varphi'_{1nx} + \frac{1}{2}u'_x\varphi_{1n} + \beta_n\varphi_{1n} + F_n\,. \tag{25}$$

Then, we obtain the equation

$$F''_{nxx} - \left(\frac{1}{4} + \eta_n(m(x,t) + \omega + \frac{\gamma}{2})\right)F_n = \eta_n G\varphi_{1n}. \tag{26}$$

Let us solve (26) in the form

$$F_n(x,t) = A_n(x,t)\phi_{1n} + B_n(x,t)h_n.$$

Likewise, in order to find $A_n(x,t)$ and $B_n(x,t)$, we obtain a system of equations resulting in

$$A_n(x,t) = -\frac{\eta_n}{2k_nb_n}\int_{-\infty}^{x} G\varphi_{1n}h_n dx,$$

$$B_n(x,t) = \frac{\eta_n}{2k_nb_n}\int_{-\infty}^{x} G\varphi_{1n}^2 dx.$$

in case of the continuous spectrum as well. Thus, on the basis of (23), the second equation of the Lax pair in this case has the form:

$$\varphi'_{1nt} = \left(\frac{1}{2\eta_n} + \gamma - u\right)\varphi'_{1nx} + \left(\frac{u'_x}{2} + \beta_n\right)\varphi_{1n} + \left(-\frac{\eta_n}{2k_nb_n}\int_{-\infty}^{x} G\varphi_{1n}h_n dx\right)\varphi_{1n} +$$
$$+\frac{\eta_n}{2k_nb_n}\int_{-\infty}^{x} G\varphi_{1n}^2 dx\, h_n \tag{27}$$

Passing to the limit in this equality when $x \to \infty$ and using the asymptotics (3), (11), (22) and (8), we obtain

$$\left(\frac{1}{2\eta_n} + \gamma\right)(-k_n)b_ne^{-k_nx} + \beta_nb_ne^{-k_nx} - \left(\frac{\eta_n}{2k_nb_n}\int_{-\infty}^{\infty} G\varphi_{1n}h_n dx\right)b_ne^{-k_nx}$$
$$+\frac{\eta_n}{2k_nb_n}\int_{-\infty}^{\infty} G\varphi_{1n}^2 dx\, e^{k_nx} == \frac{db_n}{dt}e^{-k_nx} - \dot{a}(ik_n)\frac{d(ik_n)}{dt}e^{k_nx}.$$

Substituting $\eta_n = \eta(ik_n) = -\frac{1}{\omega+\frac{\gamma}{2}}\left(-k_n^2 + \frac{1}{4}\right)$ and comparing coefficients of the exponents, we have

$$\frac{db_n(t)}{dt} = 4k_nb_n\left(\frac{\omega+\frac{\gamma}{2}}{1-4k_n^2} - \frac{\gamma}{2}\right) + \frac{1-4k_n^2}{8\left(\omega+\frac{\gamma}{2}\right)k_n}\int_{-\infty}^{\infty} G\varphi_{1n}h_n\, dx,$$

$$\frac{dk_n(t)}{dt} = i\frac{1-4k_n^2}{8\left(\omega+\frac{\gamma}{2}\right)k_nb_n\dot{a}(ik_n)}\int_{-\infty}^{\infty} G\varphi_{1n}^2 dx, n = 1,2,\dots,N.$$

Lemma 2 is proved.

Let us apply the result of Lemma 2 when

$$G = \sum_{k=1}^{N}(m'_xg_k^2 + 2(m + \omega + \frac{\gamma}{2})(g_k^2)'_x).$$

Using Lemma 1, one obtains

$$\int_{-\infty}^{\infty}(2((m+\omega+\tfrac{\gamma}{2})g_k^2)'_x - m'_xg_k^2)\varphi_1^2 dx = 2\int_{-\infty}^{\infty}(m+\omega+\tfrac{\gamma}{2})\,g_k\varphi_1(g'_{kx}\varphi_1 - g_k\varphi'_{1x})dx ==$$
$$\frac{2}{\eta_k-\eta}\int_{-\infty}^{\infty} W\{\varphi_1,g_k\}\frac{d}{dx}W\{\varphi_1,g_k\}dx = \frac{1}{\eta_k-\eta}W^2\{\varphi_1,g_k\}\Big|_{-\infty}^{\infty} = 0. \tag{28}$$

Consequently, according to Lemma 2

$$\frac{\partial R(k,t)}{\partial t} = -4ikR(k,t)\left(\frac{\omega+\frac{\gamma}{2}}{4k^2+1} + \frac{\gamma}{2}\right),\ Im\, k = 0. \tag{29}$$

Let us introduce the notation $g_n(x,t) = g(x,ik_n,t)$ and it is clear that $g_n(x,t) = c_n\phi_{1n}(x,t)$. Similar to (28) for $k \neq n$

$$\int_{-\infty}^{\infty}(2((m+\omega+\frac{\gamma}{2})g_k^2)'_x - m'_x g_k^2)\varphi_{1n}h_n dx =$$
$$= \frac{1}{\eta_k-\eta_n}\int_{-\infty}^{\infty}\left(\frac{d}{dx}W\{h_n,g_k\}W\{\varphi_{1n},g_k\} + \frac{d}{dx}W\{\varphi_{1n},g_k\}W\{h_n,g_k\}\right)dx =$$
$$= \frac{1}{\eta_k-\eta_n}W\{h_n,g_k\}W\{\varphi_{1n},g_k\}|\quad {}_{-\infty}^{\infty} = 0. \qquad (30)$$

For $k=n$, according to (13) and (4)

$$\int_{-\infty}^{\infty}(2((m+\omega+\frac{\gamma}{2})g_n^2)'_x - m'_x g_n^2)\varphi_{1n}h_n dx = = \int_{-\infty}^{\infty}(m+\omega+\frac{\gamma}{2})g_n^2 W\{h_n,\varphi_{1n}\}dx$$
$$= -2k_n b_n A_n(t).$$

Hence,

$$\frac{db_n(t)}{dt} = b_n\left(4k_n\left(\frac{\omega+\frac{\gamma}{2}}{1-4k_n^2}-\frac{\gamma}{2}\right)+\frac{4k_n^2-1}{4\left(\omega+\frac{\gamma}{2}\right)}A_n(t)\right). \qquad (31)$$

Similarly, to (30) for $k\neq n$

$$\int_{-\infty}^{\infty}(2((m+\omega+\frac{\gamma}{2})g_k^2)'_x - m'_x g_k^2)\varphi_{1n}^2 dx = = 2\int_{-\infty}^{\infty}(m+\omega+\frac{\gamma}{2})\,g_k\varphi_{1n}(g'_{kx}\varphi_{1n} - g_k\varphi'_{1nx})dx$$
$$= \frac{2}{\eta_k-\eta_n}\int_{-\infty}^{\infty}W\{\varphi_{1n},g_k\}\frac{d}{dx}W\{\varphi_{1n},g_k\}dx == \frac{1}{\eta_k-\eta_n}W^2\{\varphi_{1n},g_k\}|\quad {}_{-\infty}^{\infty} = 0.$$

For $k=n$, using the equality $g_n(x,t) = c_n\phi_{1n}(x,t)$, we obtain

$$\int_{-\infty}^{\infty}(2((m+\omega+\frac{\gamma}{2})g_n^2)'_x - m'_x g_n^2)\varphi_{1n}^2 dx = 2\int_{-\infty}^{\infty}(m+\omega+\frac{\gamma}{2})c_n\varphi_{1n}^2 W\{\varphi_{1n},c_n\varphi_{1n}\}\,dx = 0.$$

The last two equalities, we obtain

$$\int_{-\infty}^{\infty}G(x,t)\varphi_{1n}^2(x,t)dx = 0.$$

The equation for k_n in Lemma 2 can be written in the form

$$\frac{dk_n(t)}{dt} = 0, n = 1,2,\dots,N. \qquad (32)$$

Theorem. If the functions $u(x,t), g_k(x,t), k=1,2,\dots,N$ constitute a solution to the problem (1-3) hen the scattering data corresponding to Equation (4), associated with the function $u(x,t)$ vary in t according to the following relations:

$$\frac{\partial R(k,t)}{\partial t} = -4ikR(k,t)\left(\frac{\omega+\frac{\gamma}{2}}{4k^2+1}+\frac{\gamma}{2}\right), \qquad (Im\,k=0),$$
$$\frac{db_n(t)}{dt} = b_n\left(4k_n\left(\frac{\omega+\frac{\gamma}{2}}{1-4k_n^2}-\frac{\gamma}{2}\right)+\frac{4k_n^2-1}{4\left(\omega+\frac{\gamma}{2}\right)}A_n(t)\right),$$
$$\frac{dk_n(t)}{dt} = 0, n = 1,2,\dots,N.$$

Conclusion

The obtained equalities provide a complete description of the evolution of the scattering data, which enables the application of the inverse scattering method to solve the system (2–5). The inverse problem of reconstructing the function$u(x,t)$ rom the scattering data is solved through the following equations [1]:

$$\overline{\psi_1}(x,k) = \left(\frac{\xi(x)}{\xi'(x)}\right)^{\frac{1}{2}} + \int_{-\infty}^{\infty}R(k')\overline{\psi_2}(x,k')\,[\xi(x)]^{2ik'}\frac{dk'}{k'-k} + \sum_{n=1}^{N}\frac{b_n[\xi(x)]^{-2k_n}\overline{\psi_1}(x,-ik_n)}{\dot{a}(ik_n)(ik_n-k)},$$

$p=1,2,\dots,N,$

$$\overline{\psi_1}(x,-ik_p) = \left(\frac{\xi(x)}{\xi'(x)}\right)^{\frac{1}{2}} + \int_{-\infty}^{\infty}R(k')\overline{\psi_2}(x,k')[\xi(x)]^{2ik'}\frac{dk'}{k'+ik_p} + i\sum_{n=1}^{N}\frac{b_n[\xi(x)]^{-2k_n}\overline{\psi_1}(x,-ik_n)}{\dot{a}(ik_n)(k_p+k_n)}$$

$$e^{-\frac{x}{2}}[\xi(x)]^{\frac{1}{2}} = \left(\frac{\xi(x)}{\xi'(x)}\right)^{\frac{1}{2}} + \int_{-\infty}^{\infty} R(k')\overline{\psi_2}(x,k')[\xi(x)]^{2ik'}\frac{dk'}{k'+\frac{i}{2}} + i\sum_{n=1}^{N}\frac{b_n[\xi(x)]^{-2k_n}\overline{\psi_1}(x,-ik_n)}{\dot{a}(ik_n)(k_n+\frac{1}{2})}.$$

where

$$\xi(x) = exp\left\{x + \int_{\infty}^{x}\left(\sqrt{\frac{m+\omega+\frac{\gamma}{2}}{\omega+\frac{\gamma}{2}}} - 1\right)dy\right\}, \quad \overline{\psi_1}(x,k) \equiv \psi_1(x,k)[\xi(x)]^{ik}.$$

References:

[1] Dullin R., Gottwald G., Holm D. "An integrable shallow water equation with linear and nonlinear dispersion," *Phys. Rev. Lett.* 87 (9), 2001, pp. 4501-4504.

[2] Tian L., Gui G., Liu Y. "On the well-posedness problem and the scattering for the Dullin–Gottwald–Holm equation," *Comm. Math. Phys.* 257, 2005, pp. 667–701.

[3] Constantin A., Strauss W. "Stability of the Camassa–Holm solitons," *J. Nonlinear Sci.* 12, 2002, pp. 415–422.

[4] Octavian G. Mustafa "Existence and uniqueness of low regularity solutions for the Dullin-Gottwald Holm equation," *Comm. Math. Phys.* 265, 2006, p. 189-200.

[5] Christov O., Hakkaev S. "On the inverse scattering approach and action-angle variables for the Dullin Gottwald Holm equation," *Physica D*, 238, 2009.

[6] Melnikov V.K. "Exact Solutions of the Kortewedde Vries Equation with a Selfcon sistent Source," *Phys. Lett. A*, 128:9, 1988, pp. 488-492.

[7] Lixin Tian, Guilong Gui, Boling Guo, "The limit behavior of the solutions to a class of nonlinear dispersive wave equations," *J. Math. Anal. Appl.* 341, 2008, pp. 1311-1333.

[8] Hakkaev S. "Stability of peakons for an integrable shallow water equation," *Physics Letters A*. 354, 2006, pp. 137-144.

[9] Constantin A., Gerdjikov V., Ivanov R.I. "Inverse scattering transform for the Camassa-Holm equation," *Inverse Problems*. 22, 2006, p. 2197.

[10] Zhou J.B., Tian L.X., Zhang W.B., Kumar S. "Peakon-antipeakon interaction in the Dullin-Gottwald-Holm equation," *Physics Letters A*. 377, 2013, pp. 1233-1238.

UDC: 8, 81, 81'3, 81.37

GRAMMATICAL SEMANTIC EXPRESSIVE POSSIBILITIES OF REDUPLICATION

Guzal Rakhimova Yuldashovna
Associate Professor (PhD), Department of Theory of Translation and Practice, Urgench State University named after Abu Rayhan Biruni
gozal.r@urdu.uz

Annotatsiya. Ushbu maqola reduplikatsiyaning grammatik, semantik va ifodaviy imkoniyatlarini o‘rganadi, uning asosan o‘zbek tilidagi va boshqa tillardagi roliga e’tibor qaratadi. Reduplika so‘zning ma’nosini kuchaytirish, ko‘plikni belgilash, hissiy ohang qo‘shish va matn tuzilishini tashkil etishda ko‘p qirrali vosita sifatida namoyon bo‘ladi. Tadqiqotda to‘liq va qisman leksiko-semantik takrorlash hamda sintaktik parallelizm shaklidagi turli reduplikatsiya turlari tahlil qilinadi va ularning ingliz, o‘zbek va boshqa tillardagi misollari keltiriladi. Reduplika she’riyat, xalq og‘zaki ijodi va kundalik muloqotda stilistik ta’sir ko‘rsatish xususiyatiga ega ekanligi ta’kidlanadi. Shuningdek, o‘zbek tili uchun yaratilgan morfologik tahlil modullari va lemmatizatsiya hamda stemmimg jarayonlarida reduplikatsiyaning ahamiyati ko‘rsatilib, matnlarni avtomatik tahrirlash va mashina tarjimasi sifatini oshirishga qaratilgan tadqiqotlar natijalari taqdim etiladi. Tadqiqot natijalari reduplikatsiyaning til tipologiyasiga, morfologik tizimlariga bog‘liqligini, shuningdek, oddiy takrorlashdan farqli o‘laroq, uning murakkab semantik va morfosintaktik funktsiyalarini yoritadi.

Kalit so‘zlar: *reduplikatsiya, lemmatizatsiya, morfologiya, leksik-semantik takrorlash, sintaktik jarayon.*

Аннотация. В статье рассматриваются грамматические, семантические и выразительные возможности редупликации с особым вниманием к её роли в узбекском и других языках. Редупликация, как широко распространённое морфологическое и синтаксическое явление, служит многофункциональным языковым инструментом, усиливающим значение, обозначающим множественность, добавляющим эмоциональные оттенки и структурирующим дискурс. В исследовании анализируются различные типы редупликации — от полной и частичной лексико-семантической повторяемости до синтаксического параллелизма, представлены примеры из английской, узбекской и других языков. Особое внимание уделяется значимости редупликации в поэзии, устной традиции и повседневном общении, подчёркивается её стилистическое и риторическое воздействие.

В статье также обсуждается разработка морфологического анализатора и лингвистического программного модуля для узбекского языка, подчёркивается необходимость учета редупликативных форм для точной

автоматической обработки текстов, стемминга и лемматизации. Полученные результаты выделяют типологическую значимость редупликации, которая варьируется в зависимости от морфологической системы языка и чётко отличается от простой повторяемости за счёт своей семантической и морфосинтаксической сложности.

Ключевые слова: *редупликация, лемматизация, морфология, лексико-семантическое повторение, синтактическое явления.*

Abstract. This article explores the grammatical, semantic, and expressive possibilities of reduplication, focusing on its role in Uzbek and other languages. Reduplication, a widespread morphological and syntactic phenomenon, serves as a multifunctional linguistic tool that intensifies meaning, marks plurality, adds emotional nuance, and structures discourse. The study analyzes various types of reduplications—from full and partial lexical-semantic repetition to syntactic parallelism—and illustrates their functions with examples from English, Uzbek, and other languages. Particular attention is given to the significance of reduplication in poetry, oral tradition, and everyday communication, highlighting its stylistic and rhetorical impact.

The research also discusses the development of morphological analysis modules and linguistic software tailored for Uzbek, emphasizing the necessity of incorporating reduplicative forms for accurate automatic text processing, stemming, and lemmatization. The findings underscore the typological importance of reduplication, which varies according to language typology and morphology, and distinguishes it clearly from simple word repetition due to its semantic and morphosyntactic complexity.

Keywords*: Reduplication, lemmatization, morphology, lexical-semantic repletion, syntactic phenomenon.*

Introduction

As the information age progresses, automatic text editing and analysis have become rapidly developing and highly significant areas in global linguistics. Programs handling these tasks are indispensable modern tools that not only provide quick and cost-effective text processing but also improve the quality of machine translation. Morphological analysis (MA) traces its origins to the ancient Indian linguist Panini, who created 3959 rules for Sanskrit morphology in the *Aṣṭādhyāyī*. Later, the Greek-Roman grammatical tradition also studied morphology. The term “morphology” was coined in linguistics by A. Schleicher in 1859. By the 1960s-70s, research in machine morphology expanded around creating machine lexicons. Today, the world’s information technologies and linguistics have developed several effective morphological analysis technologies, notably stemming and lemmatization. Stemming works on the root base of words, while lemmatization considers inflected forms derived by affixation.

For the agglutinative Uzbek language, stemming technologies are particularly effective for automatic text analysis. Words that change with possessive and case suffixes combine under noun categories, including nouns, adjectives, numerals, pronouns, onomatopoeic words, and verbal nouns. Morpho-syntactic synthesis,

particularly for nouns, was implemented by creating databases of affixes for lexical and syntactic form generation in Access. Words with plural or semantic plurality, such as uncountable nouns, abstract nouns, body parts, personal, and toponyms, were grouped accordingly. A specific software module for grammatical formation of Uzbek nouns was created, linking affixes with word forms and generating derivatives via comprehensive databases. All program algorithms rely on data sources, including linguistic rules of the national language. Linguistic software works based on these algorithms. Morphological modules analyze and synthesize word forms—from surface forms to lexemes and vice versa—playing a critical role in linguistic processing of Uzbek texts, accelerating editing and analysis, and fostering correct Uzbek text writing skills. Reduplication is a key linguistic tool that attracts attention to text meaning and helps deliver the main idea effectively. It is characterized by emotional and expressive richness, functioning as an important connector between sentences. Some linguists regard reduplication as a symbolic feature distinguishing poetry from prose. Parallel sentence structures created by reduplication are often used rhetorically in poetic texts to strengthen impact.

Research Methodology

The study analyzes different types of reduplications syntactically and lexically, classifying them by their degree and type of repetition. Syntactic reduplication overlaps with lexical reduplication and may be termed lexical-semantic reduplication. This can occur as full or partial repetition, reflecting syntactic parallelism and lexical reiteration. The semantic unity is achieved by integration of semantically close words, enriching clarity and expressiveness. Examples are provided from English and Uzbek literature illustrating full syntactic parallelism (e.g., predicate repetition, subject repetition) and their rhetorical effects. The study further explores incomplete lexical-semantic reduplication, which repeats only parts of words or clauses to serve stylistic functions, such as focus and emphasis. Additionally, theoretical perspectives on lexical units such as reduplicative, binomials, and their morphological and semantic roles were examined in linguistics literature by researchers like J. Lich, Y. Swartvik, D. Biber, and S. Conrad.

The study identifies different types of reduplications, including echo words, idiomatic, binomial pairs, and their phonological and semantic properties. It also delves into the distinction between reduplication (morphological duplication with semantic significance) and mere repetition (phonetic or pragmatic reiteration). Statistical and corpus-based approaches to classification of reduplications are considered.

Classification of Reduplication: Reduplications consist mainly of complete or partial lexical and syntactic repetition. Lexical-semantic reduplication widens the semantic field and enhances expressiveness and clarity. Full reduplication often occurs in poetic and oral traditions, as visible in popularly repeated phrases from Uzbek songs and Shakespeare's works.

Morphological Synthesis: Morphological databases and algorithms enable the generation and analysis of noun forms and reduplicative constructs effectively. The study confirmed that Uzbek's agglutinative morphology benefits significantly from stemmer-based morphological processing.

Expressive Function: Reduplication functions predominantly in emotional intonation and stylistic emphasis in text, serving as a linguistic device for organizing discourse and highlighting key semantic information.

Phonological and Semantic Variation: Reduplications show diverse phonological patterns like initial consonant alternation, vowel changes, and affix variations, illustrating their productive and dynamic nature.

Linguistic Software Development: The linguistic module for Uzbek text editing integrates morphological analysis and synthesis, recognizing reduplications for improved automatic text processing and machine translation.

Analysis and Results

Reduplication plays an important role in linguistic expression, text cohesion, and semantic emphasis in both oral and written forms. The use of reduplication extends beyond formal literature, influencing everyday communication, folklore, and digital linguistic processing. In Uzbek, as well as in English and other languages, it enriches idiomatic expressions and stylistic devices, consequently enhancing the richness of language. The study highlights the complexity and variability of reduplicative forms, their morphological, phonological, and semantic layers, suggesting the necessity of comprehensive linguistic models for accurate computational processing. Furthermore, differentiating between reduplication and plain repetition remains a methodological challenge but is vital for natural language understanding.

The findings encourage further application of automatic and statistical linguistic tools, particularly for agglutinative languages like Uzbek, contributing to both theoretical linguistics and practical linguistic technologies such as machine translation, information retrieval, and text editing systems.

Reduplication is a highly productive and expressive linguistic device found across the world's languages. It plays a multifaceted role in grammar, stylistics, semantics, and discourse organization. This section provides a deeper discussion on the significance of reduplication, illustrated with diverse examples from Uzbek, English, and other languages. When we discuss about Semantic and Pragmatic functions we have underpinned about

Emphasis and Intensification. Reduplication is frequently used to intensify meaning or draw attention to a particular property or state.

English examples: “Do you like-like him?” clarifies romantic interest versus mere friendship. “I’m tired-tired” intensifies the degree of tiredness. Bish -bash-bosh, mumbo-jumbo (nonsense), freaky-deaky (strangely).

Uzbek example: “Qup-quruq gap” (empty talk), where the repetition adds scornful or dismissive meaning.

Plurality and Distribution. In some languages, reduplication marks plurality, frequency, or distributive meaning:

Malay/Indonesian: “buku” (book) → “buku-buku” (books).

Uzbek: While Uzbek does not routinely mark plural via reduplication, iterations like “yaxshi-yaxshi gaplar” (nice-nice words) may indicate abundance or variety in colloquial speech. Ko‘p-ko‘p odamlar (many people), ancha -muncha odamlar (several people), ming-ming tomoshabin (thousands of audiences), meva -cheva (some fruits)

Diminutives and Affectives. Reduplication can soften, endear, or render childish/cute meanings.

English: "night-night" (for "good night" to children), "choo-choo" (train sound).

Uzbek: "Aka-ukalar" (bro, pal — affectionate slang among peers). Bola-chaqalar (children), xotin -xalajlar (women).

Poetic Rhythm and Stylistic Effect. Used in poetry and songs, reduplication often serves as a tool for rhythm, resonance, and memorability.

English (Shakespeare):

"So long as men can breathe or eyes can see,
So long lives this, and this gives life to thee."

Uzbek folk song:

"Sust xotin, sulton xotin,
Ko'lkankasi maydon xotin."

The repetition supports musicality and enhances cultural flavor.

Parallelism and Cohesion. Reduplication can structure discourse by providing syntactic parallelism, giving the text cohesion and expressive power.

Example:

"Living is the art of loving, loving is the art of caring.
Caring is the art of sharing, sharing is the art of living."

Morphological Productivity. Reduplication contributes to word formation and the enrichment of the lexicon, especially in agglutinative languages.

Forming new adjectives/adverbs or vivid onomatopoeia:

English: "zig-zag," "tick-tock," "flip-flop."

Uzbek: "chap-chap" (the slapping sound of water), "jing-jing" (tinkling) shivir-shivir.

Idiomatic and Formulaic Expressions. Some reduplicative formations become established idioms or formulaic language units.

English nursery rhymes

"Humpty-Dumpty," "hocus-pocus."

Uzbek: Phrases such as "har xil har xil" (all kinds of), valdir-vuldur (ping-pong), taraq-turuq, gumbur-gumbur.

Reduplication is distinct from mere repetition:

Lexicalized reduplication creates fixed or semi-fixed meanings, often with a specific communicative function ("bye-bye" = "goodbye").

Repetition for rhetorical effect may not always alter word meaning, but enhances rhythm or dramatic focus

Expressing Emotion and Attitude. Uzbek conversational speech: "Tez-tez kel" ("Come quickly!"), with reduplication for urgency.

English: "Fancy-schmancy," expressing dismissiveness or sarcasm.

Children's Language Acquisition. Children often use and recognize reduplicatives earlier than other forms ("mama," "dada"), highlighting their cognitive and mnemonic utility.

Informal Speech. Widespread in informal, colloquial registers:

Hanky -panky, "Goody-goody," "wishy-washy" in English for pejorative or playful tone.

“Ko‘cha-mo‘cha” in Uzbek (street and the like) — informal or dismissive references. Oldi-sotdi (to trade), uncha-muncha, onda-sonda and so on.

Oral Tradition and Folklore. Reduplication features prominently in proverbs, riddles, and folklore, for both performative and aesthetic reasons.

Automatic Analysis and Natural Language Processing. In computational linguistics, identifying reduplication is crucial for accurate morphological parsing, information retrieval, and machine translation, particularly for morphologically rich and agglutinative languages like Uzbek

Ambiguity and Boundaries. Differentiating reduplication from repetition, and distinguishing partial from full reduplication, remain ongoing issues.

Semantic Opacity. Certain reduplicative forms become idiomatic and lose transparency, complicating their analysis for both human linguists and NLP systems.

Table 1. Types and Uses of Reduplication.

Type	Language	Example	Function
Full Reduplication	English	“bye-bye,” “go-go”	Diminutive/affectionate
Partial Reduplication	English	“zig-zag,” “flip-flop”	Onomatopoeic, descriptive
Lexicalized Idiom	Uzbek	“aka-maka”	Affection, camaraderie
Expressive	Uzbek	“tez-tez” (quickly)	Emphasis, urgency
Distributive	Malay	“anak-anak” (children)	Plurality/distribution
Stylistic	English/Uzbek	Song or poetry lines	Rhythm, cohesion, stylistic effect

Conclusion

Reduplication is a dynamic and context-sensitive linguistic phenomenon that enriches language expressivity, stylistic nuance, and communicative efficiency. Its varied realizations across languages highlight its role in emotional intensification, grammatical innovation, artistic expression, and computational challenges, confirming the need for ongoing interdisciplinary research and practical language technology development. The conclusions on reduplication emphasize its universal typological significance and its unique structural and semantic-functional roles across languages of different families and morphological types. Reduplication is found to be a widespread morphological process with great diversity in form and function, from full to partial repetition, and its use correlates strongly with a language's typological properties, especially word-formation strategies. Research shows that reduplication functions as a morphological doubling process, which primarily relies on identity at the morphosyntactic level rather than strictly phonological identity between the original base and the reduplicant. This insight allows for a better understanding of why reduplication patterns often show phonological variation or partial reduplication depending on phonological or morphological constraints in different languages.

From a semantic and pragmatic perspective, reduplication enhances expressive power by marking emphasis, intensification, plurality, recurrence, or affective nuance. For instance, English reduplication such as "redder and redder" captures progressive intensification over time, which differs from simple comparison without reduplication. In Uzbek and other agglutinative languages, reduplication contributes intricately to expressive and stylistic richness, playing important roles in poetry, oral tradition, and everyday speech, as well as enhancing computational linguistic analysis through

morphological synthesis. Furthermore, it is concluded that: The universality of reduplication allows it to serve as a typological feature that helps classify languages according to how reduplication interacts with syntax, morphology, and phonology. Reduplication use varies widely: languages with rich morphological word-formation tend to have more extensive reduplication systems, while isolating or analytic languages use it more limitedly.

The distinction between reduplication and simple repetition is crucial for linguistic theory and natural language processing because reduplication encodes morphosyntactic and semantic functions beyond mere reiteration of identical forms. Reduplication has important pragmatic functions such as clarifying intention, adding emotional coloring, or structuring discourse through syntactic parallelism, with effects seen in idiomatic expressions, poetry, and folklore. The complexity and variability of reduplication phenomena suggest continuing challenges for computational linguistics, especially for agglutinative languages like Uzbek, where morphological and phonological analysis must incorporate reduplicative patterns for accurate text editing, parsing, and machine translation. In summary, reduplication represents a fundamental and multifaceted linguistic mechanism that spans phonology, morphology, syntax, semantics, and pragmatics. It enhances expressivity, contributes to word formation, and provides a rich area of study for understanding language universals and diversity. This calls for ongoing interdisciplinary research, combining theoretical linguistics and computational methods, to fully grasp and utilize the expressive and structural possibilities of reduplication in natural languages.

References:

[1] Benczes R. “Just a load of hibber-gibber? Making sense of English rhyming compounds.” *Australian Journal of Linguistics* 32(3), 2012, pp. 299-326.

[2] Biber D., Conrad S., & Reppen R. “Corpus Lingusitics: Investigating Structure and Use.” Cambridge: *Cambridge University Press*, 1999.

[3] Blatna R. “Binomialy typu “techtle-mechtle” v cestine, rustine a anglictine.” *Slavia-casopis pro slovanskou filologii* 59, 1990.

[4] Inkelas Sh. and Cheryl Z. “Is grammar dependence real? A comparison between cophonological and indexed constraint approaches to morphologically conditioned phonology.” 2007, pp. 133–171.

[5] Jespersen D.C. “Arakawa's method is a finite-element method.” *Journal of computational physics* 16(4), 1974, pp. 383–390.

[6] Joan Beal “Toy boys and lager louts: Motivation by linguistic form.” In Language usage and description: Studies presented to NE Osselton on the occasion of his retirement. 1991, pp. 139–148.

[7] Minkova Donka “The Cambridge History of the English Language.” Vol. III, *Journal of English Linguistics,* 2001, pp. 1476-1776.

[8] Nadarajan S. “A crosslinguistic study of reduplication.” *Journal of English Linguistics* 29(1), 2001, pp. 83-92.

UDC: 93/94, 308, 2-43, 304

THE CATEGORY OF JUSTICE IN NAVOI'S SOCIO-ANTHROPOLOGICAL VIEWS

Gulova Anorgul Akhtamovna
Doctoral Student, Andijan State University
Gulovaanorgul2@gmail.com

Annotatsiya. Ushbu maqolada Alisher Navoiyning ijtimoiy-antropologik qarashlarida odillik kategoriyasi tahlil qilingan.

Kalit so'zlar: *adolat, ma'naviyat, ma'rifat, tafakkur, jamiyat, ta'lim, sabr.*

Аннотация. В стате анализируется категория справедливости в сотсиально-антропологических воззрениях Алишера Навои.

Ключевые слова: *справедливост, духовност, просвещение, мысл, общество, образование, терпение.*

Abstract. This article analyzes the category of justice in Alisher Navoi's socio-anthropological views.

Keywords: *justice, spirituality, enlightenment, thought, society, education, patience.*

Introduction

In his socio-anthropological views, Alisher Navoi also places special emphasis on the concepts of justice and fairness. Therefore, justice serves as the basis for the prosperity of the world and the well-being of social life. Navoi mainly uses the word "adl" in his scientific and literary works.

Adlki uch harf ila maqrun erur,
Har biriga o'zgacha mazmun erur:
"Ayn"i aning mehre erur tobnok,
Zulm qaro shomini qilmoqqa pok.
"Dol"i dag'i davlati din tojidur,
Din bila davlat eli muhtojidur.
Hurg'a gisu quyig'i "lom"i bil,
Izzu sharaf qushlarining domi bil [1].

The word "Adl" consists of three letters. But each letter in it has a different meaning. The "ayn" in it is the burning sun, purifying the dark evening of oppression. "Dol" is the crown on the head of religion and state, and religious and state figures always feel the need for it. The "lam" at the end is the hair of the free; it is a trap for birds of honor and glory. Therefore, put the crown on your head and brighten your eyes with love. Protect the oppressed who come to you for help under the shadow of justice.

Literature Review

Alisher Navoi, first of all, sets a demand for justice for himself. In particular, in the prayer section of "Lison ut-tair," in accordance with the tradition of Sufis, he asks Allah

Almighty to place the light of justice and honesty in his heart, to free him from the oppressive self, and to take him under his protection.

At the same time, Navoi, who considered the ability to distinguish truth from falsehood, truth from falsehood, as the main condition for justice, emphasized that whoever acts by distinguishing truth from falsehood, as if he had reached the level of enlightening the West and the East with justice.

According to Alisher Navoi, the supreme example of justice is not in the material world. Rather, it is the creator and ruler of the universe (Allah). God is not only the creator of existence and man, but also the creator of divine laws and rules that must be applied to the human world. These laws show and teach man the path of guidance. Therefore, the philosopher-poet describes the origin, development and end of existence and life through a sense of religious faith. It is on this basis that he describes spiritual and social issues.

After Navoi became the main figure in the country's governance after the ruler, he began to implement more and faster the work aimed at improving the well-being of the country and the life of the people. He took advantage of the wide opportunities given to him and began to realize his goals and intentions, namely, to suppress the growing rebellions in the state, to create even more conditions for the working people, in short, to introduce a just order in the kingdom, and he made the most of all the opportunities at his disposal. It is noteworthy that while working as a minister, Hazrat Navoi always acted with concern for the people. He diligently sought to mobilize the material wealth of the country's treasury for the welfare of the state and the improvement of the people's lives, not for wars and conflicts. In this regard, Navoi scholar V. Zohidov says: "Even when Navoi was in state affairs, he did not forget the people for a single breath. He tried to turn the state into a tool that serves the interests of the people and fulfills their dreams, to turn statesmen into servants of the people, and in this he himself became an example. He did his best to discipline state affairs, to cleanse government offices and the palace of scoundrels, to expose and whip them, to expose and whip them..."

Navoi emphasizes the need to benefit the people both with work, word, and heart. He calls such people real people. The meaning of the scholar's life was to act with concern for people, to share goodness, and to be kind. That is why the words "Shahi Gharibon" are inscribed on his tombstone, that is, the king of the poor, the poor, and the lonely. He was unparalleled in charity and kindness. He directed all the material blessings that came from the lands and waters of the territories he owned to charity. Navoi considers generosity to be the main aspect of patriotism and maturity. Humanity is a unique quality that makes a person human, distinguishes him from other creatures. The image of Farhod in the epic poem "Farhod and Shirin" is interpreted in the spiritual heritage of the thinker as a truly brave, humane and heroic young man. The fact that Farhod, who was familiar with science from his youth, mastered all the crafts of his time, and used the robot system as a weapon against dark forces shows the youth of our time the actions that they should also perform.

Analysis and Results

According to Navoi, loyalty is the essence of humanity, the basis of social goodness. As a supporter of eliminating the vices existing in society, the thinker emphasizes the vast possibilities of free will and puts before people the need to get rid of negative vices as much as possible. He calls on people to follow the example of good people in this regard. The scholar defines goodness as follows: "Goodness, kindness, is to bear the burden of hardship of a victim and save him from those difficulties. "Karam is to bear the weight of someone's hardship and to blossom like a flower from the tip of a thorn and not to mention the deed done, not to put it in your mouth," "Kindness is the offspring, the twin brother of karam. Whoever possesses these qualities will be honored and respected." Navoi likens the qualities of kindness and karam to parents, while modesty and loyalty are like twin children. The scholar also emphasizes that charity is the sum of all good deeds and all virtues are contained in it.

A person who has been granted a high position should devote his life only to good deeds. If he cannot do good, then at least he should not harm people and stay away from evil:

Yaxshilik gar aylamasang ish chog'i,
Aylamagin bori yomonlik dog'i...[2]

In his spiritual heritage, Alisher Navoi praised the highest ideals of humanity. At the same time, he fought for his own ideals. In his opinion, faith is the main sign of humanity. In this, by faith, the scholar means genuine faith, not imitation for the people. Creative hypocrisy, hypocrisy, and forgery are completely incompatible. As an example, one can cite his reflections on "Hypocrite Sheikhs" in the work "Mahbub-ul Qulub" and the ghazal "Sheikh".

Navoi's idea of the ideal person is reflected in the governance of the state, in the scholar's views on the community of accomplished individuals, in his thoughts on the just king, in the ruler's attitude towards the population, and in his adherence to religious and legal laws and regulations.

In the epics from the work "Khamsa," in particular, "Farhod and Shirin," "Sab'ai Sayyor" and "Saddi Iskandari," the thinker embodies the image of a "society of virtuous people" who gives the people a prosperous life, develops the state, brings happiness to people, is far from injustice and oppression, and acts with justice, and has reached the status of a perfect human being.

Alisher Navoi, addressing the Shah, emphasizes that justice is the foundation on which the life of the nation is built, and explains that a good person acquires justice. Politics is strong with justice, because it is better to lead justice and governance equally:

Adl aylaki, ul xalq hayoti bo'lmish,
Xush ul kishikim, adl sifoti bo'lmish,
Ham mulk bila adl jihoti bo'lmish,
Ham adl bila mulk saboti bo'lmish [3].

"Ochlar g'izosi bazl va atosi xonidin, yalang'ochlar libosi xizonai lutf va ehsonidin. Mulk bog'in ma'mur qilurg'a abri serob va mulk ahli ko'zin yoruturg'a mehri jahontob. O'zga mulkning raoyo va xalqi aning orzusida va yana kishvar mazlumlari aning adli duosi guftigo'sida. Yaxshi otig'a ulamo ishi rasoil tartibi va yaxshi sifotig'a shuaro varzishi qasoyid tarkibi, mug'anniylar ishtig'oli sanosi

uchun surud tuzmak va musanniflar maqoli duosi ohangida nag‘ma ko‘rguzmak. Xalq rizosidin haq rizosig‘a tolib va dodxoh so‘rarda so‘rug‘ kuni vahmi ko‘nglig‘a g‘olib [4].

Content: The food of the hungry comes from the king's generous table, the clothing of the naked comes from the king's treasury of grace. He is like a rain cloud that beautifies the flowers of the land, and like the sun that illuminates the eyes of the people of the land. The oppressed people of other countries pray for his justice. Scholars write treatises in his good name, and poets write odes describing his good qualities, and composers compose melodies in his honor.

Navoi wants to see the just, wise, and people-loving king, praised in his socio-anthropological views, in the person of his friend Husayn Boykara, with whom he grew up since youth. He always encourages him to share the sorrows and sorrows of the country’s people and to do good deeds. For example, Alisher Navoi tells his friend Abulgazi Bahodirkhan (Husayn Boykara): “It is obligatory to put the advice of the king's state first in all matters. It is obligatory to carry out the command of God even before.” Through this invitation, he calls for being just, people-loving, and humane in governing the state.

It is known that in the 8th-15th centuries, the dominant view in the Muslim East was that the king was a deputy (caliph) sent by God to rule the people. According to him, the king was considered a symbol of justice, it was important for him to implement it among the people, and justice should always be the priority in his activities. This idea is also reflected in the socio-anthropological views of Hazrat Navoi: “Odilu oqil podshoh ibodullohg‘a zillulloh. Xilofat mulki aning farmonida “inni joilun fil arz xalifa”ning sha’nida. Bukim odil podshoh ta’rifdin biyikroq erur “valadat fiz-zamon as-sulton ul-odil” andin xabar berur. Ulki aning zoti bila mubohidur xojai kavnayn debdurkim, “adli soat xabara min ibodat ul-saqlin [5].”

Content: The just and wise king is the shadow of Allah on earth. The verse “Inni jailun fil arz khalifatun” – that is, “I will make a man a caliph (vicegerent) on earth” – was said in his honor. Thus, the level of the just king is beyond description – the hadith “Wulidtu fai zamonas – sultan ul-adil” – that is, “I was born in the time of a just sultan” – that is, “I was born in the time of a just sultan” – informs about this. The owner of the two worlds, Muhammad (peace and blessings of Allah be upon him), said, “Adlu saatin khairunmin ibadatis – saqalayn” – that is, “One hour of justice is better than the worship of both worlds: the worship of humans and the worship of jinn.”

Navoi, who promoted the ideas of the sacred sources of Islam in his works, advocated that the rulers of the country should remember their Muslim identity in any situation and act in accordance with the principles of Sharia.

According to the scholar, the health or illness of a person’s body depends on the health or illness of his soul, and the prosperity or ruin of a country depends on the tyranny or justice of the ruler: “Badan salohu fasodi ko‘ngul salohu fasodig‘a tobe’-dur va mulk obodu xaroblig‘i shoh adlu zulmig‘a roje’dur” [6].

Justice is the adornment not only of rulers but also of ordinary people. No other king can match a king who is determined to act with justice.

Nechukkim, erur adl shahlarg‘a zeb,
Erur ham gado, xokrahlarg‘a zeb.

Shahekim, adolatdur oning ishi,
Teng ermas anga shohlardin kishi [7].

A king who acts with justice turns wastelands into prosperous territories. Even an infidel king, if he is just, will make the country prosperous. If a believing king is tyrannical, the state will fall into disarray. If the king is just, he will achieve the happiness of both worlds, Navoi emphasizes:

Shohki ish adl ila bunyod etar,
Adl buzuq mulkni obod etar.
Kofiri odil ani obod etib,
Mu'mini zolim ani barbod etib.
Shahki erur adl ila davron anga,
Bo'ldi sirot o'tmagi oson anga [8].

The scholar ruthlessly exposes the various tricks of tyrants, ruthlessness, and wickedness of kings: "Odil podshoh ko'zgu va bu aning uchasidur. Ul yoruq, subh, bu aning qorong'u kechasidur. Zulm aning ko'nglig'a marg'ub va fisq aning xotiriga mahbub. Mulk buzug'lig'idin zamiriga jam'iyat va ulus parishonlig'idin xotirig'a amniyat. Obodlar aning zulmidin vayrona, kabutar toqchalari boyqushg'a oshiyona. Boda seli chun bazmida to'g'yon qilib, ul sel mulk ma'muralarin vayron qilib." The scholar ruthlessly exposes all the tricks of the tyrant, the ruthless, the wicked, the kings. Content: The just king is a mirror and this is his reflection. He is the bright morning, this is his dark night. Tyranny is a comfort to his heart, and corruption is pleasant to his memory. Unity in his heart from the chaos of the country, peace in his memory from the chaos of the people. The prosperous regions are ruined by his oppression, the pigeon houses are a place for owls. The flood of wine has overflowed at his feasts and parties, ruining the prosperity of the country.

Conclusion

In conclusion, from the above socio-anthropological views of Alisher Navoi, it is clear that every person is a representative of God on earth. He should spend his life, which is given to him only once, meaningfully, constantly working on himself and striving for spiritual perfection, be just and conscientious. Especially, those who exercise authority over the people should be doubly responsible in this regard and be determined to leave a good name for themselves. Of course, justice should serve as a bright beacon for them on this path.

References:

[1] Alisher Navoiy "Hayratul-abror," MAT. J. 7. Toshkent: *Fan*, 1991, pp. 347-348.
[2] Zohidov V. "Ulug' shoir ijodining qalbi," T. 1970.
[3] Navoi A. "The role of Alisher Navoi's creative heritage in the spiritual and educational development of mankind." *Materials of the international scientific conference,* 2017, p. 328.
[4] Mutallibov S., Ochilov E. "Proverbs." Preparers for publication, T.: "*East*," 2006, p.. 18.
[5] Alisher Navoiy "Mahbub ul-qulub." MAT. 20 jildlik. J. 14. Toshkent: *Fan*, 1998, p. 8.
[6] Alisher Navoiy "Munshaot." MAT.J. 14. Toshkent: *Fan*, 1998, p. 160.
[7] Alisher Navoi "Mahbub ul-qulub," Tashkent: *Sano standart*, 2018, p. 14.
[8] Mutallibov S., Ochilov E. "Wisdoms," Prepared for publication, T.: "*Sharq*", 2006, pp. 33-34.